An Evaluation of the Predictions of Near Bottom Interaction Forces and Moments on Unmanned Undersea Vehicles

Validation, Reduction, and Implementation of the Results of a Computer Code into a Real-Time Simulation

by

Jacqueline Ruth Chatterton

B.S., Webb Institute of Naval Architecture,
1992

Submitted to the Department of Ocean Engineering
in Partial Fulfillment of the Requirements for the Degree of

MASTER OF SCIENCE
in Naval Architecture and Marine Engineering

at the
Massachusetts Institute of Technology
May, 1994

Signature of Author _____
Jacqueline Ruth Chatterton
May 1994

Certified By _____
Michael S. Triantafyllou
Thesis Advisor
Professor of Ocean Engineering

Accepted By _____
Audrey K. Fitzgerald
Supervisor, Draper Laboratory

Accepted By _____
A. Douglas Carmichael
Chairman, Departmental Committee on Graduate Students

An Evaluation of the Predictions of Near Bottom Interaction Forces and Moments on Unmanned Undersea Vehicles

Validation, Reduction, and Implementation of the Results of a Computer Code into a Real-Time Simulation

by

Jacqueline Ruth Chatterton

Submitted to the Department of Ocean Engineering on May 6, 1994
in Partial Fulfillment of the Requirements for the Degree of
Master of Science in Naval Architecture and Marine Engineering.

Abstract

The purpose of this thesis is to provide extensions to and evaluation of the proximity codes currently available at Draper Laboratory. These codes have been developed to predict the interaction force and moment which an Unmanned Undersea Vehicle (UUV) will experience when in proximity with an obstacle. The theory presented uses a potential flow model of a body operating in an ideal fluid. The body is represented by an axial distribution of singularities from which the force and moment are predicted using Lagally's theorem. The currently available code has been extended to include unsteady motion, an inclined bottom, and automatic convergence.

The validation of these codes involved performing model testing at the MIT towing tank as well as collecting previously published data and examining the theoretical trends. A theoretical database has been compiled to examine the trends associated with changes in vehicle shape and orientation.

Finally, the results of these extensions and evaluations are presented in the form of prediction equations that can be used in Draper Laboratory's real-time simulation.

Thesis Supervisor : Michael S. Triantafyllou
Title : Professor of Ocean Engineering

Acknowledgments

The author would like to begin by thanking all of the following people for their assistance in this endeavor: Audrey Fitzgerald for bringing me to MIT and providing a basis for my thesis as well as providing many insights into the theory while supervising my work, Narender Chhabra for also supervising this project and supporting my efforts over the past year, Dr. Jerry Feldman for providing reference materials, and finally, my advisor, Professor Michael Triantafyllou for encouraging me, particularly as I learned the theory I needed to start this project.

Special thanks go to my fiancé, Greg Diggs, for all of his support, understanding, and patience throughout my studies here at MIT. Without him, I never would have had the desire to finish.

Finally, I dedicate this thesis to my parents, Howard and Muffet Chatterton. Their love and encouragement has made me who I am today. Thank you and I love you both.

Jacquie Chatterton
May 6, 1994

Acknowledgement of Copyright
5/94

This thesis was prepared at The Charles Stark Draper Laboratory, Inc., under IR&D Contract 15105.

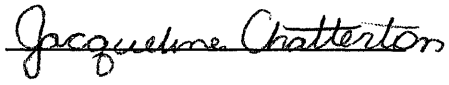

Jacqueline Chatterton

Table of Contents

List of Figures

List of Tables

Chapter 1 : Introduction

Ships experience interaction forces and moments when they come close to an obstacle. This interaction force, caused by the pressure decrease between the ship and the boundary, typically forces the ship to move closer to the obstacle. Several major disasters have occurred when navigators did not account for this force. The force has sent ships into the sides of canals, bridges, into overtaking ships, and more recently, caused the grounding of the Queen Elizabeth II. The QEII was moving at a high speed in shallow waters when the suction force between the bottom and the ship caused the QEII to run aground off Cutty Hunk Island, MA. While operating in constrained waters is an intermittent problem with large ocean-going vessels, it is a more common problem with Unmanned Undersea Vehicles (UUVs) that are required to travel close to the ocean bottom, or a host submarine. Several theoretical models have been developed to predict the interaction forces and moments that occur when the vehicle is close to an obstacle. However, these models have not been proven to relate closely to any experimental data, nor have these models been fully exercised to determine their strengths and weaknesses for various vehicle configurations.

In this thesis, three models: Slender, Baseline, and Segmented are compared. The similarities as well as differences between these methods are discussed. Chapter 2 presents the general theory and similarities, followed, in Chapter 3, by the differences and recent extensions to the codes of these models. The model testing performed for this thesis is presented in Chapter 4. These and other experimental and analytical data are used to validate these techniques in Chapter 5. Chapter 6 contains the development and discussion of a theoretical database. Finally, the conclusions and recommendations for future work can be found in Chapter 7.

Problem Definition

The purpose of this thesis is to compute the hydrodynamic force imposed by a boundary (obstacle) on an axisymmetric body moving in proximity to that boundary. The obstacle is assumed to be a wall that is generally, but not necessarily, aligned with the relative flow and parallel to the length of the axisymmetric body. The distance from the wall to the maximum diameter of the body is H. The typical problem is shown in Figure 1.

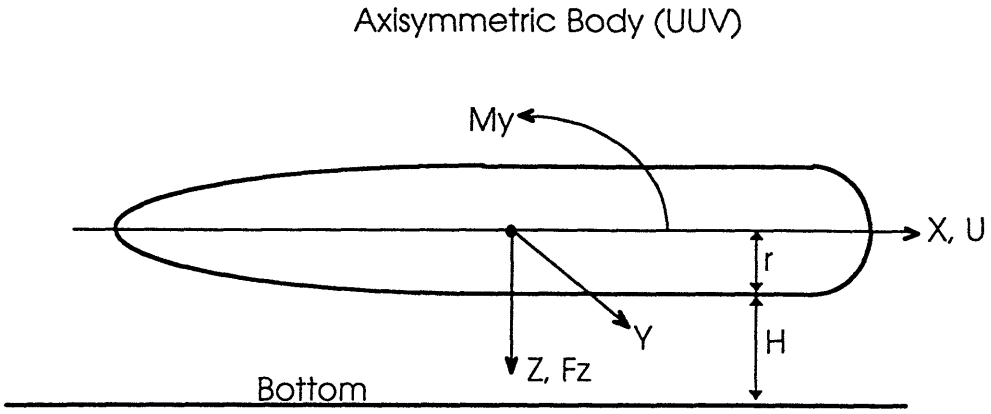

Figure 1 : Problem Definition

All three of the codes discussed in this thesis use an axial distribution of sources and dipoles to describe the body, but their methods for calculating the forces differ. Both the Baseline and the Segmented codes have been generalized to allow for other orientations of the body with respect to the wall, as shown in Figure 2.

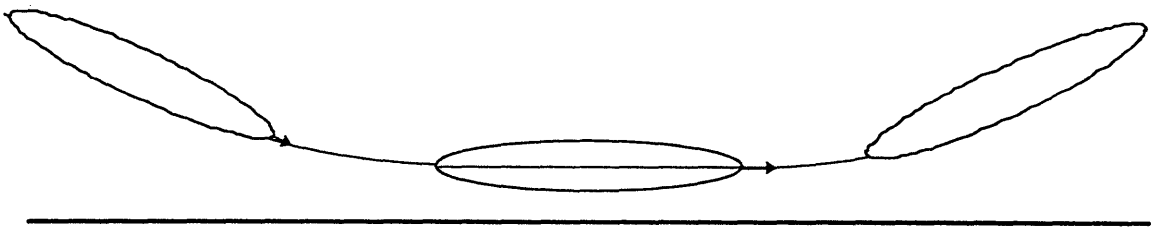

Figure 2 : UUV Orientation/ Path

In generalizing these codes, the problem was divided into three sections, the steady-state descent or ascent with the body at an incline, the unsteady turn, and the basic steady-state, constant height motion. The Baseline code now handles all three of these conditions. The Segmented code has been extended to include both the steady-state and inclined conditions. The Slender code is only applicable for the steady-state, constant height motion that it was originally written for.

Previous Work

There are several sources of previous research, primarily dealing with the interaction forces and moments developed between ships in proximity. These sources begin with model tests performed by David Taylor [21] in 1909 to determine the forces between two ships traveling next to one another. Since then, several papers have been written in an attempt to theoretically describe these forces. Those which are most relevant to this research are discussed below.

In 1965, Newman [17] published a paper on "The Force and Moment on a Slender Body of Revolution Moving Near a Wall." This paper and its results have been used extensively in evaluating the results of other methods. Newman calculated the force and moment on a body using the following assumptions:

1. The fluid is ideal and incompressible.
2. The fluid is unbounded except by the wall and the body.
3. The body is axisymmetric and slender ($r/L << 1$), and
4. The body is in proximity to the wall ($z/L << 1$).

In these assumptions, r is the radius of the body, L is the body length, and z is the distance from the body's centerline to the obstacle.

Aerodynamics theory is used and the source distribution is calculated inside the body. To allow for the presence of the wall, the source distribution is offset from the body axis. The body is considered to be fixed in space, with a free stream flowing past it in the -x direction. Lagally's

theorem [5] is then used to find the force and the moment. Newman's theory will be discussed in further detail in Chapter 3, since it is the basis for the Slender code used in this thesis.

In 1974, Fortson [7] published one of the first MIT theses in this area, "Interaction Forces Between Ships." Fortson modeled ship interactions using bodies of revolution moving in an infinite ideal fluid. He used axial distributions of sources and dipoles to represent the body and its image. He then used Lagally's theorem to calculate the forces and moments given this singularity distribution. Fortson compared his results to model tests done by Taylor [21] in 1909, and Newton [18], published in 1960. He also discussed Havelock's analytical models [8] using an ellipse and a rankine ovoid.

In 1975, Ashe [4] continued Fortson's efforts and expanded upon the previous work. In his thesis, "Trajectory Predictions for Ships Engaged in Close Proximity Operations," Ashe very clearly states his assumptions:

1. Interaction forces arise only from the potential disturbance and therefore, a rigid free surface can exist.
2. The fluid is ideal and therefore, potential theory is applicable.
3. The fluid is infinite.

Like Fortson, Ashe uses an axial distribution of dipoles to account for the wall effects. As with the previous methods, Ashe also uses Lagally's theorem to calculate the forces and moments on the body, but he includes the unsteady terms. The steady-state force is due entirely to interaction effects as shown by D'Alembert's paradox. Ashe extends the theory presented by Fortson and includes the unsteady effects associated with acceleration, vertical velocities, and rotational velocities in a quasi-steady manner. Since the forces and moments of interest are those due to the interaction, the steady state moment and unsteady values may be simplified. Ashe neglects any effects due to motions other than pitch, heave, or surge. Ashe's theoretical derivation of the

unsteady forces and moments has been used as a basis for extending the Baseline code in this thesis.

In 1985, Arcano [3] examined the forces and moments on a submarine near a sinusoidal wall. Using the previous works described above, Arcano begins with the axial distribution of sources and dipoles and a flat wall. He uses two methods in calculating the force: Lagally's theorem and "Segmented" theory. The Lagally's method is the same theory that was used in previous works. The Segmented theory divides the body into vertical segments and calculates the force using either two-dimensional or three-dimensional flow analysis, depending on the body shape. For the segmented theory, most of the body is assumed to be locally two-dimensional. However, at the nose, the flow cannot be modeled by strip theory, and therefore, the bow is treated as a hemi-ellipsoid. Arcano also examined the effects of a body traveling in proximity to a sinusoidal wall. While the sinusoidal wall effects have not been incorporated into the current codes, Arcano's segmented theory is the basis for the Segmented code.

In 1993, Fitzgerald [6] again extended the previous works. In her thesis, "A Potential Flow Model of an Unmanned Undersea Vehicle Operating Near the Ocean Bottom," Fitzgerald converted the previously mentioned codes and theories to FORTRAN. She also extended the code to allow for a body with an elliptical cross section, added the inclined bottom effects, and implemented some aspects of unsteady flow. Currently, these codes exist as subroutines in the computer program, NB_OPS located on Draper Laboratory's VAX mainframe computer. It is these codes, developed by Fitzgerald, that are examined in this thesis.

Chapter 2 : Theory

The hydrodynamic force examined in this thesis is caused by the spatial distribution of pressure on the surface of the body. The pressure difference between the top and the bottom of an axisymmetric body is caused by the contraction and acceleration of the flow between the body and the bottom. From Bernoulli's Equation, the increase in velocity can be related to a decrease in pressure.

$$P_u - P_l = 0.5\rho\left(V_l^2 - V_u^2\right),$$

where:

P = *pressure*,

V = *velocity*,

ρ = *fluid density*,

u = *upper or, above the body, and*

l = *lower or, below the body*

This pressure difference generates a suction force. Therefore, the velocity needs to be known along the surface of the body to determine the hydrodynamic forces. The problem can be solved by applying the Navier-Stokes equations, using the proper boundary equations and the proper assumptions. Navier-Stokes equation solvers are being used today for low Reynolds numbers; however, these codes often require super-computers and are computationally very expensive. For simplicity, the flow is assumed to be inviscid, steady, and irrotational; in essence, the flow is modeled as potential flow. Each of the three codes discussed in this thesis uses the potential flow assumption.

Two families of techniques are typically used to solve this problem, panel codes and line singularities. Line singularities were chosen for these codes for their simplicity and speed. Rather than distributing the singularities axially along the body, panel codes divide the surface of the body into a series of panels on the body. The singularities are then distributed on these panels.

Although they were not a subject of this thesis, basic research into panel codes has been completed and a brief description may be found in Appendix 1.

Boundary Conditions

The boundary conditions which are imposed in either theoretical method are such that Laplace's Equation, $\nabla^2\phi = 0$, is met throughout the flow. This assures the conservation of mass for a potential function. The applicable conditions are that there is no flow normal to the body surface or to the obstacle. The method of images is used to meet the requirement of no flow normal to the obstacle. The real body is matched with an identical image placed at a distance of 2 H away from the real body. In this way, the plane created between the two bodies models the effects of an obstacle at a distance H from the real body. The condition of having no flow normal to the body surface is accomplished by modeling the body with the correct combination of sources, sinks, and dipoles.

The final boundary condition is that, far away from the body, the effects of the singularities used to describe the body become negligible. In other words, the free stream is the only flow characteristic that effects the flow far away from the body. Figure 3 shows the relevant boundary conditions for this problem.

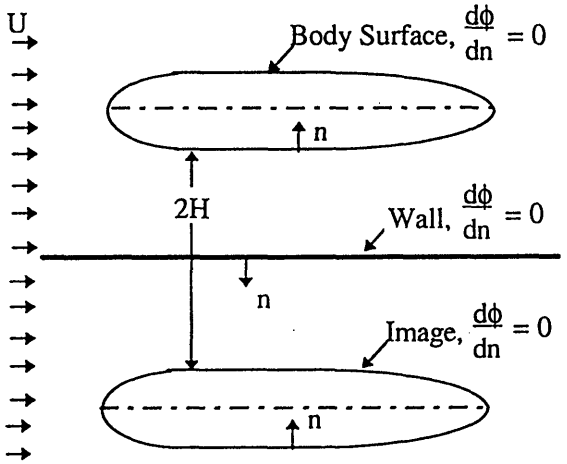

Figure 3 : Boundary Conditions for a Body Near a Wall

Inviscid vs. Viscous Fluid Effects

The theoretical methods presented here all assume that the fluid is inviscid. Therefore, one of the important issues to examine is whether this is a valid assumption. As long as the displacement thickness of the boundary layer is small in comparison to the separation distance, the fluid can be considered to be ideal. Using Newman's definition [12], the displacement thickness represents the "effective amount by which the body is 'thickened' because of the boundary layer." The following equations, derived in Sabersky, Acosta, and Hauptmann (S.A.H.), [19], define the displacement thickness:

$$\delta^* = 0.0467x\left(\frac{\nu}{U}\right)^{1/5}\left(\frac{x}{a}\right)^{1/5} \text{ for laminar flow}$$

and

$$\delta^* = 0.058\left(\frac{\nu}{U}\right)^{1/5}\left(\frac{x}{a}\right)^{4/5} \text{ for turbulent flow}$$

where:

x = *the dimension along which the boundary layer changes*

ν = *fluid viscosity*, ft^2/sec

U = *body velocity*, ft/sec

$$a \equiv \int_0^1 \left(1-\frac{u}{U}\right)\frac{u}{U}d\left(\frac{y}{\delta}\right)$$

From these equations, it is evident that the displacement thickness is dependent upon the Reynolds' number (defined below, the Reynolds' number is a good indication of laminar vs. turbulent flow). For the typical UUV (in this case, Draper Laboratory's UUV), the Reynolds' number, based on length, is found to be in the turbulent region as shown in the calculations below:

$$\mathrm{Re} = \frac{U^* L}{\nu} = 1.21 \times 10^7$$

where:

$U = 2kts \cong 3.4\, ft/s$,

$L = 35.9\, ft$, *and*

$\nu \cong 1 \times 10^{-5}\, ft^2/s$

Since the Reynolds' number in this case is shown to be well above the $R_{transition}$ range of $3x10^5$, the flow is considered to be turbulent for the case of the UUV. Therefore, the displacement thickness, δ^*, can be solved for the value below:

$$\delta^* = 0.058\left(\frac{\nu}{U}\right)^{1/5}\left(\frac{x}{a}\right)^{4/5} = 0.515\, ft$$

where:

$$a = \int_0^1 \left(1 - \frac{u_x}{U}\right)\frac{u_x}{U}\, d\left(\frac{y}{\delta}\right)$$

now taking $\frac{u_x}{U} = \left(\frac{y}{\delta}\right)^{1/7}$ *and* $\eta = \frac{y}{\delta}$,

(*from S.A.H.* [19], *pp.* 295)

$$a = \int_0^1 \left(1 - \eta^{1/7}\right)\eta^{1/7}\, d\eta = 0.0972$$

This means that, at the trailing edge of the UUV, the boundary layer thickness will have grown to be 14% of the maximum diameter. While this is significant, the separation distance is expected to be over 50% of the diameter at the extreme.

If there is a naturally occurring current between the UUV and the obstacle, viscosity effects become even more difficult to evaluate. For example, the wind across the ocean establishes a boundary layer profile that is at least as thick as the height of a sailboat main sail. The same

calculation shown above may be completed for a 1.47 ft/s current that has traveled over the ocean bottom for one day:

$$\delta^* = 0.058\left(\frac{\nu}{U}\right)^{1/5}\left(\frac{x}{a}\right)^{4/5} = 417\,ft\;!!$$

where:

$$\nu \cong 1\times10^{-5}\ ft^2/s,$$

$$U \cong 1.5\ ft/s,$$

$$x = 5280\ ft/hr = 126720\,ft,\ and$$

$$a = \int_0^1 \left(1-\frac{u_x}{U}\right)\frac{u_x}{U}\,d\left(\frac{y}{\delta}\right) = 0.0972$$

From the calculation, it is obvious that the vehicle would be traveling in the region of the boundary layer. The effects of this boundary layer will influence the interaction forces and moments on the UUV but it is not clear to what extent the forces and moments will change. If the boundary layer cannot be ignored, the inviscid flow assumption is violated. This may also be the case in situations with local currents.

If the boundary layer does influence the flow in the vicinity of the vehicle, the predicted interaction force may be more than the actual force. The UUV's bottom surface is closest to the obstacle and governs the suction force. The UUV's bottom is also located in the slower part of the current and therefore it sees a smaller inflow velocity, resulting in a smaller force. However, this analysis is speculative and can only be confirmed with a three-dimensional Navier-Stokes code.

Basic Theory

The line-source codes define the shape of an axisymmetric vehicle using a single line of sources and sinks, as shown in Figure 4.

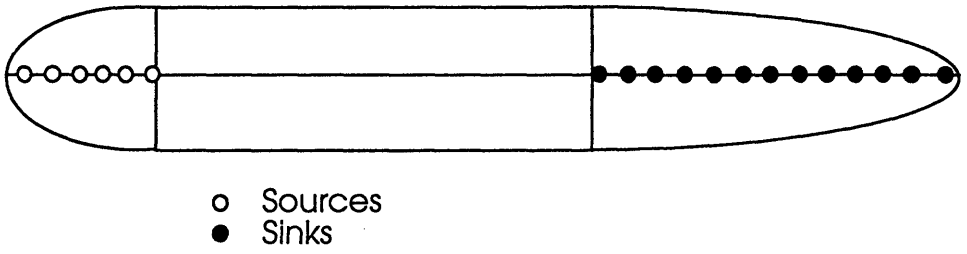

Figure 4 : Line-Source Geometry

The body is modeled using the traditional submarine configuration as described by Jackson [11]. Since the body is an axisymmetric body of revolution, it can be described by its radius as a function of its axial position, as shown in the following equations:

$$r(x_{fb}) = r_{\max}\left[1-\left(\frac{x_{fb}}{L_{fb}}\right)^{n_{fb}}\right]^{1/n_{fb}}$$

$$r(x_{pmb}) = r_{\max}$$

$$r(x_{ab}) = r_{\max}\left[1-\left(\frac{x_{ab}}{L_{ab}}\right)^{n_{ab}}\right]$$

where:

$r_{\max}$ = *maximum body radius, ft*

L = *body length, ft*

n = *fullness factor*

fb = forebody

pmb = parallel midbody

ab = afterbody

The factors n_{fb} and n_{ab} define the fullness of the forebody and afterbody, respectively. These factors are generally between two and three. The radii, slopes, and forward velocity (U) are then used to calculate the source strengths as shown:

$$m(x) = \frac{-U * r(x) * slope(x)}{2}$$

However, when the body is brought into proximity with its image, the flow field becomes distorted and is no longer uniform. One of the major differences between the Slender theory and the Baseline and Segmented theories occurs in correcting for this induced cross-flow. The Slender body theory corrects for the cross-flow by adjusting the placement of the singularities closer to the wall, while the other theories use an axial distribution of dipoles. Since both the Baseline and Segmented theories use the same method of correcting for the induced cross-flow, that method will be discussed below. The theory for the Slender body code will be discussed in the Comparison of Codes section in Chapter 3.

The process of adding the dipoles to the body definition is iterative since they will induce both axial and radial velocities that must be accounted for by reducing the source strengths and changing the dipole strengths. Five iterations are used to ensure convergence; this was shown to be acceptable by both Fortson [7] and Fitzgerald [6]. Several simplifying assumptions are used in sizing these dipoles. These assumptions are as follows:

1. The cross-flow velocity is uniform over a small axial distance.
2. The axial distance between dipoles is modeled as a cylindrical section.
3. At a particular cross-section, the body is translating laterally with a velocity equal in magnitude and opposite in direction to the perturbed cross-flow component.

The second assumption is based on the hypothesis that the change in radius is small for a small change in axial distance. The dipoles are sized using the following formula:

$$\mu(x) = \frac{q_n(x)}{4}\left(1 + \frac{A_{22}}{\rho\forall}\right) r^2(x)$$

where:

$\mu(x)$ = *dipole distribution strength,*

$q_n(x)$ = *cross flow velocity component induced normal to the body on the surface*

A_{22} = *lateral "added mass" of the body*

$\forall$ = *volume of the body*

The added mass for a cylinder is equal to the displaced volume, $\rho\forall$, simplifying the dipole strength to:

$$\mu(x) = \frac{q_n(x)}{2} r^2(x).$$

Finally, the induced cross flow velocity must be calculated. For the initial iteration, only the sources are estimated based on the axial free stream velocity. The image sources then induce a cross flow on the real body. The dipoles are sized to cancel the cross flow as shown in the above equation. However, the image dipoles will then induce both axial and radial cross flows on the real body. Therefore, the sources and dipoles are resized in an iterative procedure. In this procedure, the following potential equation, integrated over the body length, is used to derive the induced velocities:

$$\phi = \int_0^L \left[\frac{m(\xi)}{\left((x-\xi)^2 + z^2\right)^{1/2}} + \frac{\mu(\xi)(-z)}{\left((x-\xi)^2 + z^2\right)^{3/2}} \right] d\xi$$

where:

ξ = *dummy variable for axial position*

Since $\vec{q} = -\nabla\phi$, this equation can be differentiated to find the induced velocity components due to the image, show below.

$$\frac{-\partial\phi}{\partial x} = q_x = \int_0^l \frac{m(\xi)(x-\xi)}{\left[(x-\xi)^2 + z^2\right]^{3/2}} + \frac{3(x-\xi)\mu(\xi)(-z)}{\left[(x-\xi)^2 + z^2\right]^{5/2}}, \text{ and}$$

$$\frac{-\partial\phi}{\partial z} = q_z = \int_0^l \frac{m(\xi)(-z) - \mu(\xi)}{\left[(x-\xi)^2 + z^2\right]^{3/2}} + \frac{3z^2\mu(\xi)}{\left[(x-\xi)^2 + z^2\right]^{5/2}}$$

Force and Moment Calculations

Once the potential function for a rigid body moving in an ideal fluid without viscosity is determined, the interaction forces can be calculated. The pressure distribution over the body can be obtained using Bernoulli's equation. The integration of this pressure distribution over the body, will then produce the forces and moments acting on the body.

Lagally [5] was the first to comprehensively investigate both the force and moment acting on a body generated by sources. He found that the force and moment were simple functions of the singularity strengths and the free stream in the proximity of the singularities. The force and moment acting on a singularity are therefore, functions of the singularity and the velocity induced at its location by all singularities external to the body. From this analysis, the steady-state Lagally forces and moments are found to be:

$$\vec{F} = -4\pi\rho\left[m\vec{q} + \left(\vec{\mu}\cdot\vec{\nabla}\right)\vec{q}\right]$$

$$\vec{M} = \vec{r}_g \times \vec{F} + 4\pi\rho\left(\vec{q}\times\vec{\mu}\right)$$

These equations can be further simplified by considering that the location of the sources and moments can be described by the vector $\vec{r} = \xi\ \hat{i} + 0\hat{j} + 0\hat{k}$, where ξ is again the dummy variable representing axial position. Decomposing the force and moment into orthogonal components:

$$F_x(\xi) = -4\pi\rho\left[m(\xi)q_x(\xi) + \left(\mu_y(\xi)\frac{\partial}{\partial y} \right) q_x(\xi) \right]$$

$$F_y(\xi) = -4\pi\rho\left[m(\xi)q_y(\xi) + \left(\mu_y(\xi)\frac{\partial}{\partial y} \right) q_y(\xi) \right]$$

$$F_z(\xi) = -4\pi\rho\left[m(\xi)q_z(\xi) + \left(\mu_y(\xi)\frac{\partial}{\partial y} \right) q_z(\xi) \right]$$

$$M_x(\xi) = -4\pi\rho\left[\mu_y(\xi)q_z(\xi) \right]$$

$$M_y(\xi) = -\xi F_z(\xi)$$

$$M_z(\xi) = \xi F_y(\xi) + 4\pi\rho\mu_y(\xi)q_x(\xi)$$

These forces and moments are then integrated over the length of the body to give the total force and moment.

The Lagally force and moment presented above are limited to steady flow applications. However, these results were expanded to include unsteady flow in 1953 by Cummins [5]. These unsteady effects are described in detail in Chapter 3, Line-Source Codes and Extensions.

Chapter 3 : Line-Source Codes & Extensions

Comparison of Codes

All three of the codes examined in this thesis use Lagally's theorem to determine the interaction forces and moments on a body of revolution moving in an ideal fluid. However, the methods used in determining the velocity potential differ. The Slender code uses the slender body theory developed by Newman. The Baseline code uses the method described in Basic Theory, above. The Segmented code also uses this theory with deviations in the forebody to account for the shape of the nose. Since the Slender and Segmented theories deviate from the Baseline theory described above, the differences between these codes will be discussed in this section.

Slender

The Slender code has been developed directly from the paper by Newman [13], "The Force and Moment on a Slender Body of Revolution Moving Near a Wall." Two of Newman's assumptions are crucial for determining the limits on this code. These assumptions are :

1. that the body is axisymmetric and slender ($r/L << 1$), and
2. the body is in proximity to the wall ($z/L << 1$).

These assumptions allow for the use of the slender-body approach of aerodynamics in determining the source distribution inside the body as well as the corresponding image source distribution below the wall. The source distribution on the body is unchanged by the presence of the wall, but is offset from the body axis as shown in Figure 5.

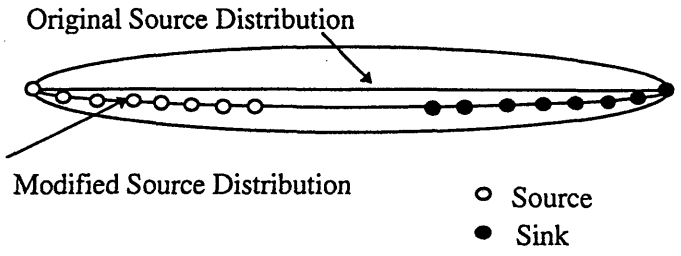

Figure 5 : Newman's Modified Source Distribution

Given a source distribution, Lagally's theorem can then be used to find the force and the moment.

Newman develops the following equations in his work:

$$m(x) = \frac{1}{4\pi} U\, S'(x) = \frac{1}{4\pi} U\, \frac{\partial(\pi\, r^2(x))}{\partial x} = \frac{U}{2} r(x) \frac{\partial r(x)}{dx}$$

where:

$m(x) = source\ strength$

$U = body\ velocity, {}^{ft}/_{s}$

$S(x) = cross - sectional\ area, \pi\, r^2(x), ft^2$

$S'(x) = {}^{dS(x)}/_{dx}$

$r(x) = body\ radius, ft$

and,

$$F_z = -\pi\rho U^2 \int_{-L/2}^{L/2} [r(x)r'(x)]^2 \left\{z^2 - r^2(x)\right\}^{-0.5} dx$$

$$M_y = \pi\rho U^2 \int_{-L/2}^{L/2} [r(x)r'(x)]^2 \left\{z^2 - r^2(x)\right\}^{-0.5} x\, dx$$

where:

$r'(x) = body\ slope, {}^{dr(x)}/_{dx}$, *and*

$z = height\ off\ bottom\ from\ the\ body's\ centerline, ft.$

Other terms are as defined above.

Segmented

The Segmented code was developed to improve upon the Baseline code's assumption that the fluid flow around the entire body is two-dimensional. Segmented theory, first suggested by Abkowitz, divides the body into two sections, the blunt forebody, and the more slender parallel midbody (pmb) and afterbody. Three-dimensional analysis is then used for the forebody, while two-dimensional analysis is used for the remainder of the submarine.

The forebody is considered to be approximately the shape of a hemi-ellipsoid. Lamb [10], in Article 15, gives the equations for computing the added mass of a prolate ellipsoid as a function of the diameters. However, the added mass of a hemi-ellipsoid is not simply half the added mass of a sphere. The actual added mass lies somewhere between the added mass of a cylinder and that of a spheroid. Therefore, the average of these two added masses is taken to approximate the added mass of a hemi-ellipsoid. This approximation is necessary, since there is no easy way to determine the added mass of an arbitrary hemi-ellipsoid, without experimentation. Fortunately, the approximation appears valid for a wide range of submarine noses.

The segmented theory is similar to the baseline code in the calculation of sources and dipoles. The method is identical, except the added mass of a hemi-ellipsoid is used in sizing of dipoles near the nose of the body. Because the added mass of a hemi-ellipsoid is larger than the added mass of a cylinder, the dipoles near the nose are stronger for the segmented theory than for the baseline method. From this, the forces and moments of the nose, and therefore for the full submarine, are expected to be larger for the Segmented calculations than for the Baseline calculations. This trend is shown in the results section.

Unsteady Motion

The unsteady effects are necessary if the simulation is to model the submarine as it approaches the bottom and "straightens out" (see Figure 6). In such a complicated landing pattern, the inflow to the body has velocity components in the U (axial), V (vertical), and ω (rotational) directions that vary with time. In addition, the orientation of the bottom to the submarine is changing with time.

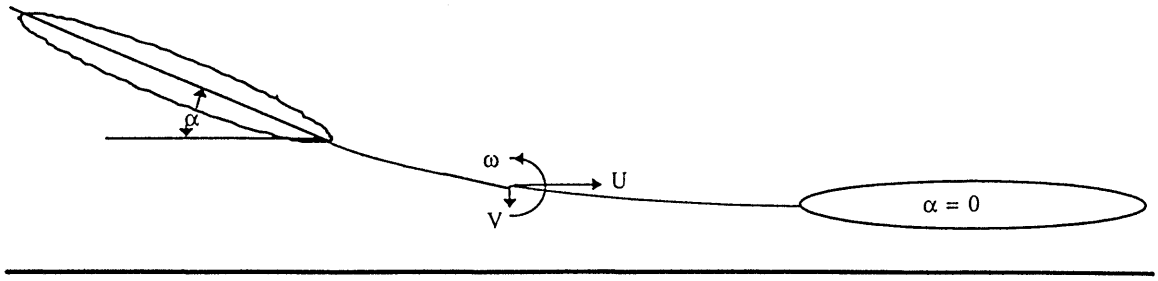

Figure 6 : Unsteady Motion

The additional vertical and rotational motions of the body must be considered when sizing the sources and dipoles to model the body. Therefore, two additional dipole distributions are used:

$$\mu_v(\xi) = \frac{V}{4}\left(1 + \frac{A_{22}}{\rho\forall}\right) r^2(\xi)$$

and

$$\mu_\omega(\xi) = \omega\xi\left(1 + \frac{A_{22}}{\rho\forall}\right) r^2(\xi)$$

where:

V = *lateral velocity*

ω = *angular velocity*

Other variables are as described in Chapter 2 : Basic Theory. When considering unsteady motions, the cross-flow induced by these additional singularities must be accounted for when

resizing the singularity distributions. Once these additions are incorporated into the modeling of the body, the forces and moments, including the unsteady motions, can be calculated.

The expressions for the force on a body due to a singularity distribution were first developed by Lagally in 1922. In 1953, Cummins [5] expanded these expressions to include unsteady motion. The force and moment on the body as described by Cummins are:

$$\vec{F} = 4\pi\left[\rho\forall\frac{d\vec{u}_0}{dt} + \vec{F}_1 + \vec{F}_2 + \vec{F}_3\right], \text{ and}$$

$$\vec{M} = 4\pi\left[\rho\forall\left(\vec{r}_g \times \frac{d\vec{u}_0}{dt}\right) + \vec{M}_1 + \vec{M}_2 + \vec{M}_3\right]$$

where :

- $\vec{u}_0$ is the translational velocity,
- $\vec{F}_1$ is the "steady-state" Lagally force,
- $\vec{F}_2$ is the "unsteady" force,
- $\vec{F}_3$ is the body rotation force,
- $\vec{r}_g$ is the distance to the centroid of the body,
- $\vec{M}_1$ is the "steady-state" Lagally moment,
- $\vec{M}_2$ is the unsteady moment, and
- $\vec{M}_3$ is the rotational moment.

$\vec{F}_3$ and $\vec{M}_3$ exist when the origin is not at the body centroid, and are shown by Cummins to be zero for both sources and doublets. The forces and moments for a source of strength m and a dipole of strength μ are as follows:

$$\vec{F}_1 = -\rho\left[m\vec{q} + (\vec{\mu}\cdot\nabla)\vec{q}\right],$$

$$\vec{F}_2 = -\rho\frac{d}{dt}\left[\vec{r}m + \vec{\mu}\right],$$

$$\vec{M}_1 = \left(\vec{r}\times\vec{F}_1\right) + \rho(\vec{q}\times\vec{\mu}), \text{ and}$$

$$\vec{M}_{23} = \frac{d}{dt}\left(\omega_j A_{3+j,\beta}\right) - \frac{d}{dt}\rho\Sigma\left[m_\beta\left(\phi_o + u_j x_j\right) - m_o\phi_\beta - \mu_{\beta j}\left(q_{oj} - u_j\right) - \mu_{oj}q_{\beta j}\right]$$

where:

$\vec{q}$ = *induced velocity at a given singularity due to all other singularities,*

$\omega_j = j -$ *component of angular velocity,*

$A_{3+j,\beta}$ = "*added mass*" *coefficient,*

$\beta = i+3,$ *where* $i = 3$ *for yaw moment,*

ϕ = *unit potentials,*

$u_j = j -$ *component of translational velocity, and*

all other terms are as defined previously.

The last term, $\vec{M}_{23}$, was derived by Landweber and Yih [11]. As mentioned in the definition for β, the component of interest in this problem is i=3, the yaw moment. Therefore, the moment, $\vec{M}_{23}$, has already been simplified slightly to examine only this component. The theory developed first by Lagally, then extended by Cummins, and later Landweber and Yih, is best summarized by Zucker [22], in his paper on "Lagally's Theorem and the Lifting Body Problem."

The unsteady motion described above has been added to the Baseline method for this thesis, using the theory first implemented by Ashe [4]. Since the forces and moments desired are those caused solely by the interaction of the body and wall, the previously stated equations can be simplified. In examining the forces, D'Alembert's paradox may be used to show that the steady-state force, in its entirety, must arise from the interaction. Therefore,

$$F_{x_{ss}} = -4\pi\rho\left[m \cdot q_x + \mu_z \frac{dq_x}{dz}\right]$$

and

$$F_{z_{ss}} = -4\pi\rho\left[m \cdot q_z + \mu_z \frac{dq_z}{dz}\right]$$

These equations are equivalent to those presented for the forces in the Basic Theory of Chapter 2. It is important to note that the term μ_z represents the summation of all three dipole distributions, μ, μ_v, and μ_ω. The evaluation of the transient force terms is not as simple since these forces may be due to the body alone rather than the interaction affects. In this case, only the sources and dipoles due to the presence of the image body are accounted for as shown below.

$$F_{x\ tr\ int} = -4\pi\rho \cdot \xi \cdot \frac{d}{dt} m_\eta(\xi)$$

and

$$F_{z\ tr\ int} = -4\pi\rho \cdot \frac{d}{dt} \mu_\eta(\xi)$$

where:

m_η = *source due to the presence of the image body*

μ_η = *dipole due to the presence of the image body*

As with the transient forces, the moment (both steady-state and transient portions) can exist without the presence of the image. Upon elimination of the terms not caused by the interaction of the body and its image, the steady-state portion of the moment becomes:

$$M_{y\ ss} = \xi \cdot F_{y\ ss} + 4\pi\rho\left[q_{xp} \cdot (\mu_\omega + \mu_v) + q_x \cdot \mu\right]$$

where:

q_{xp} = *axial velocity arising from the presence of the image*

q_x = *total axial velocity*

Finally, the transient portion of the moment may be found from the moment term defined by Landweber and Yih. In simplifying the expression for M_{23}, the term ϕ_6' can be described by a dipole of strength equal to that of μ_ω, oriented in the y direction. Therefore, the following simplifications can be made:

$m_6 = 0$
$\phi_6' = 0$
$\mu_{6j}\ (j \neq 2) = 0$
$\mu_{62} = \omega \xi R^2(\xi)\ (1+A_{22}/\rho\forall) = \mu_\omega$
$q_{62} = 0$
q_{02} = induced velocity in the z direction
u_2 = translational velocity in the z direction

The transient segment of the moment can be defined as:

$$M_{23\ tr} = \frac{d}{dt}(\omega_3 B_{66}) + 4\pi\rho \sum\left[\mu_{62}\frac{d}{dt}q_{02} + q_{02}\frac{d}{dt}\mu_{62} - u_2\frac{d}{dt}\mu_{62} - \mu_{62}\frac{d}{dt}u_2\right]$$

However, the first term as well as the terms μ_{62} and u_2 are not related to the interaction between the body and its image. The transient portion of the moment is then reduced to the following final equation:

$$M_{23\ tr} = 4\pi\rho \sum\left[\mu_{62}\frac{d}{dt}q_{02} + q_{02}\frac{d}{dt}\mu_{62}\right]$$

The expressions obtained for the total forces and moments, including the unsteady effects, are then integrated to find the total forces and moments on the body.

$$F_x = \int_{-L/2}^{L/2}\left[F_{x\,ss}(\xi) + F_{x\,tr}(\xi)\right]d\xi$$

$$F_z = \int_{-L/2}^{L/2}\left[F_{z\,ss}(\xi) + F_{z\,tr}(\xi)\right]d\xi$$

$$M_y = \int_{-L/2}^{L/2}\left[M_{y\,ss}(\xi) + M_{y\,tr}(\xi)\right]d\xi$$

Inclined Body

Both the Baseline and Segmented codes were extended to simulate a UUV traveling at some constant angle to the bottom as shown in Figure 7.

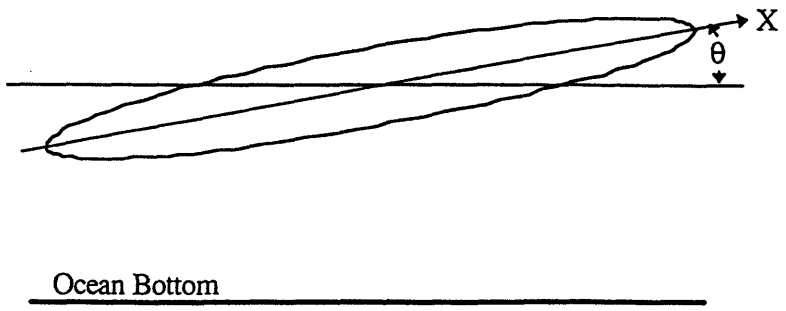

Figure 7 : Vehicle Traveling at an Incline to the Bottom

This extension was first introduced and implemented by Fitzgerald [6]. It has since been added to the Segmented theory and tested. The angle θ indicates the pitch of the vehicle and is positive for an upward pitch. The primary equation in implementing this theory is as follows :

$$z(x) = z(x_{mid}) - 2[x - x_{mid}]\sin\theta$$

where:

$$z(x_{mid}) = 2[H + R(x_{mid})\cos\theta]$$

The separation distance, z(x), is then used in finding the induced velocities on the singularity axes and the body surface.

Convergence

All of the computer models need a certain number of points to accurately describe the body geometry. When the correct number of points is chosen, the addition of more points will not significantly change the forces and moments predicted. Previously, the number of points was chosen by the user using trial and error. If a run was made with 50 points and then with 100 and the force changed by less than 5%, then 50 points were acceptable. The option of always using the

maximum number of points was unacceptable since the computation times increase by a factor of almost 5 with each doubling of the number of points. Below 300 points, the computation times are insignificant. However, for 1200 points the program will take approximately 15 minutes and for 3200 points, the program will take two hours. Given the effort involved, the possible computation time, and the consequences of not checking the required number of points for each run, a convergence criteria was developed.

The number of points for convergence were obtained from all three theories for various submarine shapes. An initial study showed that the most number of points was needed for the lowest height above the obstacle. Therefore, a height of 0.2 H', twenty percent of the diameter above the bottom, was used throughout the rest of the convergence tests. In forming the theoretical database discussed in Chapter 6, it was discovered that the number of points needed for convergence varied most with the forward fullness factor and the forebody length. These factors are important since they define the slope of the body over its steepest section, the nose. As the number of points increases, the discretization of the body becomes more accurate. The errors in discretizing the body decrease as the "steps" used to describe the body more closely represent the actual curve. This concept is shown in Figure 8. However, the computation time increases by a factor of five each time the number of points is doubled. The convergence criteria was developed to find the optimal number of points for 99% convergence with the fewest number of points.

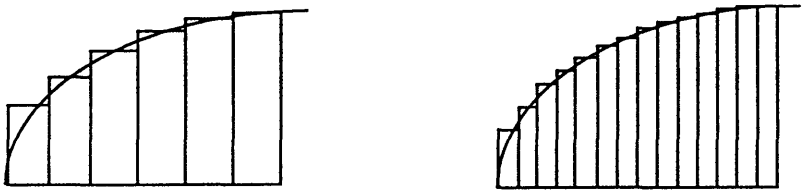

(a). Insufficient Discretization of UUV Nose

(b). Sufficient Discretization of UUV Nose

Figure 8 : Discretization of UUV Nose for Convergence

In order for the convergence criteria to hold for a wide variety of body shapes, the test matrix shown in Table 1 was used. These variables were examined in detail since they were shown to have the most influence on the number of points for convergence. All other variables were examined in the compilation of the theoretical database and had little or no affect on convergence. The height of the body off the bottom does affect convergence and might have been added to those variables examined here. However, since the codes have been developed to allow for multiple heights per run, the minimum height of 0.2 H' was chosen as a worst case scenario. The percentage length of the forebody was also used to avoid having to differentiate between geometrically similar bodies.

Table 1 : Important Convergence Factors

Variable	Range
Forward Fullness Factor, Nf	2.0 - 3.0, by 0.1
Forebody Length	5% - 30% Total Length

Once the convergence tests were completed, a factor was developed to relate the number of points to the forebody fullness and length. The factor which most accurately represented the correlation between forebody fullness, forebody length, and the number of points for convergence is:

$$Forebody\ Factor = \frac{N_f^6}{\sqrt{\%L_{fb}}}$$

Using the BASIC program, Curvefit, the equation which most accurately describes the data was found. The equation and a comparison between the actual and curve-fit data can be found in Figure 9.

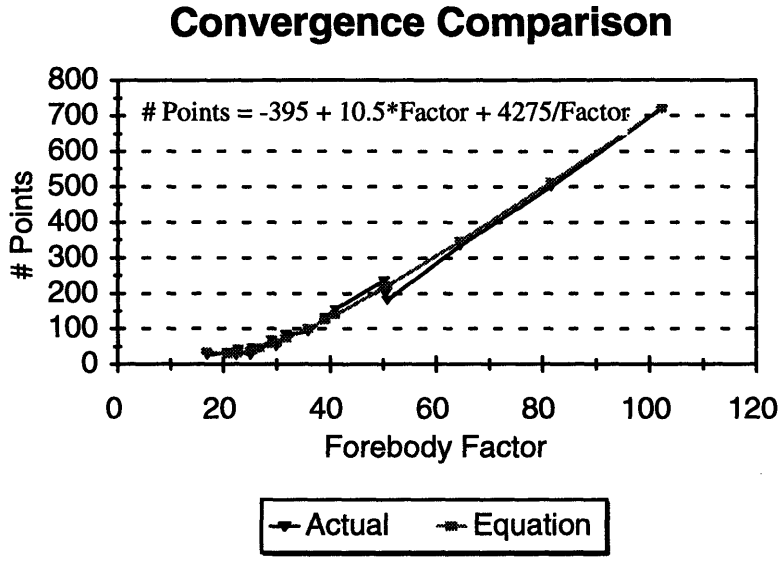

Figure 9 : Convergence Comparison

This equation has been integrated into the codes with the following guidelines to determine the correct number of points for the user.

1. The number of points calculated is always rounded up to the nearest 10 points.
2. The minimum number of points allowable is 50.

These guidelines eliminate the possibilities of having a negative number of points chosen or having an odd number of points chosen (the program requires a positive number for segmentation of the body). Since the computation time is not significant until more than 300 points are used, a minimum of 50 points is not considered to be a limitation.

The convergence criteria for the Slender and Segmented theories have been derived from those determined for the Baseline theory. The Slender code requires many more points for convergence than any of the other codes. However, there is no time penalty associated with running the Slender code at high numbers of points. Even at the maximum number of points currently allowed (6400), the Slender code produces results in a few seconds. Therefore, the number of points for the Baseline code is multiplied by 3 for the Slender code. It is important to

note that convergence has not been achieved for fullness factors above 2.6 for the Slender theory as more than 6400 points are needed for these cases. Convergence for the Segmented theory cannot be estimated quite as easily. For the Segmented theory, the force on the forebody is not computed as a sum of forces on cylindrical sections, the added mass is calculated instead. This has made the development of a convergence factor more difficult. However, the number of points needed for the Segmented code is typically close to the number needed for the Baseline theory. The exception to this rule is that the minimum number of points allowable is 100. Below 100 points, the Segmented theory had trouble converging and, once again, having this many points along the body does not significantly affect computation time.

Chapter 4 : Model Testing

Each of the previous works cited above mentions the lack of experimental data in this area. Therefore, model testing was completed at the MIT Towing Tank. The purpose of this testing was to measure the interaction forces and moments on a UUV model at various heights above the bottom of the tank in order to validate the codes.

Testing Setup

The smallest load cell available at the MIT towing tank is a six axis sensor with a full scale measurement of 100 lbs. The maximum forces in our test were expected to be on the order of 0.7 lbs, making this load cell marginally acceptable for use in this case. The most sensitive axes on this load cell are the X and Y axes. Since the primary measurement needed was the Z force, it was decided that reorienting the cell to use the X and Y axes would provide a better chance of obtaining reliable results. The only submarine model available at the MIT towing tank did not allow for this crucial reorientation of the load cell. Therefore, a new model was designed by Lt. Mark Davis and constructed by Peter Kerrebrock, both at Draper Laboratory. The new model is a typical Jackson hull type as shown by Figure 10 and the listed dimensions.

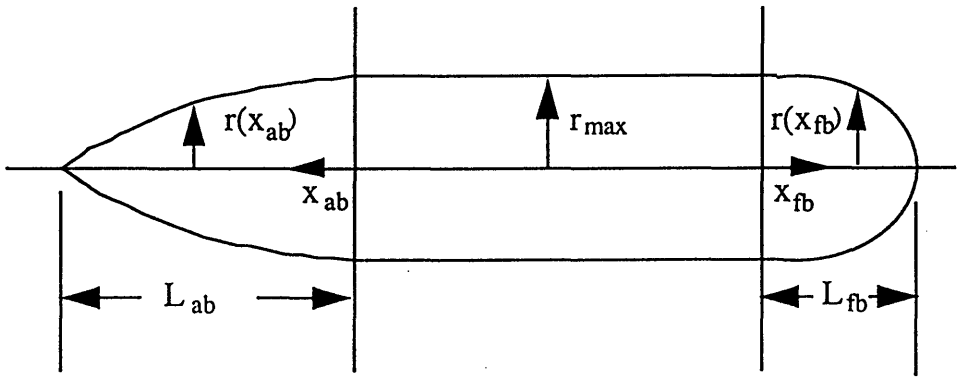

Figure 10 : Towing Tank Model

where :

Length = 32.25 in	Diameter = 5.675 in
L_{fb} = 7.0 in	N_{fb} = 3.3
L_{ab} = 14.0 in	N_{ab} = 1.75

A method also had to be developed to allow the model to be connected securely to the carriage while still allowing the distance between the model and the bottom of the tank to differ between runs. This was accomplished through the use of an adjustable strut section designed by Lt. Mark Davis (see Figure 11).

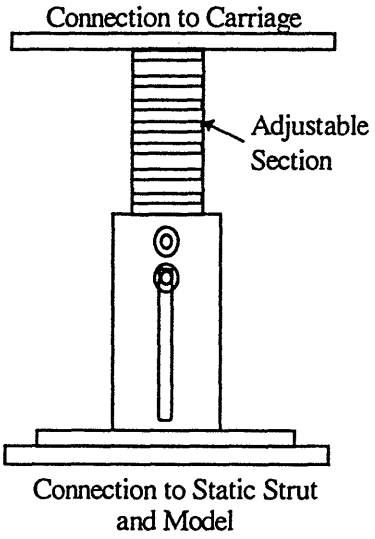

Figure 11 : Strut Configuration

Finally, the model was attached to the strut through the load cell as shown in Figure 12.

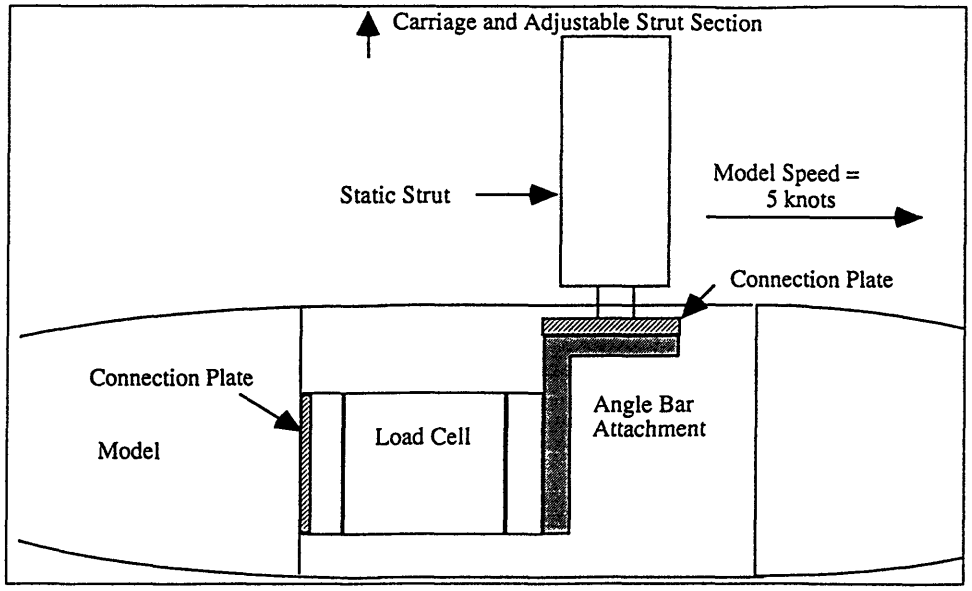

Figure 12 : Testing Setup

Calibrations

Initial calibrations showed that the dynamometer (load cell) was fluctuating for each measurement. The measurements also did not match between those taken one day and the next. Some of this may have been due to the original plate and string assembly attached to the dynamometer, shown in Figure 13.

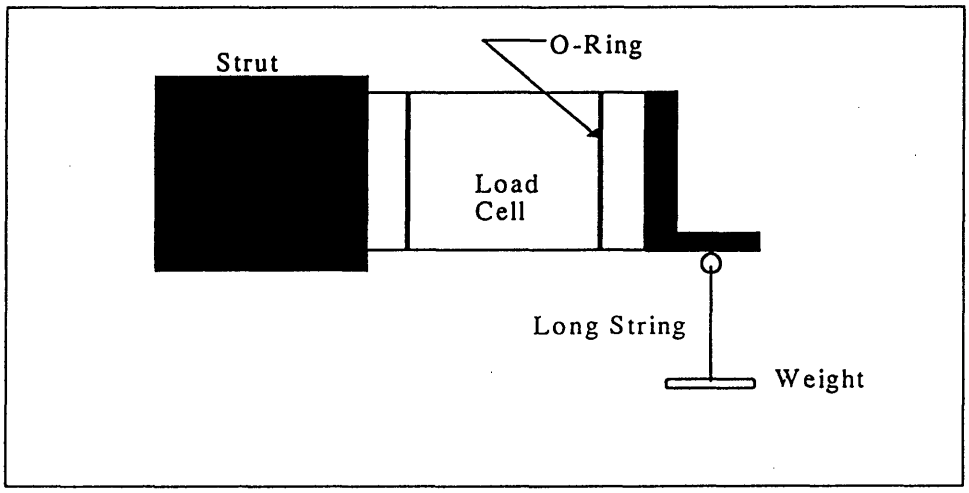

Figure 13 : Original Load Cell Orientation

The calibration setup did not adequately represent the model configuration and the string induced vibrations into the signal. Another problem encountered was in the wiring of the load cell to the electronic terminals. These terminals provided the connection between the load cell and the data collection computer. The connections between the wires and the connecting pins were very weak and the shroud (grounding wire) was not connected from the load cell through to the electronic terminal's ground. Since there were problems with the calibrations and the quality of the connections was poor, the system was rewired. The final electronics setup was as shown in Figure 14.

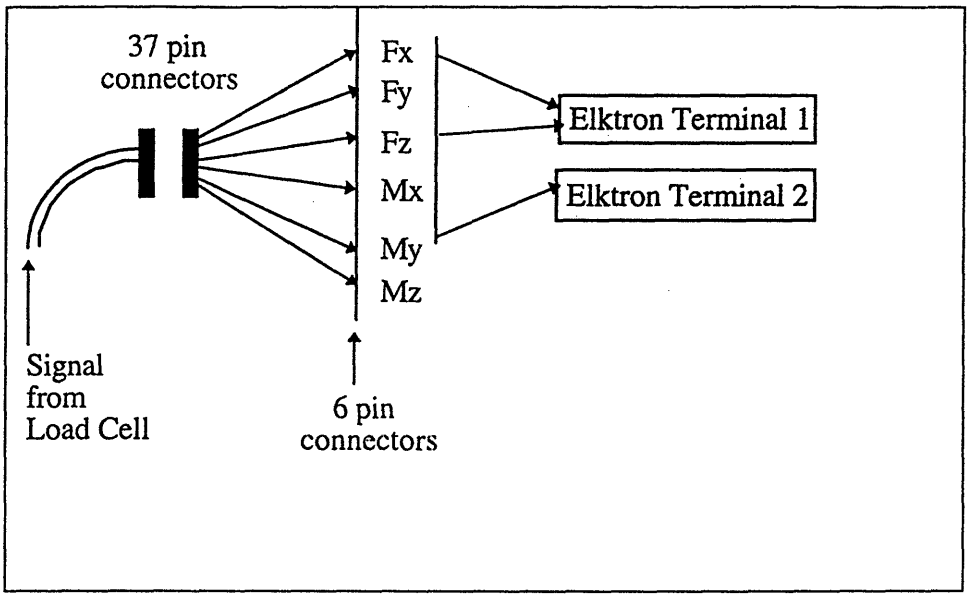

Figure 14 : Electronics Setup

The signal was sent from the load cell, through a 37 pin connector where it was split into the six measurement axes. From here, data from only three of the axes were sent on to the collection computer and recorded. During testing, only the Fy (heave), Fz (drag), and Mx (pitching) signals were recorded.

Once the wiring was redone, the voltage measurements became fairly stable. Drifting of the zero value and some hysteresis effects were noticed during calibrations. However, these fluctuations were small and did not appear to affect the results. New zeros were taken at the beginning and end of each run.

It is important to note how the load cell was setup during the final calibrations. The load cell was attached to a strut on one end while the other end was attached to an angle bar. Weights were then placed on the angle bar to do the calibrations. This setup, shown in Figure 15, was used to simulate the actual model and strut configuration.

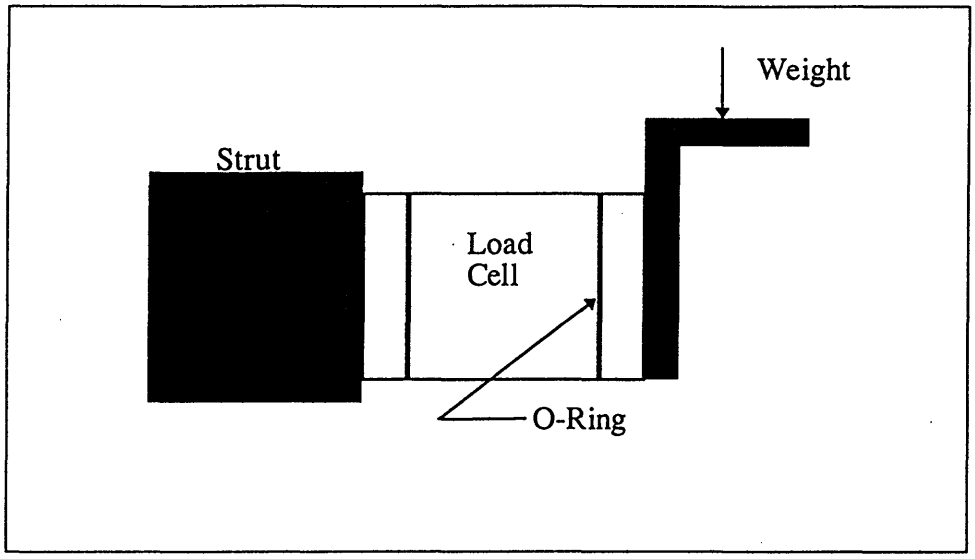

Figure 15 : Load Cell Orientation During Calibrations

Although the configuration used for the calibration measurements was intended to resemble the model configuration, the forces measured were lift forces rather than suction forces. Since the angle bar in held steady during testing, only the model moves. During calibrations, the angle moved and the "model" was held steady. By examining Figure 15, it becomes evident that a suction force measured at the connection of the load cell and model is equivalent to a lifting force measured at the load cell and angle bar connection.

The calibrations were completed by performing a regression analysis on the mean voltages obtained for each set of calibrations (heave force, pitching moment, and axial drag force). These regression equations were used to create the calibration curves in Figure 16 through Figure 18.

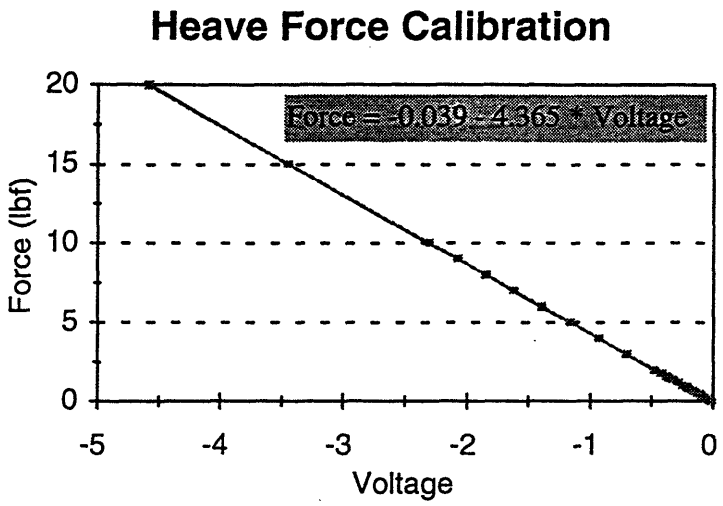

Figure 16 : Heave Force Calibration for Model Testing

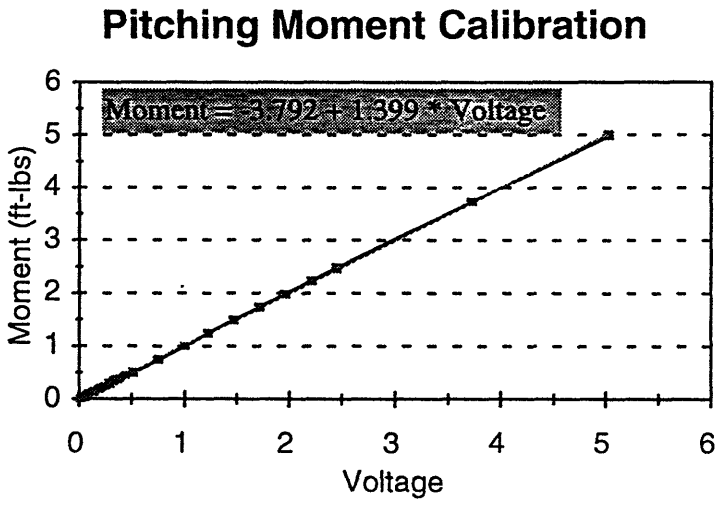

Figure 17 : Pitching Moment Calibration for Model Testing

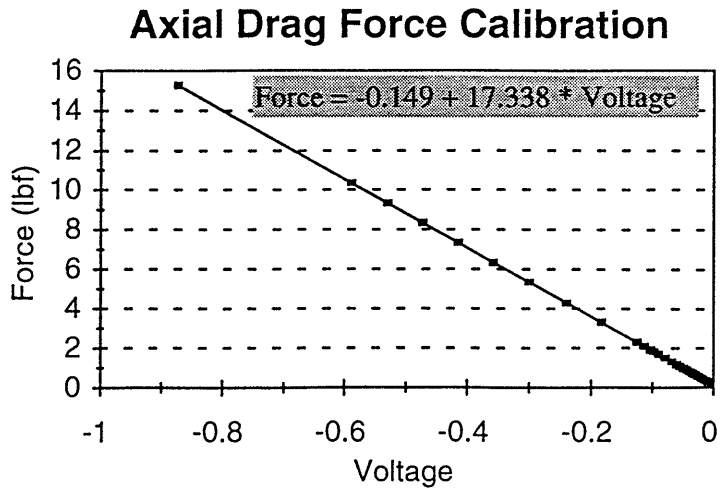

Figure 18 : Axial Drag Force Calibration for Model Testing

These curves are then used to translate voltages read from the load cell into forces and moments. Once the load cell calibrations were completed, the model was ready to be tested. The model and strut configuration was fully assembled and the electronics were connected back to the control room computer. After all of the connections were checked, testing began.

Data Collection and Analysis

Data Collection

The model was run at a constant speed of 5 knots at a series of distances from the bottom of the tank. The mean water depth of the tank was 3.9 feet and the model was run at distances between 1.25 and 13.00 inches from the bottom. These heights (H') have been non-dimensionalized by dividing them by the maximum diameter. The test matrix was as follows :

Table 2 : Test Matrix

Run #	Distance (in.)	H'
1-3	10.0	1.76
4-6	9.0	1.59
7-9	8.0	1.41
10-13	6.9	1.22
14-16	5.9	1.04
17-21	4.9	0.86
22-26	4.0	0.70
27-31	3.0	0.53
32-36	2.1	0.37
37-41	1.25	0.22
42-46	No Data Collected	--
47-51	13.0	2.29
52-56	2.25	0.40

The data were collected using MIT's Snapscope data retrieval program. The data collected generally consisted of 20 seconds of data. The model started moving at about 4 seconds and was at steady state between 6 and 14 seconds and then slowed to zero again by 16 seconds. The data were collected using an 80 Hz interval. This corresponds to 4 seconds of data or 320 points used to form an initial zero, and 5 seconds or 400 points from the steady-state portion to form an average force (or moment) for the run. An example of the raw data from run 5, with the UUV at a height of 9 inches from the bottom is shown in Figure 19. The raw data is very noisy, with 1200 points displayed in this figure.

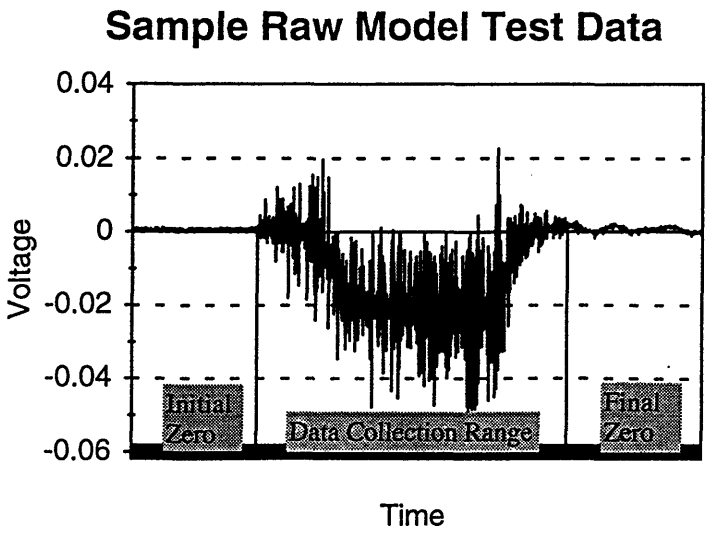

Figure 19 : Sample Raw Data from Run 5 for Model Test

Data Analysis

Various methods were considered for analyzing the test data collected during the towing tank tests. These included the standard MATLAB fast Fourier transforms and filters and the EXCEL spreadsheet fast Fourier transforms and filters. However, the simplest and first method used was to simply average the data slightly and to use the mean values.

Initial Analysis

An example of the raw test data measured was presented in Figure 19. Obviously, there is a tremendous amount of noise, and before any analysis can be completed, the data had to be cleaned up. Therefore, the voltages measured were initially averaged to obtain curves from which changes in voltage versus height from the bottom could be deduced. This method involved taking the average of 5 points on either side of the data point and placing that average at the original point. Averaging reduced some of the oscillations and noise found in the signal. Overall averages

were then taken for all of the points in the zeros range (model at rest, mean zero voltage) and all of the point in the data collection range (steady state, mean data voltage). A delta voltage was calculated by taking the difference between the mean zero voltage and the mean data voltage. However, the results of this analysis were in question once it was determined that the EXCEL program did not parse the data consistently.

MATLAB Analysis

Due to the uncertain nature of the results of the initial analysis, a second and more successful examination of the data was attempted using the MATLAB program. MATLAB was chosen for its signal processing capabilities. The procedure for analyzing the data using MATLAB is presented below.

The original data file were read into the MATLAB program for analysis. Coefficients for the filter were chosen using the Butterworth filter option on MATLAB. The Butterworth filter design used was a second order lowpass digital filter which returned the filter coefficients in terms of two vectors, A and B of length 3. The cut-off frequency Wn must be between 0 and 1.0, with 1.0 corresponding to half the sample rate. For this case, 0.02 was chosen for Wn. The filter function filters the data in vector X with the filter described by the vectors A and B. The filter is a "Direct Form II Transposed" implementation of the standard difference equation:

$$Y(n) = b(1) * x(n) + ... + b(nb+1) * x(n-nb) - a(2) * y(n-1) - ... - a(na+1) * y(n-na)$$

The order of the filter (N = 2) and the cut-off frequency of 0.2 were chosen for this data since they appeared to give a reasonably faired curve through the midsection of the original data points.

Overall averages were then taken for all of the points in the zeros range (model at rest, mean zero voltage) and all of the point in the data collection range (steady state, mean data voltage). A delta voltage was calculated by taking the difference between the mean zero voltage

and the mean data voltage. The measured voltages were converted to lifting forces and moments using the calibration curves discussed previously. The lifting forces were converted to suction forces using the assumption that at the maximum height off the bottom (13"), the force measured was purely lift. The suction force was determined by subtracting the maximum lifting force from each of the other forces measured. Although a mid water column run would be more accurate for this analysis, the adjustable range in the strut precluded this. The forces, moments and heights were non-dimensionalized using the following formulas :

$$F_z' = \frac{F_z}{\frac{1}{2}\rho\, LENGTH^2 (1.689 * FVEL)^2 10^{-4}}$$

$$M_y' = \frac{M_y}{\frac{1}{2}\rho\, LENGTH^3 (1.689 * FVEL)^2 10^{-5}},$$

and

$$H' = \frac{H}{Dia.},$$

where Fz = force measured in towing tank, converted to lbf
My = moment measured in towing tank, converted to lbf-ft
ρ = 1.9905 lbf-s^2/ft^4
LENGTH = 32.25 in.
FVEL = 5 knots
and, Dia = 5.675 in.

Listings of the filtered and the non-dimensionalized data for the heave force and pitching moment are presented in Table 3 and Table 4, respectively.

Table 3 : Model Testing Results - Heave Force

Run #	Dist. (in)	H'	Voltage	Force	Fz'
37-41	1.25	0.22	-0.0015	0.0806	1.573
32-36	2.10	0.37	-0.0056	0.0629	1.227
53-56	2.25	0.40	-0.0056	0.0629	1.226
27-31	3.00	0.53	-0.0084	0.0508	0.990
23-26	4.00	0.70	-0.0131	0.0302	0.588
17-21	4.90	0.86	-0.0143	0.0249	0.486
14-16	5.90	1.04	-0.0146	0.0234	0.457
10-13	6.90	1.22	-0.0151	0.0212	0.414
7-9	8.00	1.41	-0.0159	0.0178	0.347
4-6	9.00	1.59	-0.0209	0.0040	0.078
42-46	13.00	2.29	-0.0200	0.0000	0.000

Table 4 : Model Testing Results - Pitching Moment

Run #	Dist. (in)	H'	Voltage	Moment	My'
37-41	1.25	0.22	-0.0148	-0.0991	-7.189
32-36	2.10	0.37	-0.0187	-0.0936	-6.791
53-56	2.25	0.40	-0.0081	-1.0083	-7.862
27-31	3.00	0.53	-0.0122	-1.0026	-7.444
23-26	4.00	0.70	-0.0234	-0.0871	-6.317
17-21	4.90	0.86	-0.0287	-0.0797	-5.781
14-16	5.90	1.04	-0.0333	-0.0733	-5.318
10-13	6.90	1.22	-0.0250	-0.0848	-6.154
7-9	8.00	1.41	-0.0289	-0.0793	-5.757
4-6	9.00	1.59	-0.0345	-0.0716	-5.197
42-46	13.00	2.29	-0.0001	-0.0000	0.000

Chapter 5 : Experimental Results

Model Testing Data

The towing tank results were first presented in Tables 3 and 4 above. These results are now plotted and compared to the Baseline theory in Figure 20 and Figure 21.

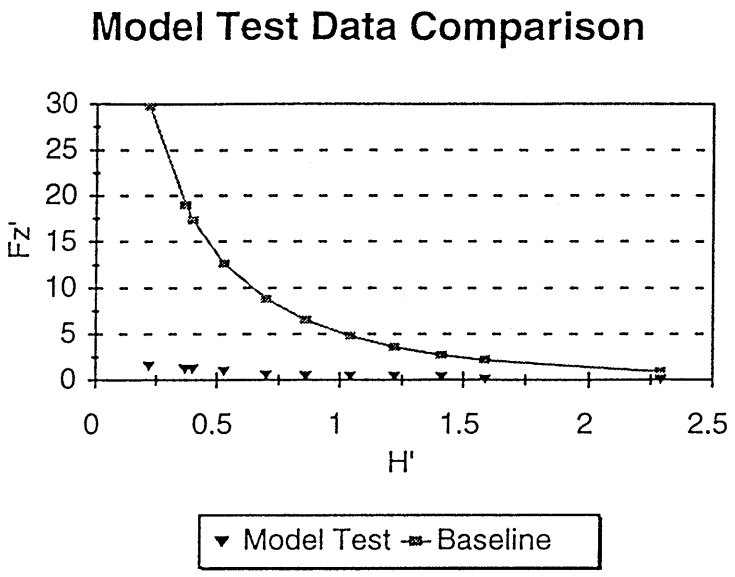

Figure 20 : Fz' vs. H' for Model Test Data and Theoretical Comparison

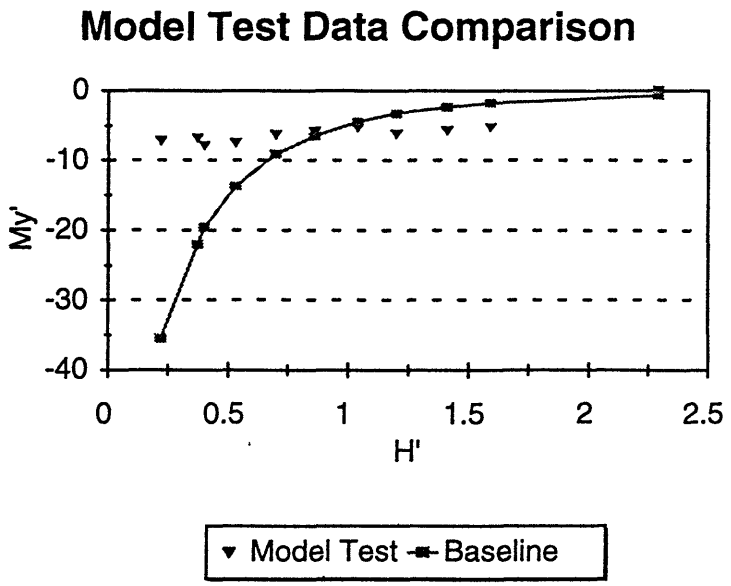

Figure 21 : My' vs. H' for Model Test Data and Theoretical Comparison

The plot of suction force vs. height off the bottom shows that the forces measured are well below those which were expected. Particularly within one diameter, the results deviate substantially. While there is certainly some error in the model test results, not all of this discrepancy may be due to the model tests. Only in theory can the suction forces approach infinity as the bottom clearance approaches zero. Therefore, the deviation of the experimental results from the theoretical may not be as critical as it may first appear. However, this deviation does warrant some future study into its possible causes.

The pitching moment measured does follow the expected trends. As the proximity to the bottom increases, the pitching moment also increases. This indicates, as predicted, that a body with a blunt nose (in comparison to the stern) will experience a bow-in moment. However, given the variation in the signal, any analysis other than examination of trends was deemed unwise.

Published Data

Previously published data is very scarce and, for the most part, classified. After an extensive library search, the only non-classified data available were found to be those for Rankine ovoids. Therefore, it is primarily these data, first discussed by Fortson [7], which will be examined in this section. Figure 22 data is presented to compare the results of the three theoretical methods to analytical data for an ellipse and a rankine ovoid with a L/D ratio of 6.0.

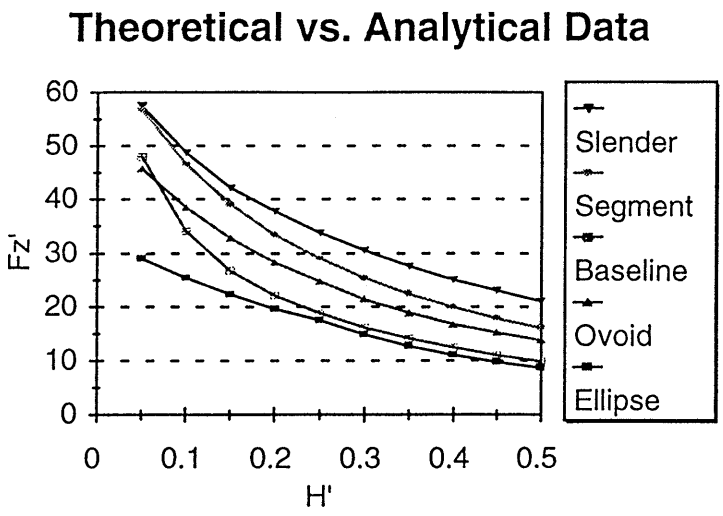

Figure 22 : Fz' vs. H' for Theoretical and Analytical Models

As shown in the Figure, the Baseline method shows the closest correlation to the analytical results for the given range of heights.

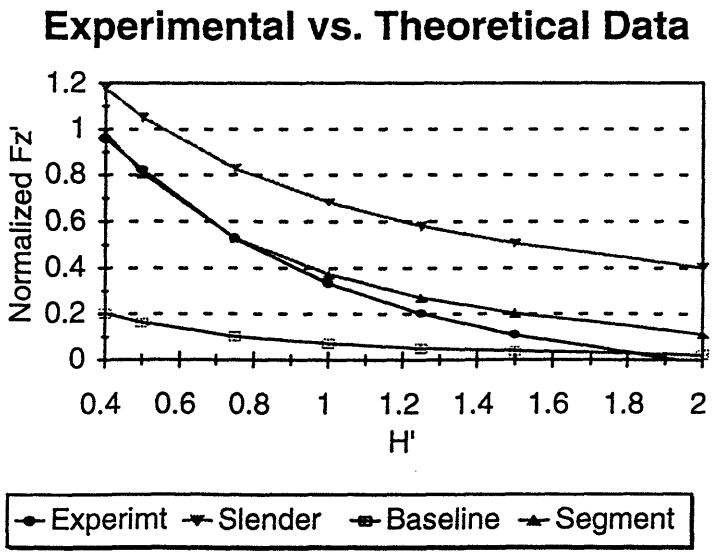

Figure 23 : Comparison of Results for a Typical Submarine

First presented by Arcano [3], data for a typical submarine are shown below in Figure 23. As shown in the Figure, the Segmented theory provides the closest approximation to the actual data when the submarine is within 1.0 diameter. However, once the submarine has moved further from the bottom, the Baseline theory proves to be more accurate. The predictions of Slender theory are well above the experimental data.

In summary, it is unclear whether the Baseline or Segmented theory is more accurate. For the data presented, the Baseline and Segmented methods are equally valid. The Slender theory consistently predicts that the forces will be higher than the experimental measurements. However, it is interesting that the results from the Slender code converge to those from the other methods when the body is extremely close to the obstacle.

Chapter 6 : Theoretical Results

Database Development

For all three codes, a theoretical database was developed to aid in determining equations that could be used in a time-domain simulation of UUV operations near the ocean floor. The matrix used to develop the database is shown in Table 5.

Table 5 : Theoretical Database Matrix

Variable	Range
L/D, Varying Diameter	4.0 - 14.0
L/D, Varying Pmb	4.0 - 14.0
Forebody Length	0.5D - 3.0D
Afterbody Length	1.0D - 5.0D
Forebody Fullness Factor	2.0 - 3.0
Afterbody Fullness Factor	2.0 - 3.0

The database was developed using Draper Laboratory's UUV, with the dimensions shown below, as a reference body shape.

Length (L) = 35.9 ft. Maximum Diameter (D) = 3.67 ft.

Forebody length (Lfb) = 5.15 ft. Afterbody Length (Lab) = 10.0 ft

Forebody Fullness Factor (Nf) = 2.2 Afterbody Fullness Factor (Na) = 2.0

Parallel Midbody Length (Lpmb) = 20.75 ft. Length/Diameter Ratio (L/D) = 9.78

Location of Origin = 17.95 ft. from the bow. This is the mid-point on the vehicle.

Data Analysis

The data collected for the theoretical database proved to be very useful in determining the accuracy and dependability of these codes. The following section describes some of the results derived from these databases. When all three of the codes yielded similar results, those of the Baseline theory have been presented to reduce the repetition of figures. However, all results from these databases can be found in Appendix 2. In most of the figures, the forces, moments, and heights were non-dimensionalized using the following formulas:

$$F_z' = \frac{F_z}{\frac{1}{2}\rho\, LENGTH^2 (1.689 * FVEL)^2 10^{-4}},$$

$$M_y' = \frac{M_y}{\frac{1}{2}\rho\, LENGTH^3 (1.689 * FVEL)^2 10^{-5}},$$

$$M_{arm}' = \frac{-M_y}{F_z \cdot LENGTH}, \text{ and}$$

$$H' = \frac{H}{Dia.}$$

where:

F_z = *suction force, lbf*

M_y = *pitching moment, lbf − ft*

ρ = *fluid density, lbf − s² / ft⁴*

LENGTH = body length, ft.

FVEL = body velocity, knots

H = height above bottom, ft., and

Dia = maximum diameter, ft.

The moment is represented by the moment arm in most of the figures to more clearly show how the moment changes with body shape. Using this representation, the moment arm varies from 0.5 to -0.5, or from bow to stern, respectively. The moment is centered at the midpoint of the body.

The Baseline UUV

The UUV was used as a baseline in developing databases for all three of the codes. The baseline forces and moments calculated for each of the codes are plotted in Figure 24 and Figure 25.

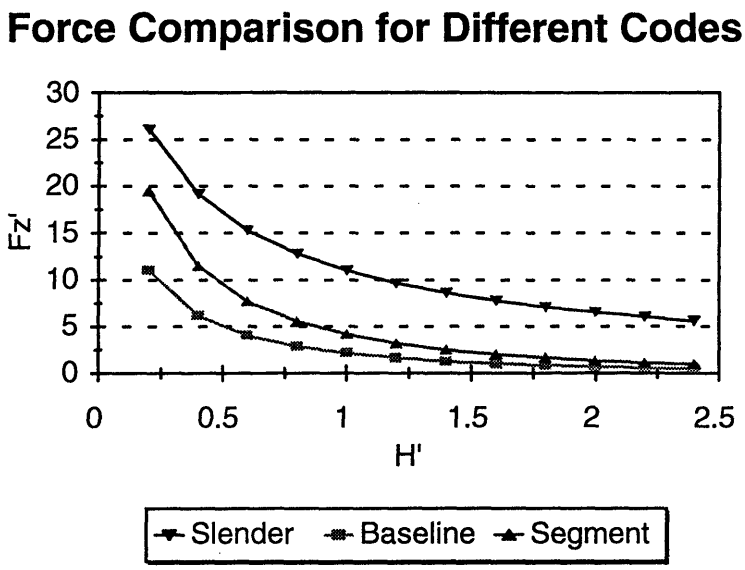

Figure 24 : Fz' vs. H' for UUV at 5 knots

As expected, the heave force decreases rapidly with distance from the bottom for all codes. The results from the Baseline and Segmented codes show a smaller heave force than the Slender theory. These differences are similar to the ones presented in Fortson, Arcano, and Hong. Each of these authors has noted the discrepancy, but presented no information on the validity of these results. In fact, Hong [10] states "it is unclear which is more accurate."

The more interesting feature is in Figure 25 where the corresponding moment arm trends do not agree with one another.

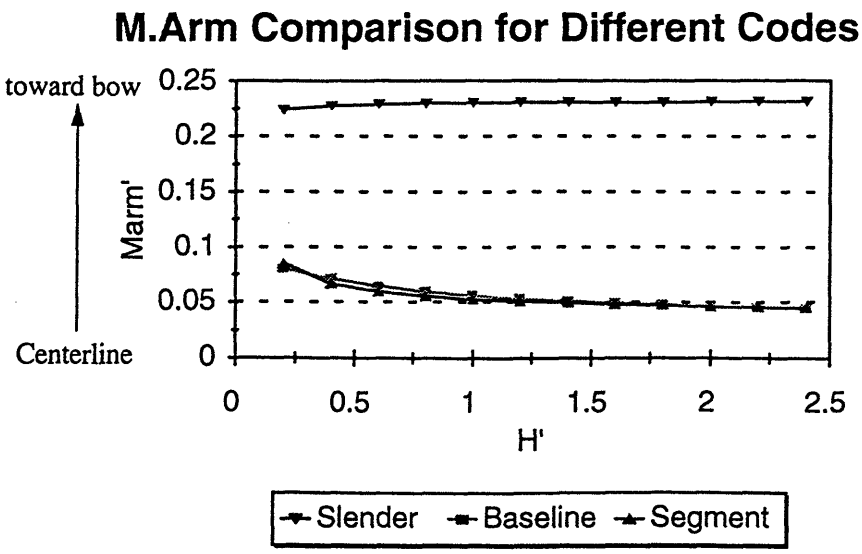

Figure 25 : Marm' vs. H' for UUV at 5 knots

In examining these curves, it can be shown that the Slender body trend is questionable. A positive moment arm corresponds to a moment arm forward of the midbody. As the body approaches the bottom, the blunter forebody will have less clearance than the more slender stern. This difference in clearance is shown in Figure 26. The discrepancy between bow and stern will cause the force on the bow to increase more rapidly, producing a moment that moves toward the bow with decreasing height. As shown in Figure 25, the moment arm for the Baseline and Segmented theories moves toward the bow as expected. The moment arm for the Slender theory moves toward the stern. Therefore, the Slender theory is found to produce questionable results with regard to the moments.

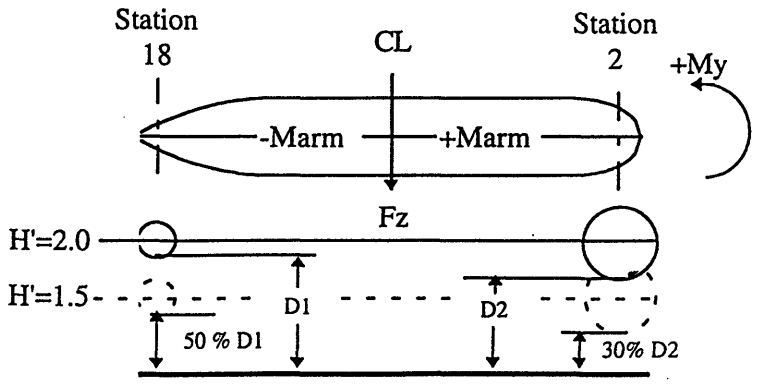

Figure 26 : Moment Arm Discrepancy

Variation of Forces/Moments due to Vehicle Velocity

As predicted by all theories, the suction forces and corresponding moments on a vehicle maneuvering close to the ocean bottom are proportional to the square of its velocity. The results of computed forces for three different velocities are presented in Figure 27 for the Baseline code. These data are plotted for the dimensional Fz (in lbf), to show the dependence on velocity. Figure 27 is redrawn in Figure 28 with the V^2 dependence taken out, showing that heave (suction) force is directly proportional to velocity squared. For this reason, the forces presented throughout this paper are non-dimensionalized by V^2.

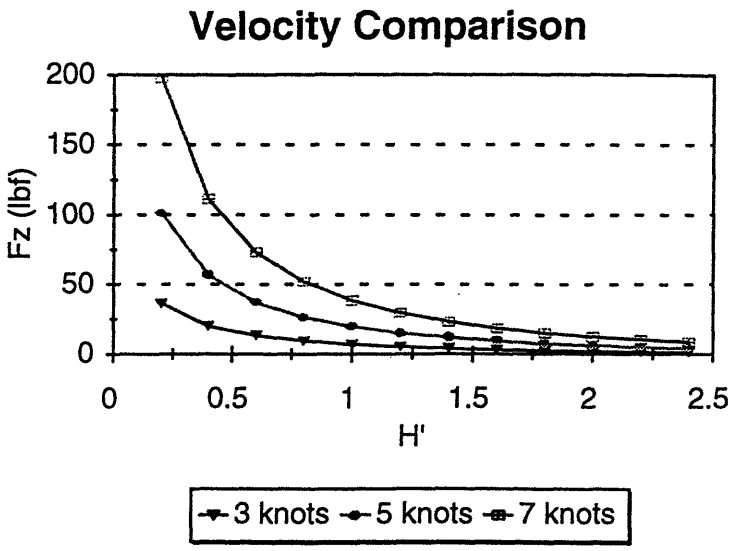

Figure 27 : Fz vs. H' for the UUV at Varying Speeds

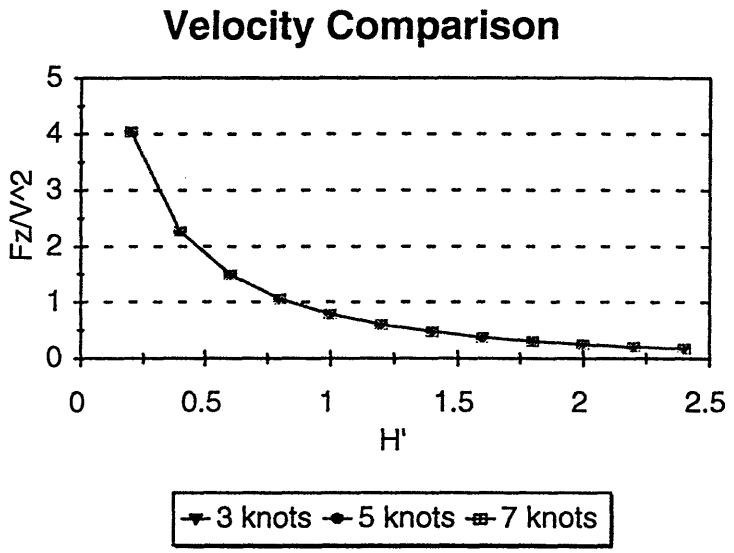

Figure 28 : Fz/V^2 vs. H' for the UUV at Varying Speeds

The moment is proportional to velocity in the same way as the force. This trend can be seen in Figure 29 and Figure 30.

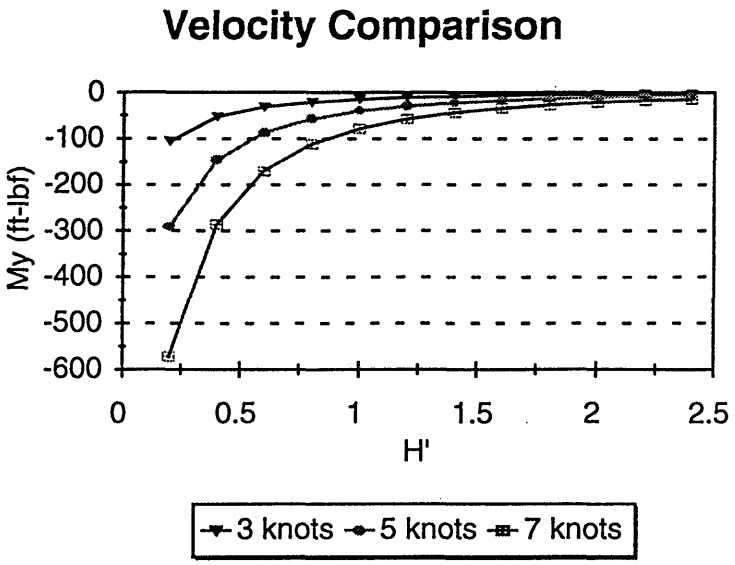

Figure 29 : My vs. H' for UUV at Varying Speeds

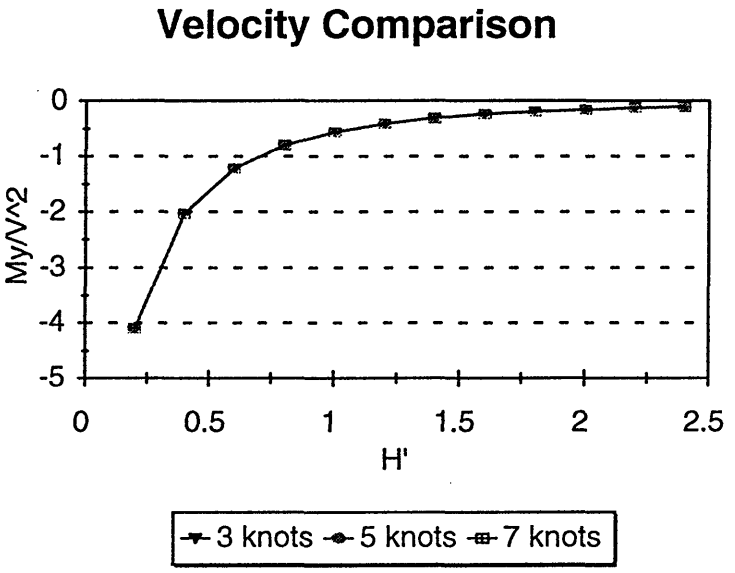

Figure 30 : My/V^2 vs. H' for the UUV at Varying Speeds

Variation of Forces/Moments due to Vehicle Size

Another important result is that the heave suction force is directly proportional to the characteristic length squared. That is:

$$F_{z-uuv} / L_{uuv}^2 = F_{z-half\ uuv} / (0.5 L_{uuv})^2$$

or

$$4 * F_{z-half\ uuv} = F_{z-uuv}$$

This relationship is presented in Figure 31. For this reason, the forces presented throughout this paper are non-dimensionalized based upon Length^2.

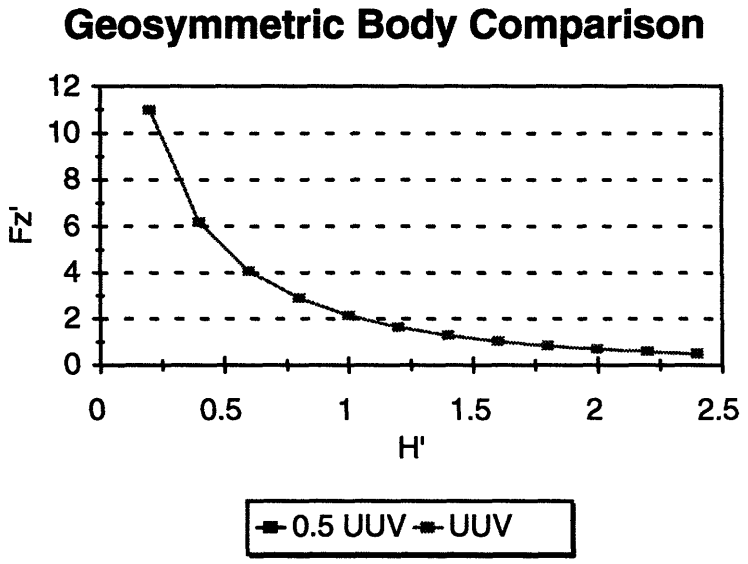

Figure 31 : Fz' vs. H' for UUV and Half Scale UUV at 5 knots - Baseline Method

The moments are also directly proportional to the characteristic length. However, they are proportional to length cubed. Since moment arms (-My/Fz) are a more intuitive variable for viewing the changing moment, they are used throughout this paper. In non-dimensionalizing the moment arms the dependence on vehicle length has been accounted for as shown in Figure 32.

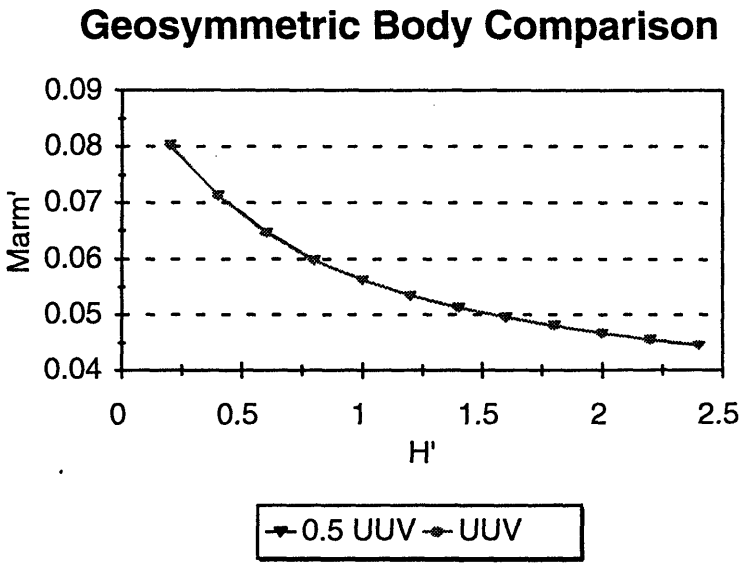

Figure 32 : Marm' vs. H' for UUV and Half Scale UUV at 5 knots - Baseline Method

By taking the velocity and length dependencies out of the force and moment calculations, the data shown in the following sections is now valid for Draper Laboratory's UUV traveling at any speed and for any vehicle which is geometrically similar to the UUV.

Variations of Forces/Moments with L/D Ratios

Another important variable for computing suction forces and their corresponding moments is the length/diameter (L/D) ratio. For these runs, the L/D ratio was varied from 4.0 to 14.0 using two methods. The first method examined the changes in forces and moments due to a variation in diameter. The suction forces for all three cases are similar and the typical trend is shown in Figure 33 for the Baseline theory. The only notable difference in trend between the three methods is that the Slender theory results do not converge to one value at higher levels, but remain as separate curves.

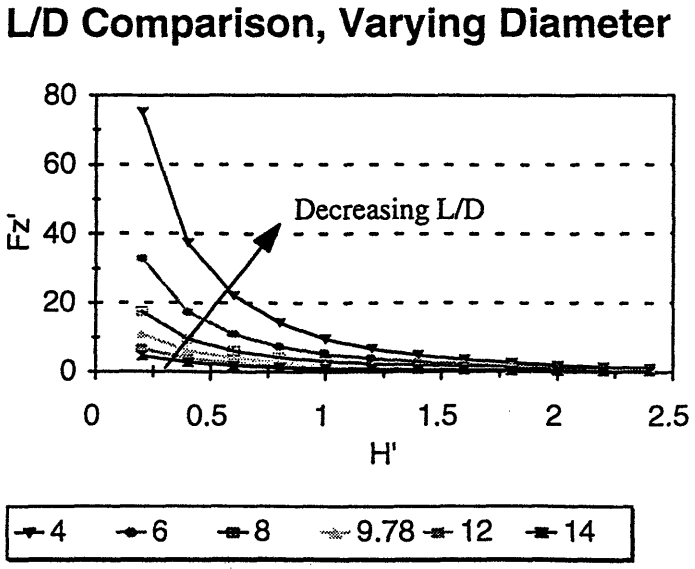

Figure 33 : Fz' vs. H' with Varying Diameters for UUV - Baseline Method

Although the suction force trends are similar for all three methods, the corresponding moment arms are very different as shown in Figure 34 through Figure 36.

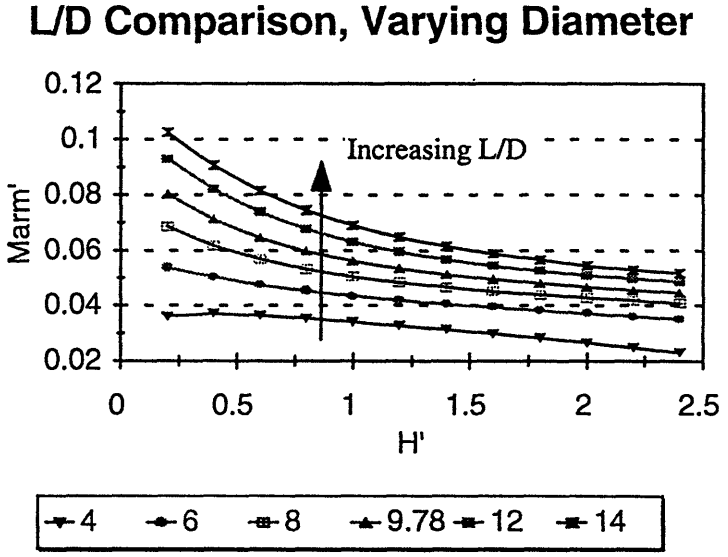

Figure 34 : Marm' vs. H' for UUV with Varying Diameters - Baseline Method

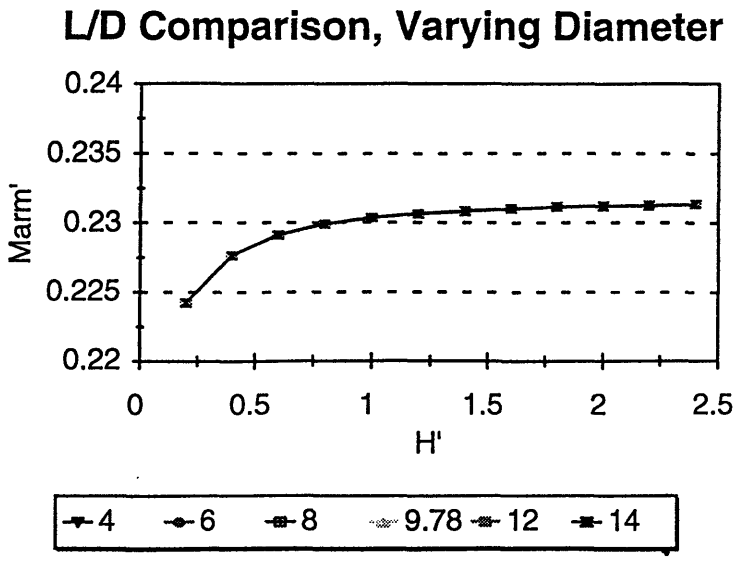

Figure 35 : Marm' vs. H' for UUV with Varying Diameters - Slender Method

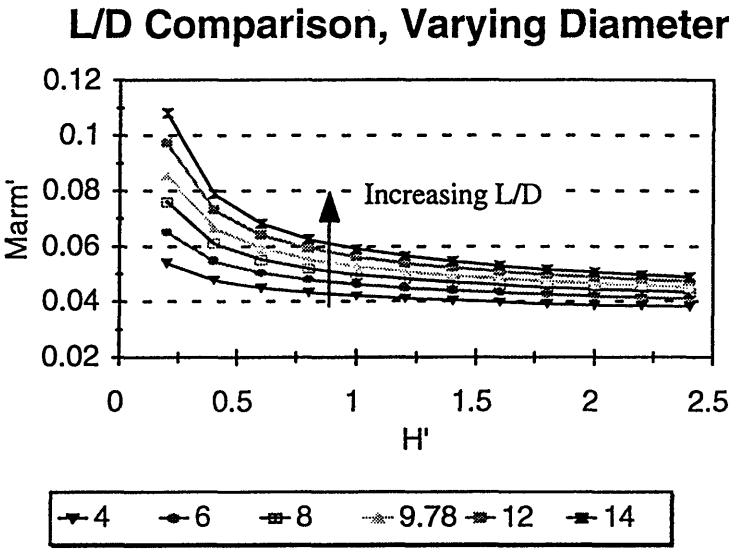

Figure 36 : Marm' vs. H' for UUV with Varying Diameters - Segmented Method

These figures reflect the differences in calculation methods between the codes. The Slender body theory was intended for application to slender bodies only. The lower L/D ratios are obviously for bodies that are more full. Since the slender theory was not written for anything but

slender bodies, it is unable to distinguish between these cases. The Baseline and Segmented theory differences reflect the more accurate segmented model at the nose. The Segmented theory produces a larger bow-in moment, due to its three-dimensional representation of the nose of the UUV.

The second method of varying the L/D ratio was to change the length of the parallel middle body (pmb) and therefore, change the length of the UUV. In these cases, the lengths of the nose and tail were kept constant. The results of varying the pmb were the same as those for varying the diameter with one exception. When the non-dimensionalized moment arms were examined, the trends reversed even though the dimensional forces and moments showed the same trends as the L/D ratios for varying diameter. This trend reversal is because the length of the body changed by significant amounts over the L/D range and the forces and moments are non-dimensionalized by L^2 and L^3, respectively. As the L/D ratio increased, the moment arms moved toward the centerline, becoming more positive, as shown in Figure 37.

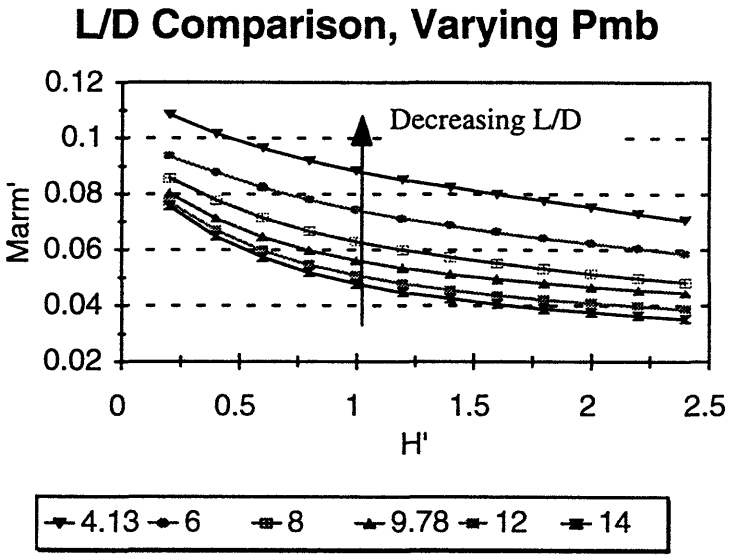

Figure 37 : Marm' vs. H' for UUV with Varying Pmb Length

This shows that the length of the body plays a greater role in the moment arm determination than the diameter, proving why the data has been non-dimensionalized based on length rather than diameter.

Variations of Forces/Moments with Forebody & Afterbody Lengths

The forebody and afterbody lengths made little difference in the force computations for both the Baseline and Segmented theories, as shown in Figure 38. In both of these variations, the overall length of the UUV was kept constant while the length of the forebody or afterbody was changed. However, since the trends were similar for the forebody and the afterbody, only the forebody results are shown here.

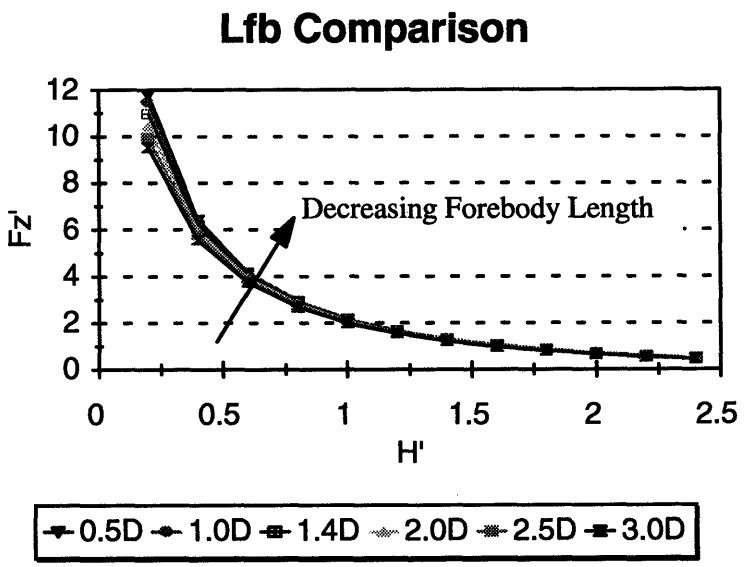

Figure 38 : Fz' vs. H' for UUV with Varying Forebody Lengths - Baseline Method

The change in moment arm with changing forebody lengths is shown in Figure 39. This figure is representative of both the Baseline and Segmented theories. The Slender theory shows the opposite trend as discussed in the previous section on the Baseline UUV.

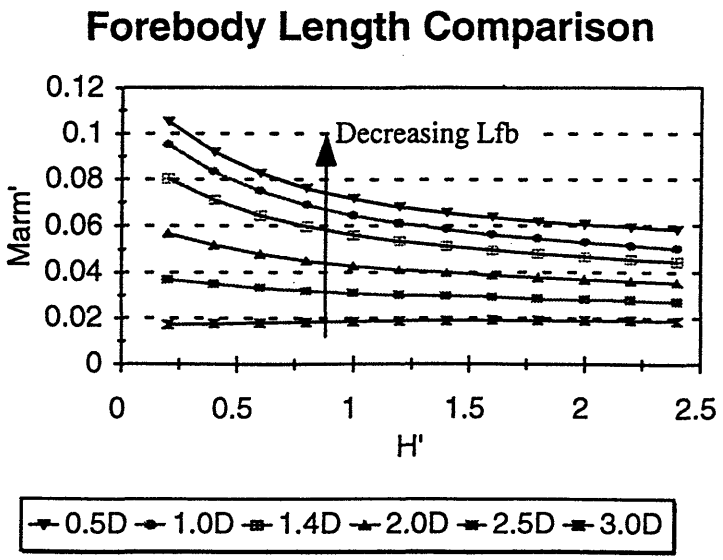

Figure 39 : Marm' vs. H' for UUV with Varying Forebody Lengths - Baseline Method

The trend in moment arm for varying forebody and afterbody lengths agrees with theory. For a very short forebody, the moment arm becomes more negative, representing a bow-in moment. This shows that a very short nose will produce more of a moment. The moment then becomes less as the forebody increases. If the forebody were to continue to be lengthened while the afterbody stayed its original length, the moment arm would even reverse, producing a bow-out moment. This effect can be seen in the figure of the afterbody lengths, shown in Appendix 2.

Variations of Forces/Moments with Fullness Factors

The fullness factors cause little change in the force and moment values for the Baseline and Segmented cases. The Slender theory shows some change with the forebody fullness factor, but the magnitude is small. Figure 40 and Figure 41 show these trends for both the forebody and afterbody fullness factors for the Baseline theory.

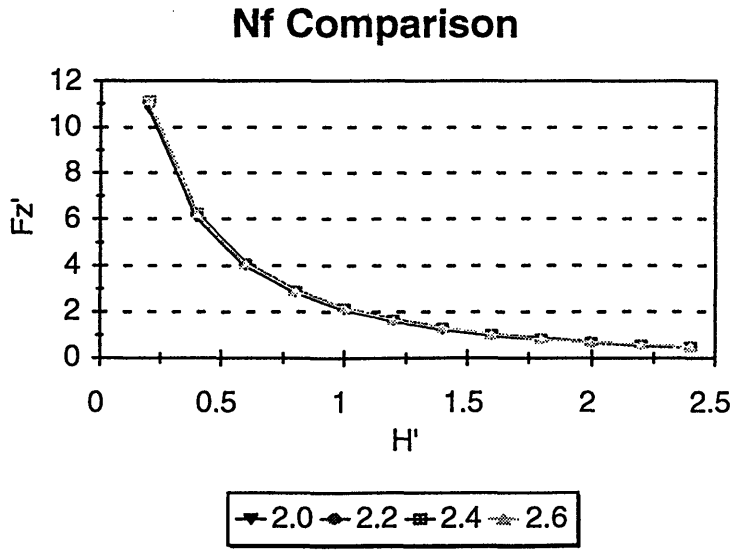

Figure 40 : Fz' vs. H' for UUV with Varying Forebody Fullness Factors - Baseline Method

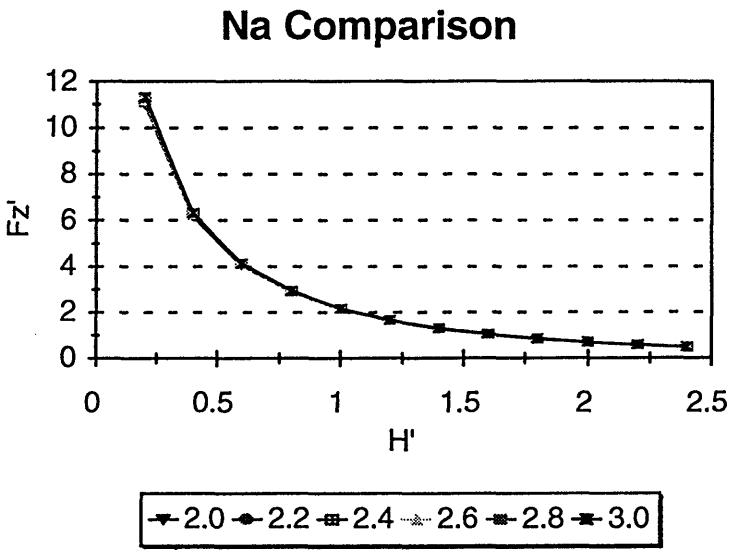

Figure 41 : Fz' vs. H' for UUV with Varying Afterbody Fullness Factors - Baseline Method

It is important to note that the forebody fullness factor plays a major role in the convergence criteria discussed in Chapter 3. For this reason, the forebody fullness factors were only varied between 2.0 and 2.6 to avoid excessive computation times. In all three cases, the moment arm increases with decreasing forebody fullness, as shown in Figure 42.

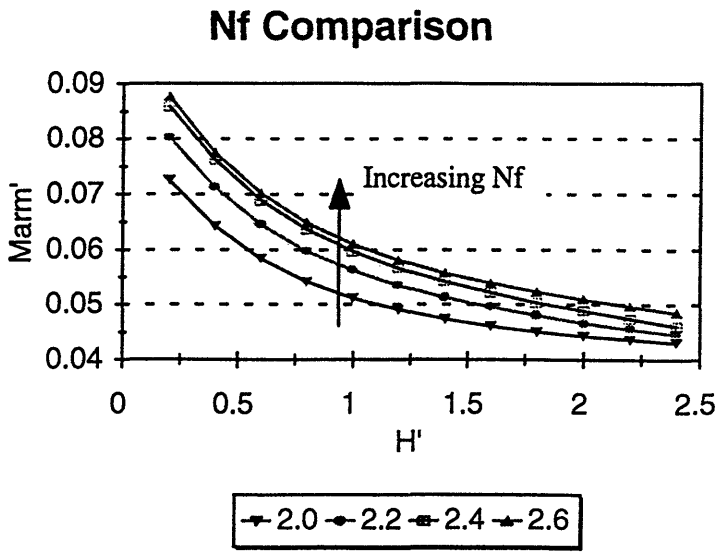

Figure 42 : Marm' vs. H' for UUV with Varying Forebody Fullness Factors - Baseline Method

The figure shows that the moment arm moves toward the bow of the body as the forebody fullness increases. This is because, when the body has a very full forebody, the flow is greatly accelerated over the forebody relative to the afterbody, causing the body to have a larger bow in moment. As the forebody fullness decreases, accelerated flow over the stern approaches that of the bow, causing the moment arm to move toward the center of the vehicle. Figure 43 shows the corresponding trend for the afterbody fullness factor. In this Figure, the more full afterbody causes further acceleration of the flow over the afterbody, resulting in the moment arm moving toward the stern. As the afterbody becomes slender, the stern has less influence, resulting in the moment arm moving toward the bow.

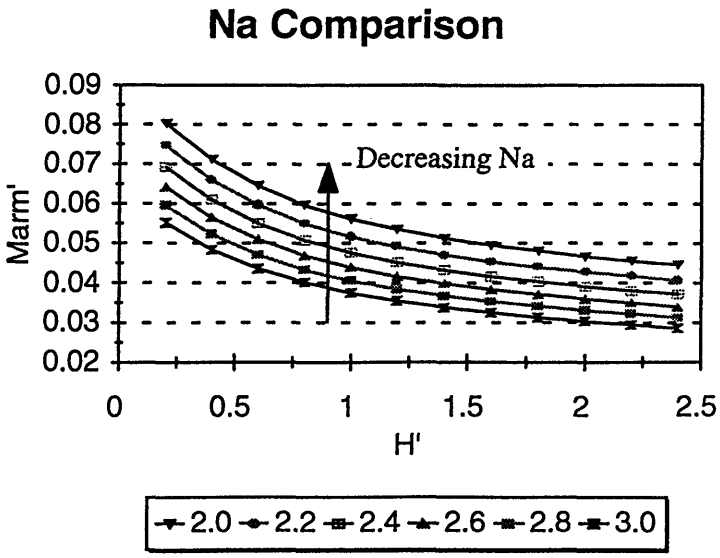

Figure 43 : Marm' vs. H' for UUV with Varying Afterbody Fullness Factors - Baseline Method

Variations of Forces/Moments with Pitching Angles

When the vehicle is either approaching or departing from the ocean bottom, the angle of attack causes the flow to be modified. As defined in Chapter 3, the pitch angle is positive for a body departing from the bottom (bow up) and negative for a body approaching the bottom (bow down). In either case, the pitch angle will cause the flow to be constricted more than if the body was at a constant height. Note that only the interaction forces are being taken into account in this case. The pitching angle (see Figure 44) causes the force to increase in all cases.

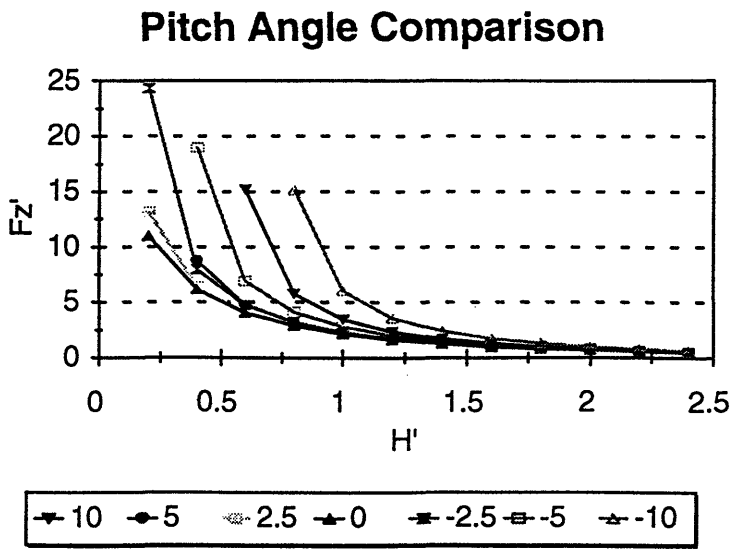

Figure 44 : Fz' vs. H' for the UUV with Varying Pitch Angles - Baseline Method

Since the general relationship between the force and the height is exponential, the effects of moving part of the UUV closer to the bottom, outweigh the effects of moving an equal length of the UUV away from the bottom. In the neutral position of zero pitch angle, the interaction force is at a minimum. It is also interesting that the more slender stern produces less of an increase in force when the body is given a positive pitch angle, as seen in the rightmost two curves where +10 degrees produces a smaller force than -10 degrees of pitch angle. If the submarine was symmetrical in both the forebody and afterbody, the sign of the pitch angle would not affect the force.

The moment arm trend for the inclined body for the Segmented theory is shown in Figure 45. When the body is given a positive pitch angle, this angle counteracts the body's natural tendency to have a bow-in moment, while a negative pitch reinforces the body's bow-in moment.

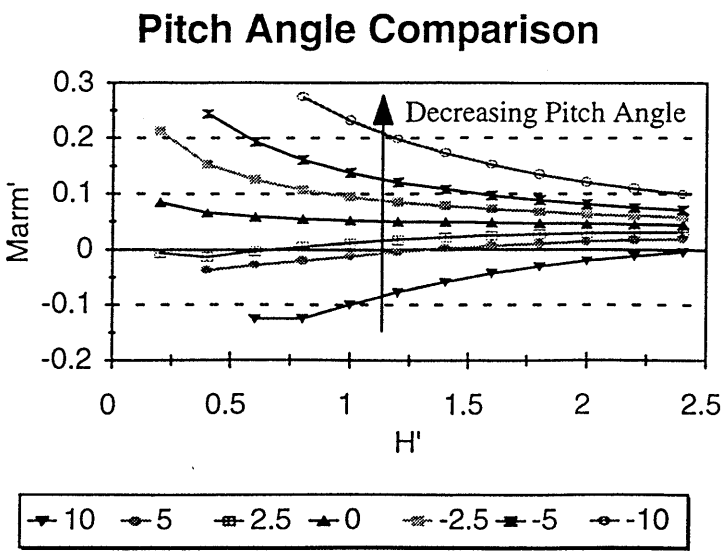

Figure 45 : Marm' vs. H' for the UUV with Varying Pitch Angles - Segmented Method

Unsteady Motion

The addition of unsteady motion to the potential flow theory was implemented as described in Chapter 3. Although there is no experimental data available to validate these results, several test cases were run to check the implementation. Careful examination of these test cases shows that the addition of unsteady motion follows reasonable trends.

Vertical Motion

The first test case to be examined involved the addition of a vertical velocity to the body. The results from this test are shown in Figure 46 and Figure 47. From the coordinate frame, Figure 1, a positive vertical velocity is downward.

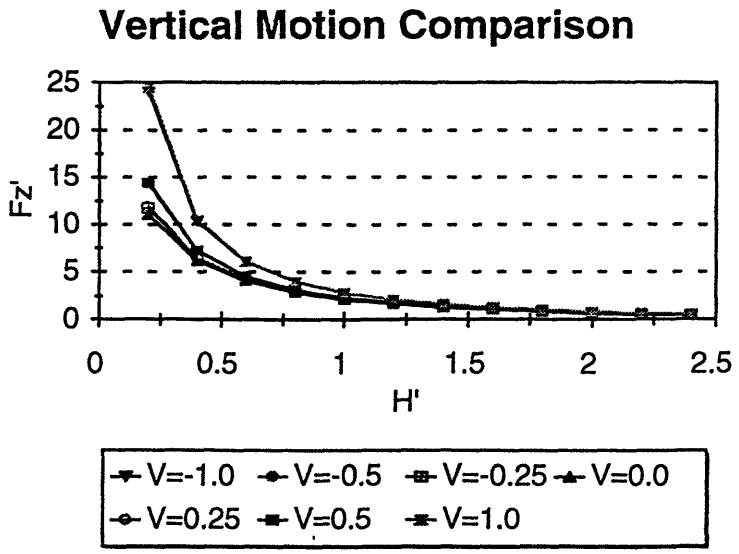

Figure 46 : Fz' vs. H' for Varying Vertical Velocities

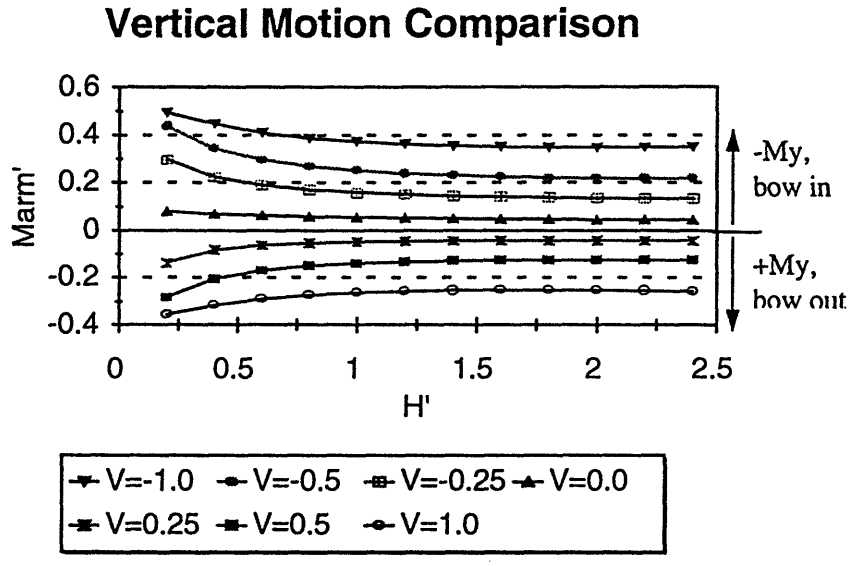

Figure 47 : Marm' vs. H' for Varying Vertical Velocities

The plot of forces shows that, when a vertical velocity is added, the force increases. This phenomenon is analogous to the pitching angle result. However, the moment arm comparison is even more indicative of the expected trends. From this plot it is evident that the addition of a

positive vertical velocity causes the vehicle to overcome its inherent bow-in moment, while a negative vertical velocity enforces the bow-in moment. Since a negative vertical velocity enforces the moment, if the vehicle attempts to escape from the bottom by using an upward, vertical velocity, the vehicle will pitch even closer to the wall.

Trajectory Profile

Once the vertical velocities were checked, a trajectory profile was examined to show how the forces and moments would change throughout the vehicle's entire descent to the bottom. For this test case, the trajectory path was chosen by assuming that the body would descend from H' = 2.0 to H' = 0.5 in roughly one boat length. The appropriate vertical and rotational velocities were then chosen to enable this transition given a steady horizontal speed of 2 knots. Figure 48 shows the path taken as well as the forces and moments measured along this path. The forces and moments have been normalized to show all three curves in one figure.

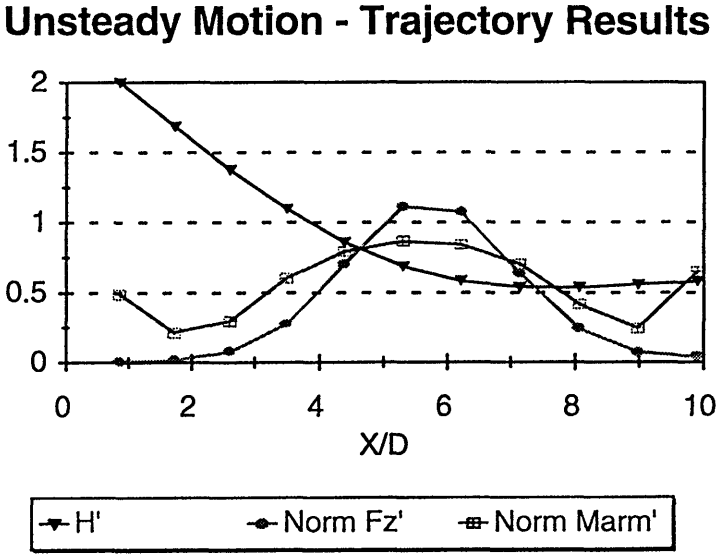

Figure 48 : UUV Trajectory Path, Forces and Moments

From this figure, it is evident that the forces and moments on the vehicle will be the greatest when the vehicle is turning to level off. The effects of these increased forces and moments decrease again once the vehicle is at its new, lower altitude. Once again, these trends appear to be reasonable for the given case. However, more testing is needed to fully verify these results.

Simulation Equations

The final step in examining the theoretical data was to develop simulation equations from the trends examined in the previous section. These regression equations allow a potential user of the simulation to determine these forces and moments without having to run the computer programs for each time-step. The simplification of these methods into simulation equations began with the realization that the general trend of the force and moment curves is similar to an exponential decay, with the general form:

$$F_z' \text{ or } M_y' = C_1 (\textit{Shape Variable})^{C_2}$$

The constants, C_1 and C_2, were found by fitting straight lines to logarithmic plots of F_z' and M_y' for a given shape variable such as L/D. These plots were then used to find expressions for C_1 and C_2 as functions of another variable such as H'. Simulation equations were computed for the Baseline forces and moments as well as the Segmented forces and moments. These results can be found in Figure 49 through Figure 52 and the equations presented below. In each case, the two curve fits presented are averaged to form the curve which is closest to the actual program result. Percentage differences between these results and the actual data are given in Table 6.

Baseline Forces:

$$Eqn1 \Rightarrow F_z' = 16.0*10^{\left(-0.0925\frac{L}{D}\right)} * H'^{\left(0.047\frac{L}{D}-1.791\right)}$$

$$Eqn2 \Rightarrow F_z' = 1637*10^{(-1.015H')} * \left(L/D\right)^{(0.430H'-2.255)}$$

and

$$Best\ Fit \Rightarrow F_z' = \frac{(Eqn1 + Eqn2)}{2}$$

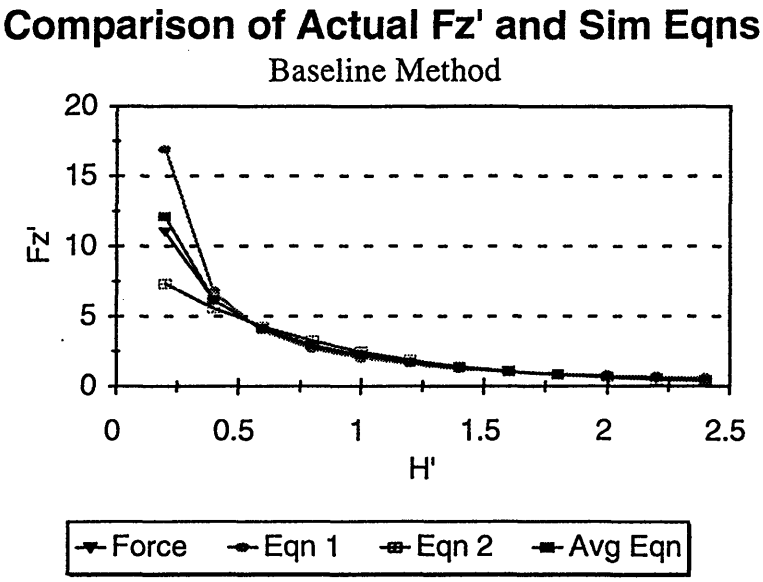

Figure 49 : Comparison of Fz' vs. Simulation Equations - Baseline Method

Baseline Moments:

$$Eqn1 \Rightarrow M_y' = -4.16*10^{\left(-0.061\frac{L}{D}\right)} * H'^{\left(0.0345\frac{L}{D}-1.906\right)}$$

$$Eqn2 \Rightarrow M_y' = -313.33*10^{(-1.157H')} * \left(L/D\right)^{(0.462H'-1.649)}$$

and

$$Best\ Fit \Rightarrow M_y' = \frac{(Eqn1 + Eqn2)}{2}$$

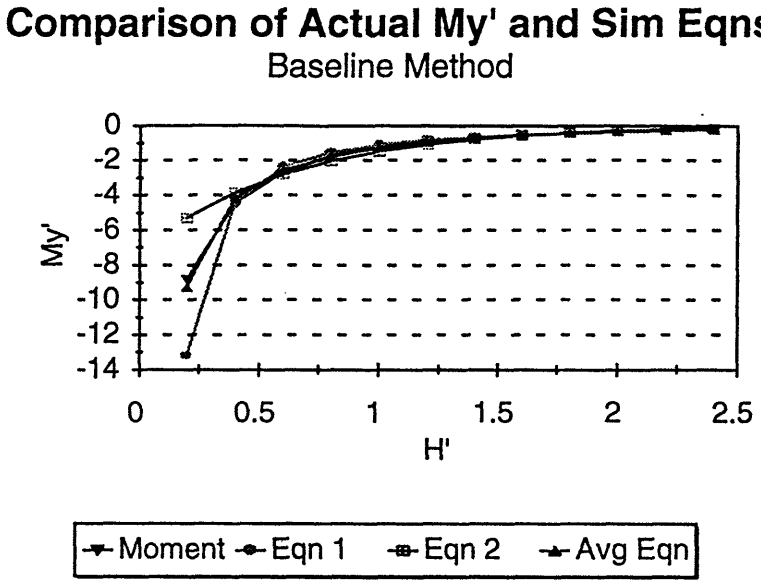

Figure 50 : Comparison of My' and Simulation Equations - Baseline Method

Segmented Forces:

$$Eqn1 \Rightarrow F_z' = 31.55*10^{\left(-0.0939\frac{L}{D}\right)} * H'^{\left(0.0513\frac{L}{D}-1.7905\right)}$$

$$Eqn2 \Rightarrow F_z' = 3435.58*10^{(-1.028H')} * \left(L/D\right)^{(0.4596H'-2.316)}$$

and

$$Best\ Fit \Rightarrow F_z' = \frac{(Eqn1 + Eqn2)}{2}$$

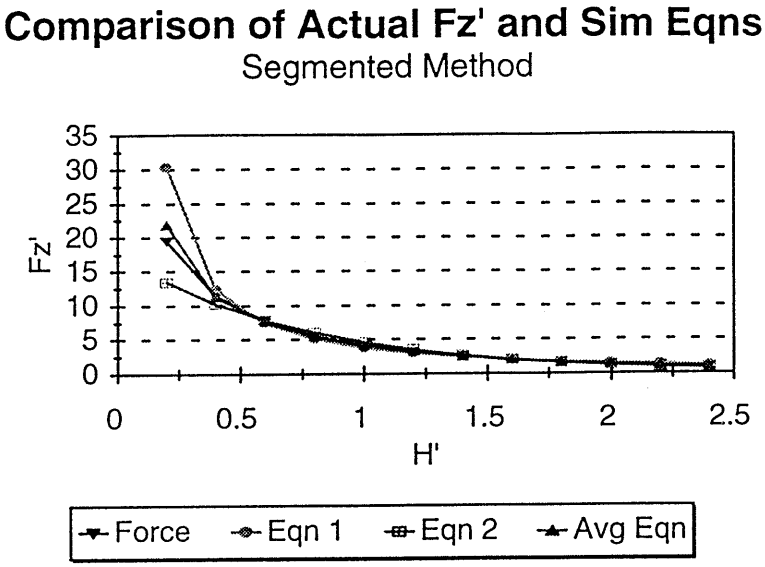

Figure 51 : Comparison of Fz' vs. Simulation Equations - Segmented Method

Segmented Moments:

$$Eqn1 \Rightarrow M_y' = 11.89*10^{\left(-0.0783\frac{L}{D}\right)} * H'^{\left(0.0346\frac{L}{D}-1.867\right)}$$

$$Eqn2 \Rightarrow M_y' = 912*10^{(-1.0075H')} * \left(L/D\right)^{(0.336H'-1.872)}$$

and

$$Best\ Fit \Rightarrow M_y' = \frac{(Eqn1 + Eqn2)}{2}$$

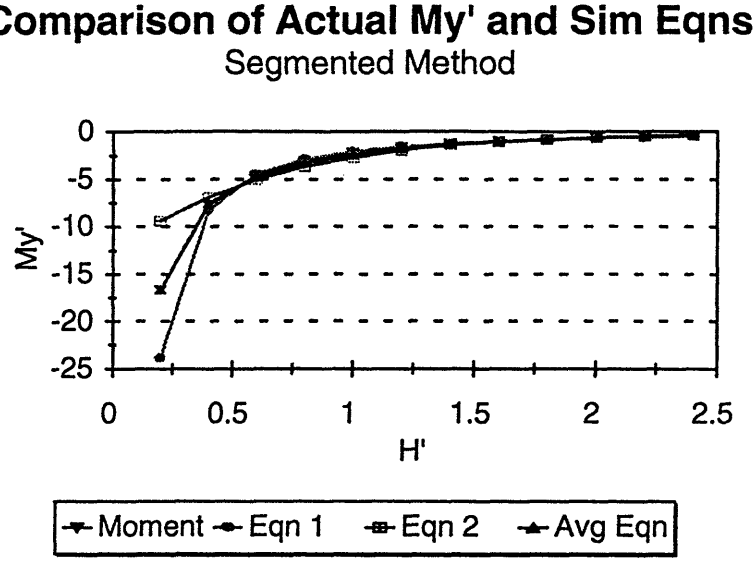

Figure 52 : Comparison of My' vs. Simulation Equations - Segmented Method

Table 6 : Percentage Differences Between Program Results and Simulation Equations

H'	Baseline Force	Baseline Moment	Segmented Force	Segmented Moment
0.2	9.81	4.59	12.30	-0.27
0.4	-0.52	-5.93	-1.28	-1.40
0.6	0.53	-2.21	-1.05	3.29
0.8	2.65	1.95	0.84	6.76
1.0	4.15	4.67	2.41	8.31
1.2	4.79	5.16	3.33	8.21
1.4	4.69	4.61	3.65	6.99
1.6	4.22	3.16	3.55	5.05
1.8	3.51	1.27	3.28	2.88
2.0	2.72	-0.37	3.05	0.78
2.2	2.29	-1.90	3.00	-1.08
2.4	2.16	-3.06	3.28	-2.49

As shown in the above table, the curvefits approximate the actual results very well. The only time the percentage difference is greater than 10% is for the Segmented force when the body is only 0.2 diameters away from the obstacle. However, the region for which any of these analytic equations should be valid is rather sharply defined. These equations encompass the conventional 6 to 10 range for L/D values, with enough leeway for somewhat more radical designs. Operational height from the bottom to the keel of the ship should be no less than half the diameter of the UUV and no more than twice the diameter. The equations again encompass a greater range. A submarine is not expected to travel closer than half its diameter from the bottom, and as it passes more than twice its diameter away, the forces and moments become negligible. For the regions of interest, the maximum error in mathematical equation results as compared to computer code results is 8.3% which makes for an acceptable estimate.

Chapter 7 : Conclusions and Recommendations

This thesis examined some of the theoretical methods available for determining the interaction forces and moments on a UUV traveling close to an obstacle. Each of these methods involved the use of an axial distribution of singularities to represent the body. The forces and moments were then calculated using Lagally's theorem, or an extension of this theorem.

In examining the experimental and theoretical results presented in Chapters 5 and 6, the following conclusions have been developed regarding these codes.

1. Both the Baseline and Segmented methods have proven to give reasonable answers for a wide variety of UUV shapes and sizes.
   - The Baseline method is currently the only method available that allows for unsteady motions and irregular vehicle shapes (elliptical cross-sections). The Baseline method also correlates very well with the ellipse and rankine ovoid data presented in Chapter 5.
   - The Segmented method is the only code which accounts for the three-dimensional effects at the nose. This method correlates very well with the typical submarine data presented in Chapter 5. The Segmented theory is also the only method that allows for the addition of appendages.
2. Although both methods have merits, the Baseline method is currently recommended for integration into Draper Laboratory's simulation until further data from model testing is available.
   - The Baseline method applies to a wider range of vehicle conditions and shapes than the Segmented method.
   - The Segmented method is highly dependent on the added mass coefficient calculated for the forebody. While the current estimate enables the Segmented code to match the data for a typical submarine rather closely, there is no indication as to the code's accuracy for other body shapes.
3. The Slender code is applicable for only theoretical models and is not recommended for integration into Draper Laboratory's simulation.

- The Slender code is applicable only for a very slender body (L/D > 15), very close to the obstacle (H' < 0.5). However, it is unlikely that any vehicle will be traveling this close to the bottom at any substantial speed.
- Given that the moments calculated using this theory are the opposite of what is expected, the results obtained using the Slender code are questionable.

One of the purposes of this thesis was to exercise the codes over a wide variety of vehicle shapes. Prior to this thesis, each author examined only one test case to validate their work. By examining many cases, the trends produced could be evaluated. The following table summarizes the conclusions, developed in Chapter 6, reached concerning a variety of body shapes. Note that the changes in force and moment are listed for each variable as it *decreases*.

Table 7 : Theoretical Database Results

Decreasing Variable	Force Influence Fz'	Moment Influence Marm'
L/D Ratio	increases	to stern
Lfb	increases very little	to bow
Lab	increases very little	to stern
Nf	no change	to stern
Na	no change	to bow
Pitch Angle	increases	to bow

The overall purpose of this thesis was to extend and evaluate the theoretical methods available for predicting the interaction forces and moments on UUVs traveling in proximity to an obstacle. In examining these codes and the various literature available on this subject, the following areas for future work have been discovered. First, little experimental data currently exists. Further validation of these codes must involve more rigorous model testing. Comparison of these codes to panel codes currently being developed here at MIT may also aid in the validation of

these methods. Additional extensions to the model could include irregular bottoms, high angles-of-attack, and operation near the ocean surface.

References :

1. Abkowitz, M.A., Ashe, G.M., and Fortson, R.M., "Interaction Effects of Ships Operating in Proximity in Deep and Shallow Water," Eleventh Symposium on Naval Hydrodynamics, March-April 1976.
2. Abkowitz, M.A., Stability and Motion Control of Ocean Vehicles, MIT Press, Cambridge, MA., 1969.
3. Arcano, J.T., "The Force and Moment on a Submerged Axisymmetric Body Moving Near a Sinusoidal Wall," MIT Thesis, Ocean Engineering, 1985.
4. Ashe, G.M., "Trajectory Predictions for Ships Engaged in Close Proximity Operations," MIT Thesis, Ocean Engineering, 1975.
5. Cummins, W.E. "The Forces and Moments Acting on a Body Moving in an Arbitrary Potential Stream," DTMB Report 780, Washington, D.C., June 1953.
6. Fitzgerald, A.K., "A Potential Flow Model of an Unmanned Undersea Vehicle Operating Near the Ocean Bottom," Tufts University Thesis, Mechanical Engineering, 1993.
7. Fortson, R.M., "Interaction Forces Between Ships," MIT Thesis, Ocean Engineering, 1974.
8. Havelock, T.H., "The Forces on a Circular Cylinder Submerged in a Uniform Stream," The Collected Papers of Sir Thomas Havelock on Hydrodynamics, Edited by C. Wigley, Office of Naval Research, Department of the Navy, ONR/ACR-103, 1963, pp. 420-428.
9. Hess, J.L., and Smith, A.M.O., "Calculation of Non-Lifting Potential Flow About Arbitrary Three-Dimensional Bodies," Douglas Aircraft Co. Report No. E.S. 40622, Long Beach, CA, March 1962.
10. Hong, Young, "Forces and Moments Acting on a Submersible Moving Beneath the Free Surface or Near a Wall," DTNSRDC Report SHD-1233-01, July, 1987.
11. Jackson, H., Submarine Design Trends, MIT Professional Summer, 1986.
12. Korvin-Kroukovsky, B.V., Chabrow, F.R., Belous, P.M., and Sutherland, W.H., "Theoretical and Experimental Investigation of the Interaction of a Free Fluid Surface and a Body of

Revolution Moving under it," Experimental Towing Tank, Stevens Institute of Technology Report 390, 1950.

13. Lamb, Sir H., Hydrodynamics, 6th Edition, Dover Publications, New York, 1932.
14. Landweber, L. and Yih, C.S., "Forces, Moments, and Added Masses for Rankine Bodies," Journal of Fluid Mechanics, Vol. 1, pp. 319-336, September 1956.
15. McCreight, W.R., "Force and Moment on a Slender Body of Revolution Moving in Water of Finite Depth," MIT Thesis, Ocean Engineering, 1970
16. Newman, J.N., Marine Hydrodynamics, MIT Press, Cambridge, MA., 1978.
17. Newman, J.N., "The Force and Moment on a Slender Body of Revolution Moving Near a Wall," DTMB Report 2127, Washington, D.C., 1965.
18. Newton, R.N., "Some Notes on Interaction Effects Between Ships Close Aboard in Deep Water," First Symposium on Ship Maneuverability, DTMB Report 1461, Washington, D.C., October 1960, pp. 1-24.
19. Sabersky, R.H., Acosta, A.J., and Hauptmann, E.G., Fluid Flow, Macmillan Publishing Company, New York, 1989.
20. Streeter, V.L., Handbook of Fluid Dynamics, McGraw-Hill Book Company, Inc., New York, 1961.
21. Taylor, D.W., "Some Model Experiments on Suction of Vessels," Transactions of the Society of Naval Architects and Marine Engineers, Vol. 17, 1909, pp. 2-22.
22. Zucker, R.D., "Lagally's Theorem and the Lifting Body Problem," Journal of Ship Research, Vol. 14, pp. 135-141, June 1970.

Appendix 1 : Panel Codes

The codes examined in this thesis are line-source codes, meaning that the singularities used to describe the body are distributed axially along the center of the body. In panel code methods, the body is divided into panels, or segments. One of the most comprehensive treatments of this subject is a paper titled "Calculation of Non-Lifting Potential Flow About Arbitrary Three-Dimensional Bodies" by Hess and Smith [9]. Currently, work is being done at MIT by Professor Milgram and Soren Jensen to develop a panel code to model the near-bottom interactions of UUVs. This appendix attempts to describe the basic differences between panel codes and line-source codes. When using a panel code, the singularities are then divided among panels rather than along the axis of the UUV, as shown in Figure 53.

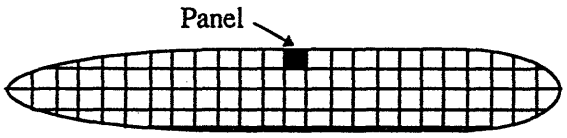

Figure 53 : Panel Code Description

Although the use of panels is computationally more intensive, there are several advantages to this type of body representation. First, the body may be more accurately described by having the singularities lie on the surface they are representing. Another advantage is that appendages such as fins or bow thrusters can be incorporated into the body description. In the current model, these appendages can only be added using their added mass coefficients as described in the Segmented theory.

Once the body is defined as given set of singularities, the boundary conditions and Lagally's theorem may be used to compute the total force and moment on the body.

Appendix 2 : Theoretical Database Results

The results from the theoretical database presented in Chapter 6, are shown below. These results include the forces, moments, moment arms, and plots for each shape variation examined.

Baseline Results

Forces

L/D Comparison, varying Diameter

H'	4	6	8	9.78	12	14
0.2	75.235	32.797	17.416	11.001	6.801	4.687
0.4	37.334	17.373	9.561	6.175	3.903	2.734
0.6	22.176	10.915	6.183	4.062	2.608	1.849
0.8	14.291	7.418	4.319	2.881	1.875	1.342
1	9.681	5.29	3.163	2.141	1.411	1.019
1.2	6.794	3.898	2.394	1.644	1.097	0.798
1.4	4.901	2.944	1.857	1.294	0.873	0.64
1.6	3.615	2.267	1.467	1.037	0.708	0.523
1.8	2.718	1.773	1.177	0.844	0.584	0.434
2	2.078	1.406	0.956	0.696	0.487	0.365
2.2	1.613	1.127	0.785	0.579	0.41	0.31
2.4	1.268	0.913	0.65	0.486	0.348	0.265

L/D Comparison, varying PMB

H'	4.13	6	8	9.78	12	14
0.2	54.775	28.539	16.491	11.001	7.34	5.41
0.4	26.576	15.46	9.19	6.175	4.135	3.052
0.6	15.348	9.768	5.987	4.062	2.733	2.021
0.8	9.601	6.626	4.197	2.881	1.95	1.445
1	6.321	4.697	3.078	2.141	1.46	1.086
1.2	4.322	3.433	2.33	1.644	1.131	0.844
1.4	3.045	2.569	1.805	1.294	0.898	0.673
1.6	2.201	1.959	1.424	1.037	0.728	0.548
1.8	1.626	1.518	1.14	0.844	0.599	0.454
2	1.224	1.192	0.924	0.696	0.5	0.381
2.2	0.937	0.948	0.756	0.579	0.421	0.323
2.4	0.729	0.762	0.625	0.486	0.358	0.277

Moments

L/D Comparison, varying Diameter

H'	4	6	8	9.78	12	14
0.2	-27.17	-17.61	-11.96	-8.836	-6.314	-4.803
0.4	-13.91	-8.758	-5.914	-4.403	-3.201	-2.48
0.6	-8.111	-5.193	-3.514	-2.625	-1.925	-1.507
0.8	-5.068	-3.366	-2.299	-1.723	-1.269	-1
1	-3.31	-2.306	-1.599	-1.204	-0.89	-0.704
1.2	-2.231	-1.64	-1.16	-0.88	-0.653	-0.518
1.4	-1.54	-1.199	-0.868	-0.664	-0.495	-0.394
1.6	-1.082	-0.896	-0.665	-0.514	-0.386	-0.308
1.8	-0.771	-0.68	-0.518	-0.406	-0.307	-0.246
2	-0.555	-0.523	-0.41	-0.325	-0.248	-0.199
2.2	-0.402	-0.407	-0.329	-0.264	-0.204	-0.164
2.4	-0.293	-0.32	-0.266	-0.217	-0.169	-0.137

L/D Comparison, varying PMB

H'	4.13	6	8	9.78	12	14
0.2	-56.63	-26.68	-14.13	-8.836	-5.663	-4.096
0.4	-26.99	-13.58	-7.16	-4.403	-2.772	-1.981
0.6	-14.81	-8.04	-4.284	-2.625	-1.635	-1.158
0.8	-8.835	-5.159	-2.8	-1.723	-1.066	-0.751
1	-5.582	-3.486	-1.938	-1.204	-0.742	-0.521
1.2	-3.682	-2.445	-1.396	-0.88	-0.542	-0.379
1.4	-2.511	-1.763	-1.036	-0.664	-0.41	-0.287
1.6	-1.76	-1.299	-0.786	-0.514	-0.319	-0.223
1.8	-1.262	-0.975	-0.607	-0.406	-0.253	-0.177
2	-0.922	-0.742	-0.476	-0.325	-0.205	-0.144
2.2	-0.684	-0.572	-0.377	-0.264	-0.168	-0.118
2.4	-0.515	-0.446	-0.302	-0.217	-0.139	-0.098

Baseline Results

Forebody Length Comparison

H'	0.5D	1.0D	1.4D	2.0D	2.5D	3.0D
0.2	11.781	11.464	11.001	10.376	9.909	9.496
0.4	6.414	6.349	6.175	5.926	5.725	5.536
0.6	4.166	4.15	4.062	3.933	3.825	3.718
0.8	2.935	2.933	2.881	2.804	2.738	2.672
1	2.174	2.176	2.141	2.091	2.047	2.002
1.2	1.667	1.669	1.644	1.609	1.577	1.544
1.4	1.311	1.313	1.294	1.267	1.243	1.218
1.6	1.051	1.052	1.037	1.016	0.997	0.978
1.8	0.856	0.857	0.844	0.827	0.812	0.796
2	0.706	0.706	0.696	0.681	0.668	0.655
2.2	0.588	0.588	0.579	0.567	0.556	0.544
2.4	0.495	0.494	0.486	0.475	0.466	0.456

Afterbody Length Comparison

H'	1.0D	2.0D	2.72D	3.0D	4.0D	5.0D
0.2	12.594	11.634	11.001	10.783	10.099	9.563
0.4	6.805	6.448	6.175	6.075	5.736	5.442
0.6	4.384	4.208	4.062	4.005	3.803	3.613
0.8	3.071	2.97	2.881	2.845	2.712	2.577
1	2.266	2.201	2.141	2.116	2.022	1.921
1.2	1.734	1.687	1.644	1.626	1.555	1.476
1.4	1.363	1.327	1.294	1.28	1.223	1.159
1.6	1.093	1.064	1.037	1.026	0.98	0.926
1.8	0.891	0.866	0.844	0.835	0.796	0.75
2	0.736	0.715	0.696	0.687	0.654	0.615
2.2	0.615	0.596	0.579	0.572	0.543	0.509
2.4	0.518	0.501	0.486	0.48	0.454	0.425

Forebody Length Comparison

H'	0.5D	1.0D	1.4D	2.0D	2.5D	3.0D
0.2	-12.4	-10.87	-8.836	-5.903	-3.648	-1.627
0.4	-5.89	-5.287	-4.403	-3.071	-1.99	-0.977
0.6	-3.443	-3.11	-2.625	-1.885	-1.266	-0.67
0.8	-2.24	-2.023	-1.723	-1.263	-0.872	-0.49
1	-1.56	-1.405	-1.204	-0.896	-0.633	-0.372
1.2	-1.139	-1.022	-0.88	-0.662	-0.475	-0.29
1.4	-0.862	-0.768	-0.664	-0.504	-0.367	-0.23
1.6	-0.67	-0.593	-0.514	-0.393	-0.289	-0.185
1.8	-0.531	-0.467	-0.406	-0.312	-0.231	-0.151
2	-0.428	-0.374	-0.325	-0.251	-0.188	-0.124
2.2	-0.35	-0.303	-0.264	-0.205	-0.154	-0.103
2.4	-0.289	-0.248	-0.217	-0.169	-0.127	-0.086

Afterbody Length Comparison

H'	1.0D	2.0D	2.72D	3.0D	4.0D	5.0D
0.2	0.243	-5.222	-8.836	-10.06	-13.89	-16.87
0.4	-0.051	-2.588	-4.403	-5.045	-7.133	-8.833
0.6	-0.091	-1.548	-2.625	-3.016	-4.32	-5.415
0.8	-0.084	-1.022	-1.723	-1.98	-2.857	-3.606
1	-0.069	-0.718	-1.204	-1.384	-2.001	-2.535
1.2	-0.055	-0.527	-0.88	-1.01	-1.461	-1.852
1.4	-0.042	-0.399	-0.664	-0.762	-1.1	-1.394
1.6	-0.032	-0.31	-0.514	-0.589	-0.849	-1.073
1.8	-0.025	-0.245	-0.406	-0.465	-0.668	-0.842
2	-0.019	-0.197	-0.325	-0.372	-0.534	-0.67
2.2	-0.014	-0.16	-0.264	-0.302	-0.432	-0.54
2.4	-0.01	-0.131	-0.217	-0.248	-0.353	-0.441

Baseline Results

Forebody Fullness Factor Comparison

H'	2.0	2.2	2.4	2.6
0.2	10.782	11.001	11.158	11.152
0.4	6.062	6.175	6.25	6.23
0.6	3.991	4.062	4.106	4.089
0.8	2.832	2.881	2.911	2.897
1	2.105	2.141	2.163	2.152
1.2	1.616	1.644	1.661	1.652
1.4	1.272	1.294	1.307	1.3
1.6	1.019	1.037	1.048	1.042
1.8	0.829	0.844	0.853	0.849
2	0.683	0.696	0.703	0.6995
2.2	0.568	0.579	0.585	0.583
2.4	0.477	0.486	0.492	0.4895

Forebody Fullness Factor Comparison

H'	2	2.2	2.4	2.60
0.2	-7.826	-8.836	-9.59	-9.783
0.4	-3.9	-4.403	-4.763	-4.83
0.6	-2.33	-2.625	-2.833	-2.87
0.8	-1.535	-1.723	-1.855	-1.881
1	-1.078	-1.204	-1.293	-1.314
1.2	-0.793	-0.88	-0.942	-0.96
1.4	-0.603	-0.664	-0.709	-0.725
1.6	-0.47	-0.514	-0.547	-0.562
1.8	-0.374	-0.406	-0.43	-0.444
2	-0.303	-0.325	-0.344	-0.357
2.2	-0.248	-0.264	-0.278	-0.29
2.4	-0.206	-0.217	-0.227	-0.238

Afterbody Fullness Factor Comparison

H'	2.0	2.2	2.4	2.6	2.8	3.0
0.2	11.001	11.061	11.125	11.19	11.255	11.32
0.4	6.175	6.204	6.233	6.263	6.292	6.32
0.6	4.062	4.078	4.095	4.111	4.127	4.142
0.8	2.881	2.891	2.902	2.912	2.922	2.931
1	2.141	2.149	2.156	2.163	2.17	2.176
1.2	1.644	1.65	1.656	1.661	1.666	1.671
1.4	1.294	1.299	1.303	1.307	1.311	1.315
1.6	1.037	1.041	1.045	1.049	1.052	1.055
1.8	0.844	0.848	0.851	0.854	0.857	0.86
2	0.696	0.699	0.702	0.705	0.707	0.709
2.2	0.579	0.582	0.585	0.587	0.589	0.592
2.4	0.486	0.489	0.491	0.494	0.496	0.498

Afterbody Fullness Factor Comparison

H'	2	2.2	2.4	2.60	2.8	3
0.2	-8.836	-8.257	-7.71	-7.194	-6.709	-6.251
0.4	-4.403	-4.096	-3.809	-3.543	-3.294	-3.062
0.6	-2.625	-2.435	-2.259	-2.096	-1.946	-1.807
0.8	-1.723	-1.594	-1.476	-1.368	-1.268	-1.177
1	-1.204	-1.112	-1.029	-0.952	-0.882	-0.817
1.2	-0.88	-0.811	-0.75	-0.693	-0.641	-0.594
1.4	-0.664	-0.612	-0.565	-0.522	-0.482	-0.446
1.6	-0.514	-0.473	-0.436	-0.403	-0.372	-0.344
1.8	-0.406	-0.373	-0.344	-0.317	-0.293	-0.27
2	-0.325	-0.299	-0.275	-0.254	-0.234	-0.216
2.2	-0.264	-0.243	-0.223	-0.206	-0.19	-0.175
2.4	-0.217	-0.199	-0.183	-0.168	-0.155	-0.143

Baseline Results

Pitch Angle Comparison

H'	10	5	2.5	0	-2.5	-5	-10
0.2			13.086	11.001	24.149		
0.4		8.774	6.357	6.175	7.921	18.806	
0.6	15.204	4.823	4.09	4.062	4.722	6.874	
0.8	5.779	3.21	2.881	2.881	3.204	4.107	14.98
1	3.475	2.309	2.134	2.141	2.322	2.792	6.009
1.2	2.375	1.737	1.636	1.644	1.754	2.029	3.559
1.4	1.732	1.349	1.286	1.294	1.364	1.538	2.398
1.6	1.317	1.071	1.03	1.037	1.085	1.201	1.731
1.8	1.03	0.865	0.838	0.844	0.877	0.958	1.306
2	0.823	0.709	0.69	0.696	0.719	0.777	1.017
2.2	0.669	0.588	0.575	0.579	0.597	0.639	0.81
2.4	0.552	0.492	0.482	0.486	0.499	0.532	0.657

Pitch Angle Comparison

H'	10	5	2.5	0	-2.5	-5	-10
0.2			-12.22	-8.836	-19.79		
0.4		-5.153	-4.293	-4.403	-5.985	-18.68	
0.6	2.756	-2.647	-2.524	-2.625	-3.236	-5.658	
0.8	-1.397	-1.894	-1.762	-1.723	-1.896	-2.779	-19.56
1	-1.576	-1.501	-1.328	-1.204	-1.179	-1.484	-5.579
1.2	-1.512	-1.234	-1.042	-0.88	-0.766	-0.822	-2.317
1.4	-1.38	-1.033	-0.839	-0.664	-0.516	-0.459	-0.991
1.6	-1.232	-0.873	-0.687	-0.514	-0.356	-0.25	-0.365
1.8	-1.088	-0.743	-0.57	-0.406	-0.251	-0.125	-0.051
2	-0.957	-0.636	-0.478	-0.325	-0.179	-0.05	0.111
2.2	-0.841	-0.548	-0.404	-0.264	-0.13	-0.004	0.192
2.4	-0.739	-0.474	-0.344	-0.217	-0.094	0.025	0.23

Moment Arms

L/D Comparison, varying Diameter

H'	4	6	8	9.78	12	14
0.2	0.0361	0.0537	0.0686	0.0803	0.0928	0.1025
0.4	0.0373	0.0504	0.0619	0.0713	0.082	0.0907
0.6	0.0366	0.0476	0.0568	0.0646	0.0738	0.0815
0.8	0.0355	0.0454	0.0532	0.0598	0.0677	0.0745
1	0.0342	0.0436	0.0506	0.0562	0.0631	0.0691
1.2	0.0328	0.0421	0.0485	0.0535	0.0595	0.0649
1.4	0.0314	0.0407	0.0467	0.0513	0.0567	0.0616
1.6	0.0299	0.0395	0.0453	0.0496	0.0545	0.0589
1.8	0.0284	0.0384	0.044	0.0481	0.0526	0.0567
2	0.0267	0.0372	0.0429	0.0467	0.0509	0.0545
2.2	0.0249	0.0361	0.0419	0.0456	0.0498	0.0529
2.4	0.0231	0.035	0.0409	0.0447	0.0486	0.0517

L/D Comparison, varying PMB

H'	4.13	6	8	9.78	12	14
0.2	0.1086	0.0935	0.0857	0.0803	0.0772	0.0757
0.4	0.1016	0.0878	0.0779	0.0713	0.067	0.0649
0.6	0.0965	0.0823	0.0716	0.0646	0.0598	0.0573
0.8	0.092	0.0779	0.0667	0.0598	0.0547	0.052
1	0.0883	0.0742	0.063	0.0562	0.0508	0.048
1.2	0.0852	0.0712	0.0599	0.0535	0.0479	0.0449
1.4	0.0825	0.0686	0.0574	0.0513	0.0457	0.0426
1.6	0.08	0.0663	0.0552	0.0496	0.0438	0.0407
1.8	0.0776	0.0642	0.0532	0.0481	0.0422	0.039
2	0.0753	0.0622	0.0515	0.0467	0.041	0.0378
2.2	0.073	0.0603	0.0499	0.0456	0.0399	0.0365
2.4	0.0706	0.0585	0.0483	0.0447	0.0388	0.0354

Baseline Results

Forebody Length Comparison

H'	0.5D	1.0D	1.4D	2.0D	2.5D	3.0D
0.2	0.1053	0.0948	0.0803	0.0569	0.0368	0.0171
0.4	0.0918	0.0833	0.0713	0.0518	0.0348	0.0176
0.6	0.0826	0.0749	0.0646	0.0479	0.0331	0.018
0.8	0.0763	0.069	0.0598	0.045	0.0318	0.0183
1	0.0718	0.0646	0.0562	0.0429	0.0309	0.0186
1.2	0.0683	0.0612	0.0535	0.0411	0.0301	0.0188
1.4	0.0658	0.0585	0.0513	0.0398	0.0295	0.0189
1.6	0.0637	0.0564	0.0496	0.0387	0.029	0.0189
1.8	0.062	0.0545	0.0481	0.0377	0.0284	0.019
2	0.0606	0.053	0.0467	0.0369	0.0281	0.0189
2.2	0.0595	0.0515	0.0456	0.0362	0.0277	0.0189
2.4	0.0584	0.0502	0.0447	0.0356	0.0273	0.0189

Afterbody Length Comparison

H'	1.0D	2.0D	2.72D	3.0D	4.0D	5.0D
0.2	-0.002	0.0449	0.0803	0.0933	0.1375	0.1764
0.4	0.0007	0.0401	0.0713	0.083	0.1244	0.1623
0.6	0.0021	0.0368	0.0646	0.0753	0.1136	0.1499
0.8	0.0027	0.0344	0.0598	0.0696	0.1053	0.1399
1	0.003	0.0326	0.0562	0.0654	0.099	0.132
1.2	0.0032	0.0312	0.0535	0.0621	0.094	0.1255
1.4	0.0031	0.0301	0.0513	0.0595	0.0899	0.1203
1.6	0.003	0.0291	0.0496	0.0574	0.0866	0.1159
1.8	0.0028	0.0283	0.0481	0.0557	0.0839	0.1123
2	0.0025	0.0276	0.0467	0.0541	0.0817	0.1089
2.2	0.0022	0.0268	0.0456	0.0528	0.0796	0.1061
2.4	0.0019	0.0261	0.0447	0.0517	0.0778	0.1038

Baseline Results

Forebody Fullness Factor Comparison

H'	2.0	2.2	2.4	2.6
0.2	0.0726	0.0803	0.0859	0.0877
0.4	0.0643	0.0713	0.0762	0.0775
0.6	0.0584	0.0646	0.069	0.0702
0.8	0.0542	0.0598	0.0637	0.0649
1	0.0512	0.0562	0.0598	0.0611
1.2	0.0491	0.0535	0.0567	0.0581
1.4	0.0474	0.0513	0.0542	0.0558
1.6	0.0461	0.0496	0.0522	0.0539
1.8	0.0451	0.0481	0.0504	0.0523
2	0.0444	0.0467	0.0489	0.051
2.2	0.0437	0.0456	0.0475	0.0497
2.4	0.0432	0.0447	0.0461	0.0486

Afterbody Fullness Factor Comparison

H'	2.0	2.2	2.4	2.6	2.8	3.0
0.2	0.0803	0.0746	0.0693	0.0643	0.0596	0.0552
0.4	0.0713	0.066	0.0611	0.0566	0.0524	0.0484
0.6	0.0646	0.0597	0.0552	0.051	0.0472	0.0436
0.8	0.0598	0.0551	0.0509	0.047	0.0434	0.0402
1	0.0562	0.0517	0.0477	0.044	0.0406	0.0375
1.2	0.0535	0.0492	0.0453	0.0417	0.0385	0.0355
1.4	0.0513	0.0471	0.0434	0.0399	0.0368	0.0339
1.6	0.0496	0.0454	0.0417	0.0384	0.0354	0.0326
1.8	0.0481	0.044	0.0404	0.0371	0.0342	0.0314
2	0.0467	0.0428	0.0392	0.036	0.0331	0.0305
2.2	0.0456	0.0418	0.0381	0.0351	0.0323	0.0296
2.4	0.0447	0.0407	0.0373	0.034	0.0313	0.0287

Baseline Results

Pitch Angle Comparison

H'	10	5	2.5	0	-2.5	-5	-10
0.2			0.0934	0.0803	0.0819		
0.4		0.0587	0.0675	0.0713	0.0756	0.0993	
0.6	-0.018	0.0549	0.0617	0.0646	0.0685	0.0823	
0.8	0.0242	0.059	0.0612	0.0598	0.0592	0.0677	0.1306
1	0.0454	0.065	0.0622	0.0562	0.0508	0.0532	0.0928
1.2	0.0637	0.071	0.0637	0.0535	0.0437	0.0405	0.0651
1.4	0.0797	0.0766	0.0652	0.0513	0.0378	0.0298	0.0413
1.6	0.0935	0.0815	0.0667	0.0496	0.0328	0.0208	0.0211
1.8	0.1056	0.0859	0.068	0.0481	0.0286	0.013	0.0039
2	0.1163	0.0897	0.0693	0.0467	0.0249	0.0064	-0.011
2.2	0.1257	0.0932	0.0703	0.0456	0.0218	0.0006	-0.024
2.4	0.1339	0.0963	0.0714	0.0447	0.0188	-0.005	-0.035

Baseline Results

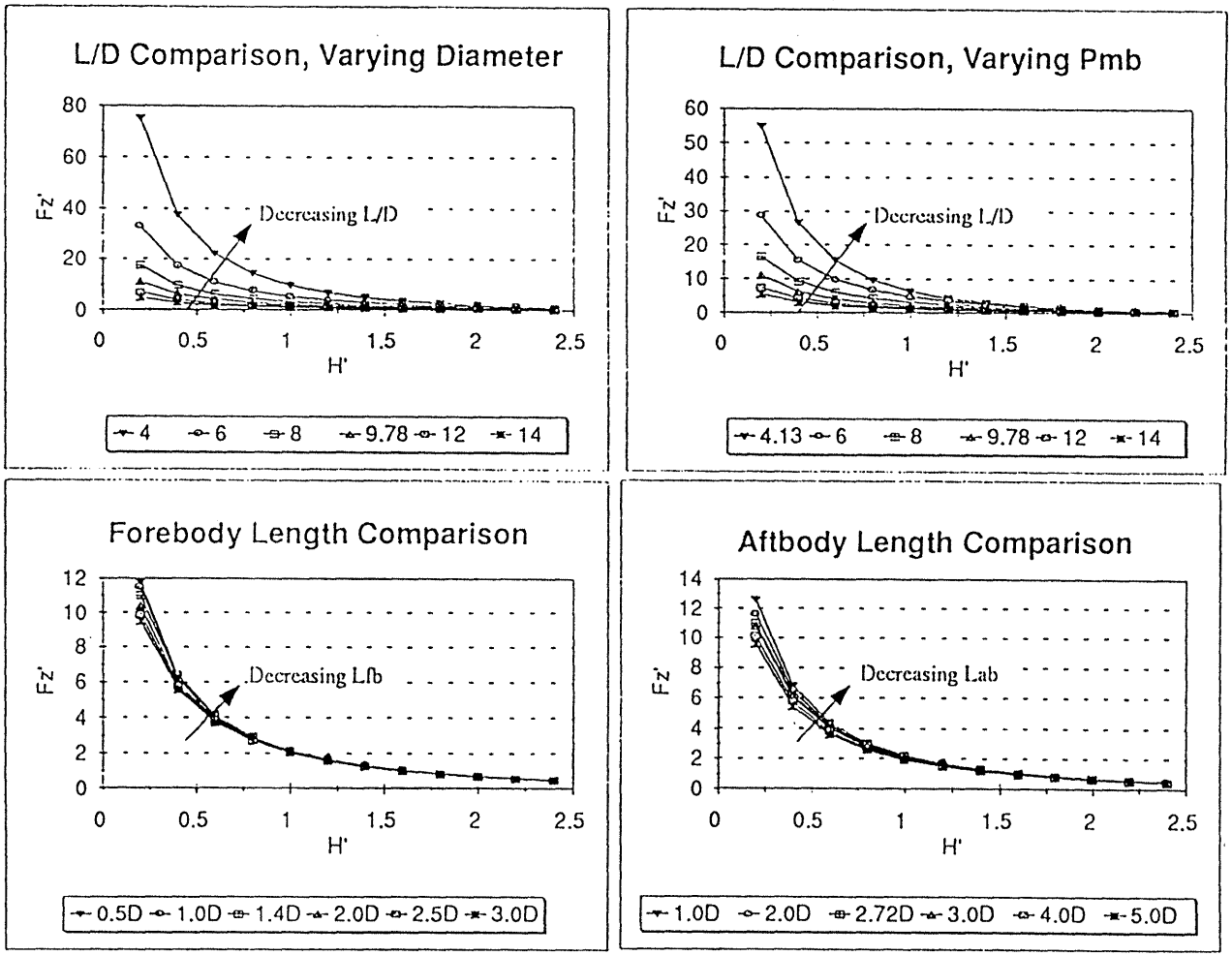

Baseline Results

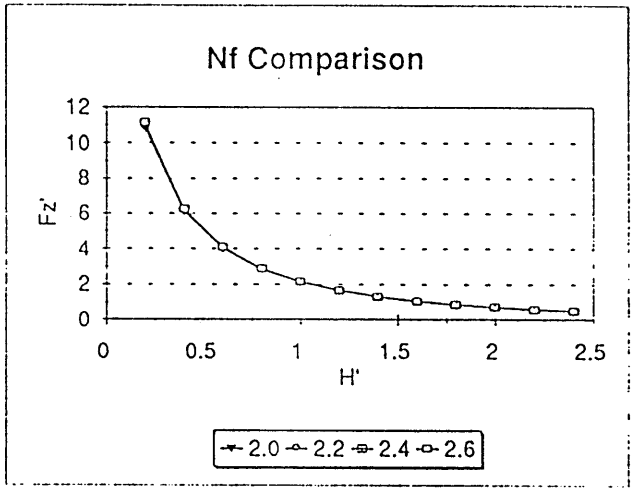

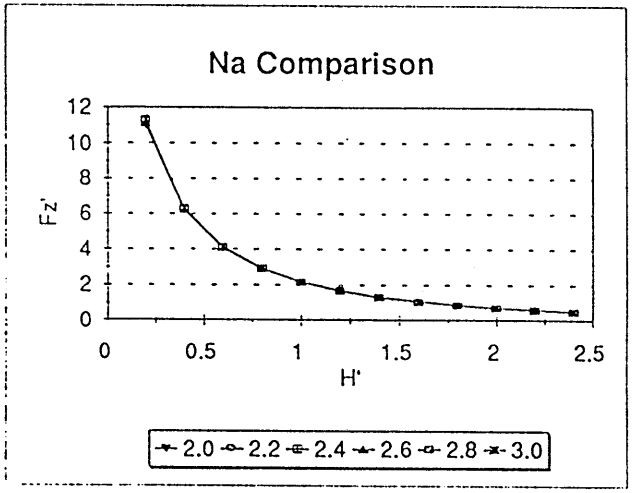

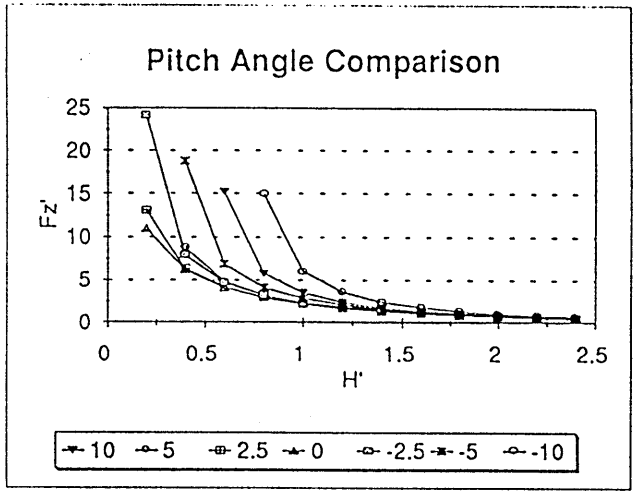

Baseline Results

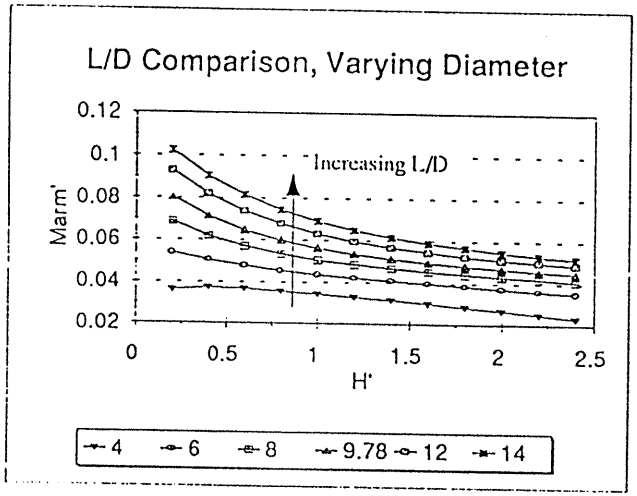

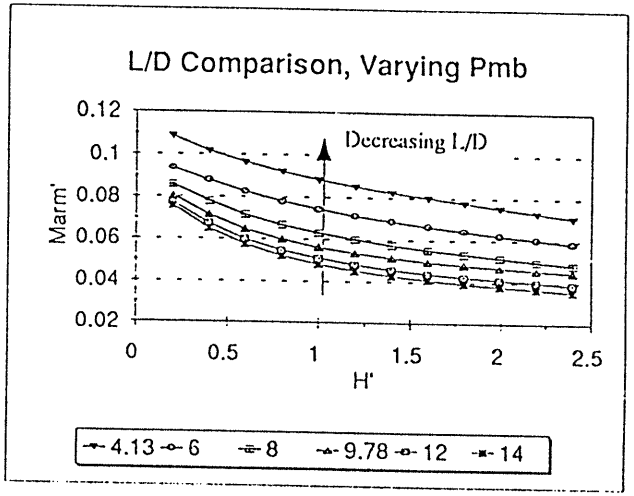

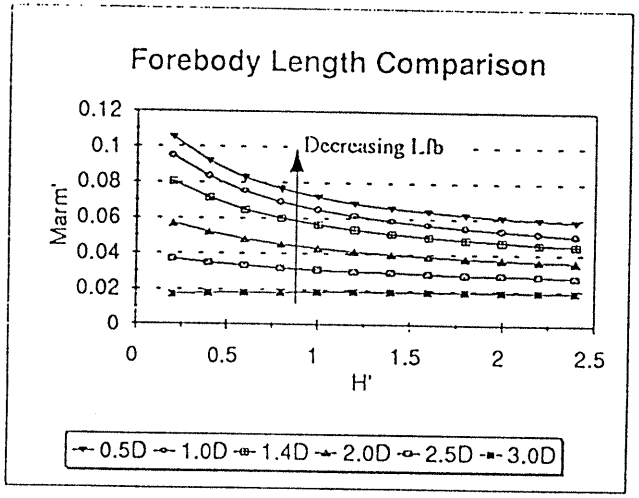

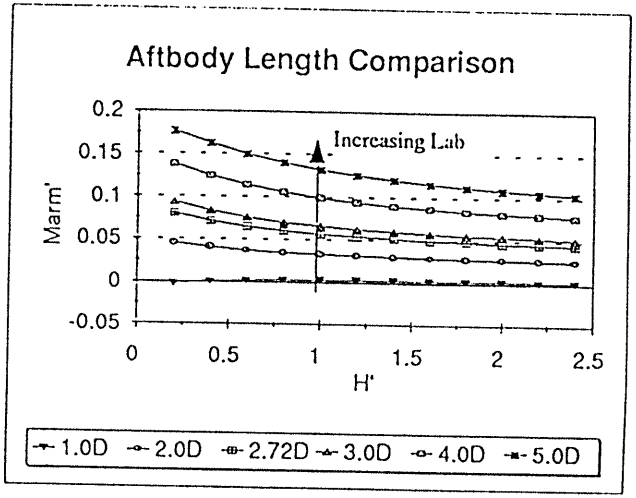

Baseline Results

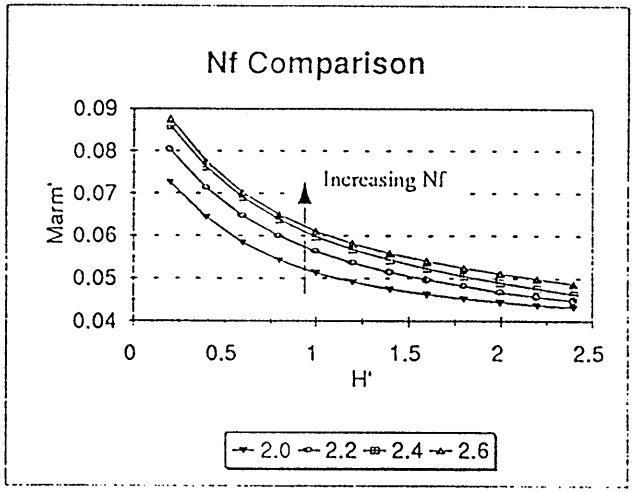

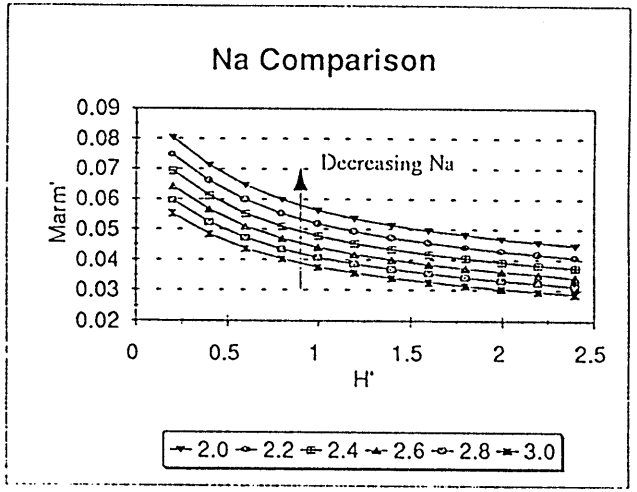

Slender Results

Forces

L/D Comparison, varying Diameter

H'	4	6	8	9.78	12	14
0.2	381.5	113.03	47.687	26.085	14.135	8.8951
0.4	280.58	83.134	35.072	19.185	10.395	6.5419
0.6	224.02	66.376	28.003	15.317	8.3	5.2233
0.8	187.08	55.43	23.385	12.791	6.9314	4.3616
1	160.85	47.659	20.105	10.998	5.9598	3.7502
1.2	141.19	41.832	17.649	9.6534	5.2309	3.2922
1.4	125.88	37.295	15.732	8.6068	4.6641	2.9353
1.6	113.59	33.657	14.199	7.7669	4.2082	2.6481
1.8	103.52	30.67	12.939	7.0782	3.835	2.4131
2	95.098	28.176	11.887	6.5016	3.5228	2.2173
2.2	87.95	26.057	10.994	6.0131	3.2584	2.0508
2.4	81.809	24.24	10.226	5.5932	3.031	1.9072

L/D Comparison, varying PMB

H'	4.13	6	8	9.78	12	14
0.2	146.06	68.839	38.872	26.085	17.21	12.669
0.4	107.4	50.606	28.583	19.185	12.652	9.3147
0.6	85.771	40.398	22.82	15.317	10.1	7.436
0.8	71.598	33.733	19.056	12.791	8.4332	6.2091
1	61.579	29.002	16.383	10.998	7.2504	5.3385
1.2	54.041	25.456	14.381	9.6534	6.3641	4.6858
1.4	48.176	22.695	12.821	8.6068	5.6737	4.1774
1.6	43.478	20.48	11.57	7.7669	5.1199	3.7695
1.8	39.617	18.661	10.544	7.0782	4.6652	3.4354
2	36.392	17.143	9.685	6.5016	4.2856	3.1555
2.2	33.661	15.856	8.9578	6.0131	3.9639	2.9186
2.4	31.309	14.748	8.3316	5.5932	3.687	2.7147

Moments

L/D Comparison, varying Diameter

H'	4	6	8	9.78	12	14
0.2	-855.5	-253.5	-106.9	-58.49	-31.7	-19.95
0.4	-638.8	-189.3	-79.85	-43.68	-23.67	-14.89
0.6	-513.3	-152.1	-64.16	-35.1	-19.02	-11.97
0.8	-430.1	-127.4	-53.76	-29.41	-15.93	-10.03
1	-370.5	-109.8	-46.32	-25.34	-13.73	-8.639
1.2	-325.7	-96.49	-40.71	-22.27	-12.07	-7.594
1.4	-290.6	-86.11	-36.33	-19.87	-10.77	-6.776
1.6	-262.4	-77.75	-32.8	-17.94	-9.723	-6.119
1.8	-239.3	-70.89	-29.91	-16.36	-8.865	-5.579
2	-219.9	-65.15	-27.49	-15.03	-8.146	-5.127
2.2	-203.4	-60.27	-25.43	-13.91	-7.537	-4.743
2.4	-189.3	-56.08	-23.66	-12.94	-7.012	-4.413

L/D Comparison, varying PMB

H'	4.13	6	8	9.78	12	14
0.2	-361.2	-160.6	-88.32	-58.49	-37.69	-27.56
0.4	-268.5	-119.6	-65.88	-43.68	-28.14	-20.59
0.6	-215.4	-95.98	-52.91	-35.1	-22.61	-16.55
0.8	-180.3	-80.38	-44.33	-29.41	-18.95	-13.87
1	-155.3	-69.22	-38.18	-25.34	-16.32	-11.95
1.2	-136.4	-60.83	-33.56	-22.27	-14.35	-10.5
1.4	-121.7	-54.27	-29.95	-19.87	-12.8	-9.371
1.6	-109.9	-49	-27.04	-17.94	-11.56	-8.462
1.8	-100.2	-44.67	-24.65	-16.36	-10.54	-7.715
2	-92.04	-41.05	-22.65	-15.03	-9.685	-7.09
2.2	-85.14	-37.97	-20.96	-13.91	-8.96	-6.559
2.4	-79.2	-35.33	-19.5	-12.94	-8.336	-6.103

Slender Results

Forebody Length Comparison

H'	0.5D	1.0D	1.4D	2.0D	2.5D	3.0D
0.2	58.997	33.321	26.085	20.483	18.027	16.256
0.4	43.444	24.528	19.185	15.039	13.227	11.916
0.6	34.778	19.591	15.317	11.998	10.55	9.5
0.8	29.06	16.364	12.791	10.016	8.8059	7.9279
1	24.995	14.071	10.998	8.609	7.5689	6.8128
1.2	21.945	12.352	9.6534	7.5559	6.642	5.9783
1.4	19.568	11.012	8.6068	6.7355	5.9207	5.3288
1.6	17.661	9.9385	7.7669	6.0773	5.343	4.8077
1.8	16.095	9.0572	7.0782	5.5377	4.8686	4.3812
2	14.786	8.3207	6.5016	5.0873	4.4715	4.0244
2.2	13.676	7.6951	6.0131	4.7043	4.1353	3.7219
2.4	12.721	7.1577	5.5932	4.3758	3.847	3.4619

Forebody Length Comparison

H'	0.5D	1.0D	1.4D	2.0D	2.5D	3.0D
0.2	-223.1	-94.68	-58.49	-30.49	-18.21	-9.353
0.4	-165.3	-70.39	-43.68	-22.94	-13.89	-7.332
0.6	-132.4	-56.46	-35.1	-18.5	-11.26	-6.009
0.8	-110.7	-47.27	-29.41	-15.52	-9.478	-5.086
1	-95.32	-40.7	-25.34	-13.39	-8.188	-4.409
1.2	-83.72	-35.76	-22.27	-11.78	-7.21	-3.89
1.4	-74.67	-31.9	-19.87	-10.51	-6.442	-3.481
1.6	-67.41	-28.8	-17.94	-9.496	-5.822	-3.149
1.8	-61.44	-26.25	-16.36	-8.66	-5.312	-2.875
2	-56.46	-24.13	-15.03	-7.96	-4.884	-2.645
2.2	-52.22	-22.32	-13.91	-7.365	-4.52	-2.449
2.4	-48.58	-20.76	-12.94	-6.853	-4.206	-2.28

Afterbody Length Comparison

H'	1.0D	2.0D	2.72D	3.0D	4.0D	5.0D
0.2	39.274	28.856	26.085	25.383	23.403	22.361
0.4	28.756	21.196	19.185	18.676	17.226	16.469
0.6	22.916	16.913	15.317	14.914	13.757	13.158
0.8	19.118	14.121	12.791	12.455	11.491	10.991
1	16.427	12.138	10.998	10.71	9.8808	9.4522
1.2	14.413	10.654	9.6534	9.401	8.6732	8.2978
1.4	12.847	9.4979	8.6068	8.3816	7.7332	7.3981
1.6	11.591	8.5698	7.7669	7.5635	6.9782	6.6768
1.8	10.561	7.8094	7.0782	6.8922	6.3591	6.0849
2	9.7002	7.174	6.5016	6.3319	5.8423	5.5899
2.2	8.9713	6.6344	6.0131	5.8565	5.4039	5.17
2.4	8.3435	6.172	5.5932	5.4474	5.0264	4.8088

Afterbody Length Comparison

H'	1.0D	2.0D	2.72D	3.0D	4.0D	5.0D
0.2	7.4487	-44.64	-58.49	-62	-69.46	-74.67
0.4	4.1788	-33.62	-43.68	-46.22	-51.57	-55.35
0.6	2.8945	-27.11	-35.1	-37.12	-41.34	-44.34
0.8	2.2211	-22.76	-29.41	-31.09	-34.59	-37.09
1	1.8083	-19.63	-25.34	-26.78	-29.78	-31.92
1.2	1.5292	-17.27	-22.27	-23.53	-26.16	-28.04
1.4	1.328	-15.42	-19.87	-21	-23.34	-25.01
1.6	1.1752	-13.93	-17.94	-18.96	-21.07	-22.58
1.8	1.0552	-12.7	-16.36	-17.29	-19.2	-20.58
2	0.9586	-11.67	-15.03	-15.88	-17.65	-18.91
2.2	0.8785	-10.8	-13.91	-14.69	-16.32	-17.49
2.4	0.8113	-10.05	-12.94	-13.67	-15.19	-16.27

Slender Results

Forebody Fullness Factor Comparison

H'	2.0	2.2	2.4	2.6
0.2	23.427	26.085	28.928	33.112
0.4	17.149	19.185	21.351	24.551
0.6	13.664	15.317	17.073	19.671
0.8	11.399	12.791	14.27	16.458
1	9.7938	10.998	12.275	14.166
1.2	8.5927	9.6534	10.778	12.444
1.4	7.6581	8.6068	9.611	11.099
1.6	6.9096	7.7669	8.6743	10.02
1.8	6.296	7.0782	7.9062	9.1345
2	5.7825	6.5016	7.2632	8.3925
2.2	5.3473	6.0131	6.7181	7.7637
2.4	4.9741	5.5932	6.2492	7.2219

Forebody Fullness Factor Comparison

H'	2	2.2	2.4	2.60
0.2	-44.62	-58.49	-73.16	-94.46
0.4	-33.08	-43.68	-54.84	-71.1
0.6	-26.5	-35.1	-44.13	-57.33
0.8	-22.17	-29.41	-37.01	-48.12
1	-19.08	-25.34	-31.9	-41.51
1.2	-16.76	-22.27	-28.05	-36.51
1.4	-14.95	-19.87	-25.03	-32.59
1.6	-13.49	-17.94	-22.61	-29.44
1.8	-12.3	-16.36	-20.62	-26.85
2	-11.3	-15.03	-18.95	-24.68
2.2	-10.45	-13.91	-17.53	-22.84
2.4	-9.725	-12.94	-16.31	-21.25

Afterbody Fullness Factor Comparison

H'	2.0	2.2	2.4	2.6	2.8	3.0
0.2	26.085	26.329	26.607	26.913	27.236	27.572
0.4	19.185	19.37	19.581	19.81	20.05	20.3
0.6	15.317	15.467	15.637	15.821	16.014	16.215
0.8	12.791	12.917	13.06	13.213	13.375	13.544
1	10.998	11.107	11.23	11.362	11.502	11.647
1.2	9.6534	9.7503	9.858	9.9744	10.096	10.224
1.4	8.6068	8.6928	8.7885	8.8919	9.0018	9.1149
1.6	7.7669	7.8442	7.9312	8.0248	8.1238	8.226
1.8	7.0782	7.1479	7.2273	7.3132	7.4025	7.496
2	6.5016	6.5669	6.6398	6.7181	6.8008	6.8868
2.2	6.0131	6.073	6.1404	6.2133	6.2895	6.3689
2.4	5.5932	5.6498	5.7118	5.7792	5.851	5.925

Afterbody Fullness Factor Comparison

H'	2	2.2	2.4	2.60	2.8	3
0.2	-58.49	-56.83	-55.08	-53.27	-51.43	-49.55
0.4	-43.68	-42.43	-41.14	-39.8	-38.43	-37.05
0.6	-35.1	-34.1	-33.06	-31.99	-30.9	-29.79
0.8	-29.41	-28.57	-27.7	-26.81	-25.89	-24.97
1	-25.34	-24.62	-23.87	-23.1	-22.31	-21.52
1.2	-22.27	-21.64	-20.98	-20.3	-19.61	-18.91
1.4	-19.87	-19.31	-18.72	-18.12	-17.5	-16.88
1.6	-17.94	-17.44	-16.91	-16.36	-15.81	-15.24
1.8	-16.36	-15.9	-15.41	-14.92	-14.41	-13.9
2	-15.03	-14.61	-14.17	-13.71	-13.24	-12.77
2.2	-13.91	-13.51	-13.1	-12.68	-12.25	-11.82
2.4	-12.94	-12.57	-12.19	-11.8	-11.4	-10.99

Slender Results

Moment Arms

L/D Comparison, varying Diameter

H'	4	6	8	9.78	12	14
0.2	0.22	0.22	0.22	0.22	0.22	0.22
0.4	0.23	0.23	0.23	0.23	0.23	0.23
0.6	0.23	0.23	0.23	0.23	0.23	0.23
0.8	0.23	0.23	0.23	0.23	0.23	0.23
1	0.23	0.23	0.23	0.23	0.23	0.23
1.2	0.23	0.23	0.23	0.23	0.23	0.23
1.4	0.23	0.23	0.23	0.23	0.23	0.23
1.6	0.23	0.23	0.23	0.23	0.23	0.23
1.8	0.23	0.23	0.23	0.23	0.23	0.23
2	0.23	0.23	0.23	0.23	0.23	0.23
2.2	0.23	0.23	0.23	0.23	0.23	0.23
2.4	0.23	0.23	0.23	0.23	0.23	0.23

L/D Comparison, varying PMB

H'	4.13	6	8	9.78	12	14
0.2	0.25	0.23	0.23	0.22	0.22	0.22
0.4	0.25	0.24	0.23	0.23	0.22	0.22
0.6	0.25	0.24	0.23	0.23	0.22	0.22
0.8	0.25	0.24	0.23	0.23	0.22	0.22
1	0.25	0.24	0.23	0.23	0.23	0.22
1.2	0.25	0.24	0.23	0.23	0.23	0.22
1.4	0.25	0.24	0.23	0.23	0.23	0.22
1.6	0.25	0.24	0.23	0.23	0.23	0.22
1.8	0.25	0.24	0.23	0.23	0.23	0.22
2	0.25	0.24	0.23	0.23	0.23	0.22
2.2	0.25	0.24	0.23	0.23	0.23	0.22
2.4	0.25	0.24	0.23	0.23	0.23	0.22

Slender Results

Forebody Length Comparison

H'	0.5D	1.0D	1.4D	2.0D	2.5D	3.0D
0.2	0.38	0.28	0.22	0.15	0.10	0.06
0.4	0.38	0.29	0.23	0.15	0.10	0.06
0.6	0.38	0.29	0.23	0.15	0.11	0.06
0.8	0.38	0.29	0.23	0.16	0.11	0.06
1	0.38	0.29	0.23	0.16	0.11	0.06
1.2	0.38	0.29	0.23	0.16	0.11	0.07
1.4	0.38	0.29	0.23	0.16	0.11	0.07
1.6	0.38	0.29	0.23	0.16	0.11	0.07
1.8	0.38	0.29	0.23	0.16	0.11	0.07
2	0.38	0.29	0.23	0.16	0.11	0.07
2.2	0.38	0.29	0.23	0.16	0.11	0.07
2.4	0.38	0.29	0.23	0.16	0.11	0.07

Afterbody Length Comparison

H'	1.0D	2.0D	2.72D	3.0D	4.0D	5.0D
0.2	-0.02	0.15	0.22	0.24	0.30	0.33
0.4	-0.01	0.16	0.23	0.25	0.30	0.34
0.6	-0.01	0.16	0.23	0.25	0.30	0.34
0.8	-0.01	0.16	0.23	0.25	0.30	0.34
1	-0.01	0.16	0.23	0.25	0.30	0.34
1.2	-0.01	0.16	0.23	0.25	0.30	0.34
1.4	-0.01	0.16	0.23	0.25	0.30	0.34
1.6	-0.01	0.16	0.23	0.25	0.30	0.34
1.8	-0.01	0.16	0.23	0.25	0.30	0.34
2	-0.01	0.16	0.23	0.25	0.30	0.34
2.2	-0.01	0.16	0.23	0.25	0.30	0.34
2.4	-0.01	0.16	0.23	0.25	0.30	0.34

Slender Results

Forebody Fullness Factor Comparison

H'	2.0	2.2	2.4	2.6
0.2	0.19	0.22	0.25	0.29
0.4	0.19	0.23	0.26	0.29
0.6	0.19	0.23	0.26	0.29
0.8	0.19	0.23	0.26	0.29
1	0.19	0.23	0.26	0.29
1.2	0.20	0.23	0.26	0.29
1.4	0.20	0.23	0.26	0.29
1.6	0.20	0.23	0.26	0.29
1.8	0.20	0.23	0.26	0.29
2	0.20	0.23	0.26	0.29
2.2	0.20	0.23	0.26	0.29
2.4	0.20	0.23	0.26	0.29

Afterbody Fullness Factor Comparison

H'	2.0	2.2	2.4	2.6	2.8	3.0
0.2	0.22	0.22	0.21	0.20	0.19	0.18
0.4	0.23	0.22	0.21	0.20	0.19	0.18
0.6	0.23	0.22	0.21	0.20	0.19	0.18
0.8	0.23	0.22	0.21	0.20	0.19	0.18
1	0.23	0.22	0.21	0.20	0.19	0.18
1.2	0.23	0.22	0.21	0.20	0.19	0.18
1.4	0.23	0.22	0.21	0.20	0.19	0.19
1.6	0.23	0.22	0.21	0.20	0.19	0.19
1.8	0.23	0.22	0.21	0.20	0.19	0.19
2	0.23	0.22	0.21	0.20	0.19	0.19
2.2	0.23	0.22	0.21	0.20	0.19	0.19
2.4	0.23	0.22	0.21	0.20	0.19	0.19

Slender Results

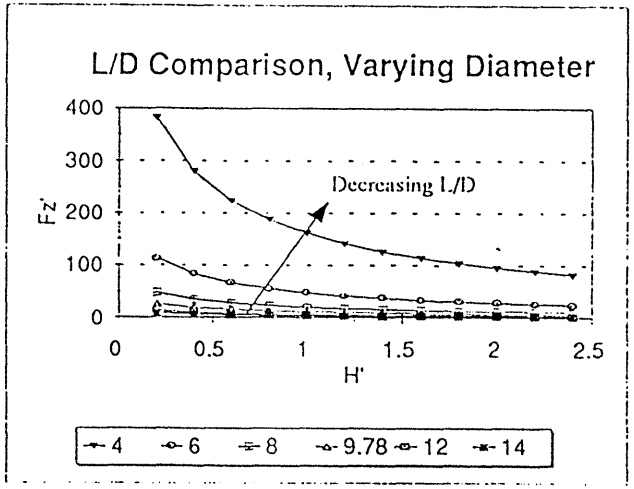

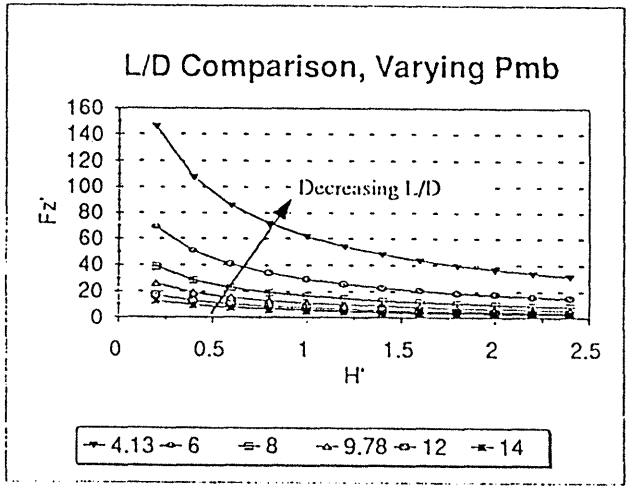

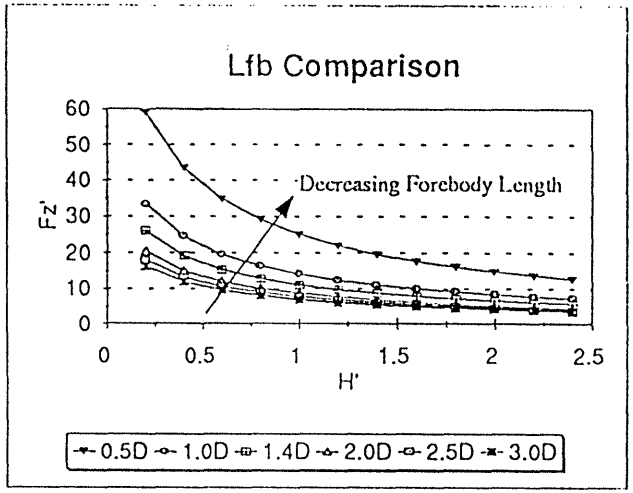

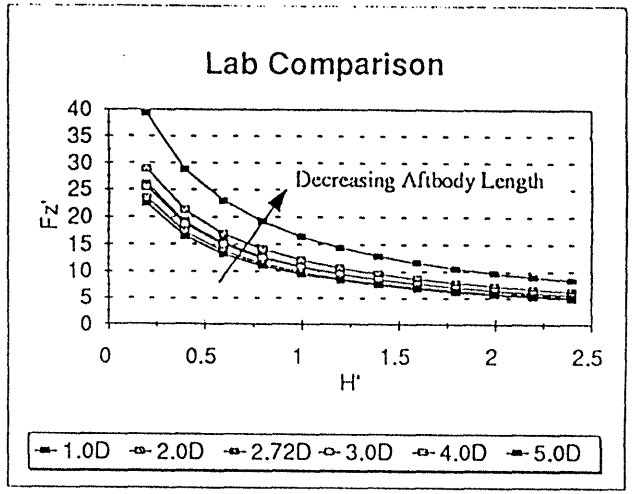

Slender Results

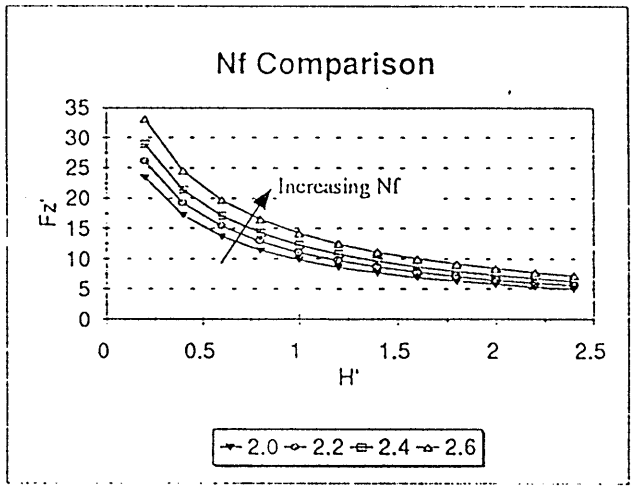

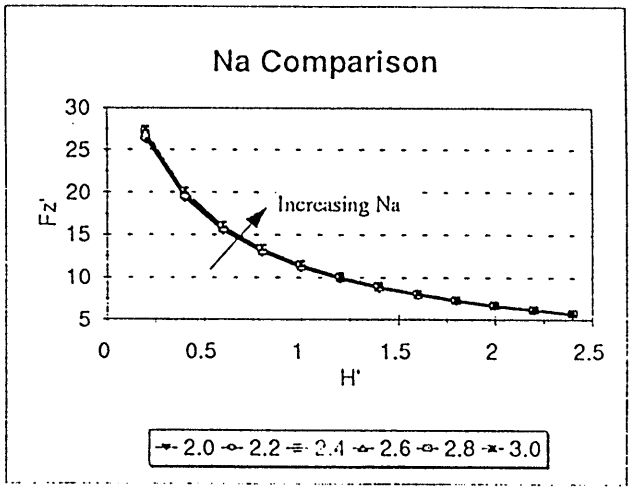

Slender Results

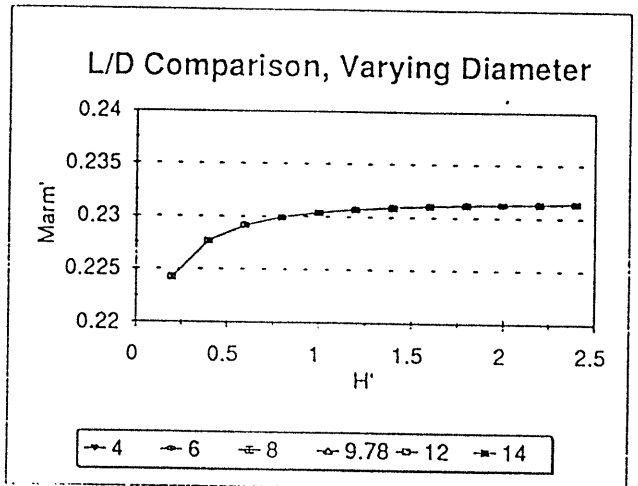

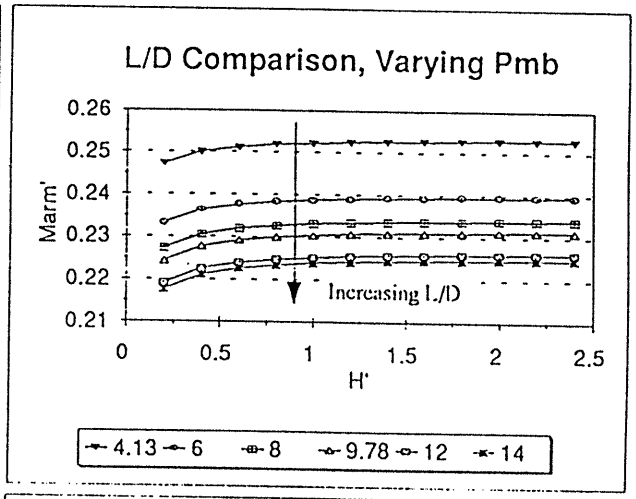

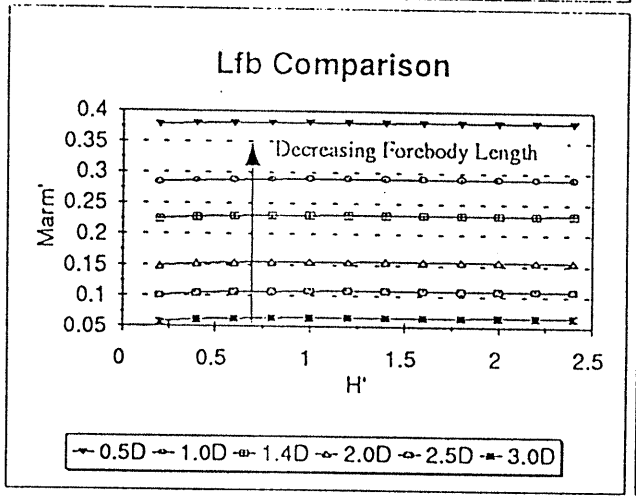

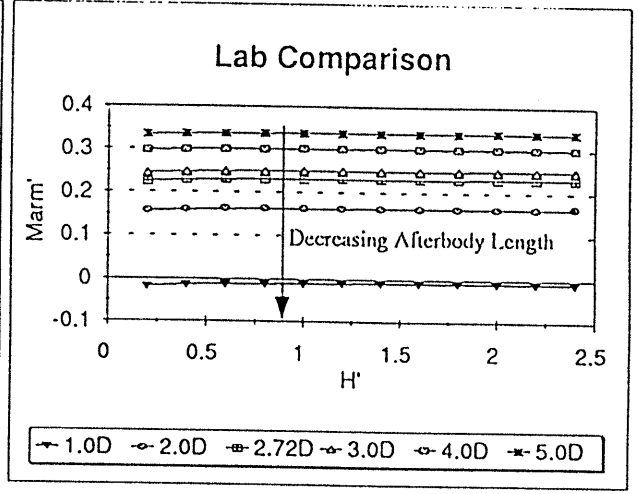

Slender Results

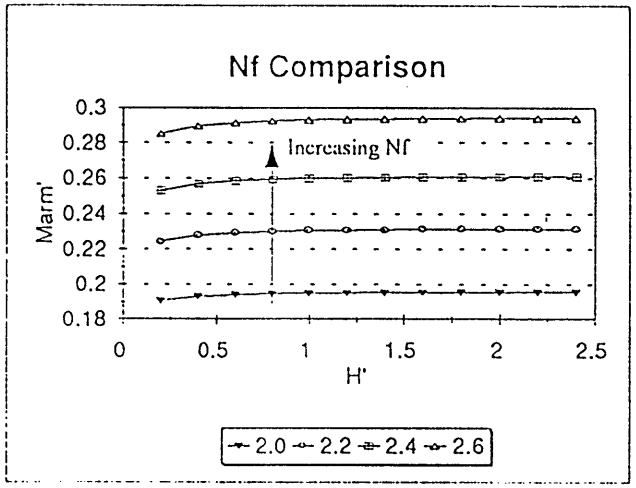

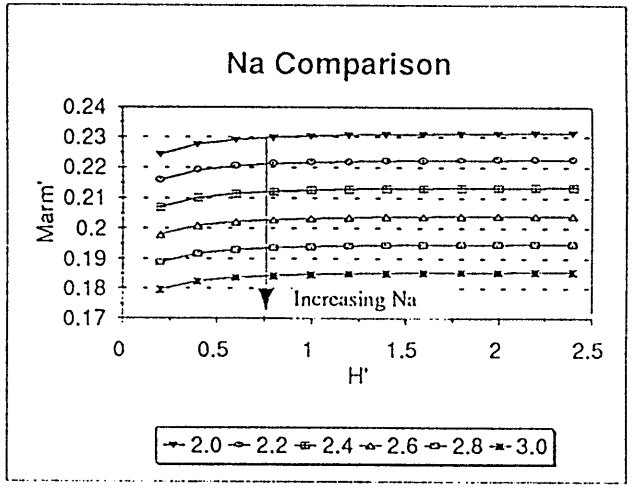

Segmented Results

Forces

L/D Comparison, varying Diameter

H'	4	6	8	9.78	12	14
0.2	139.32	60.16	31.407	19.481	11.761	7.9345
0.4	71.917	33.25	18.071	11.511	7.137	4.9121
0.6	43.129	21.148	11.878	7.7223	4.8849	3.4129
0.8	27.89	14.45	8.3631	5.5355	3.5609	2.5186
1	18.922	10.332	6.1546	4.1419	2.7047	1.9333
1.2	13.288	7.6277	4.6717	3.1942	2.115	1.5275
1.4	9.5871	5.7662	3.6305	2.5208	1.6918	1.2327
1.6	7.0728	4.4432	2.8722	2.0258	1.3774	1.0118
1.8	5.3179	3.476	2.3065	1.6515	1.1369	0.8421
2	4.0657	2.7558	1.8746	1.3621	0.9498	0.7093
2.2	3.1551	2.2107	1.5395	1.1347	0.8018	0.6038
2.4	2.4805	1.7908	1.2751	0.9531	0.6821	0.5179

L/D Comparison, varying PMB

H'	4.13	6	8	9.78	12	14
0.2	89.076	49.632	28.743	19.481	12.888	9.5181
0.4	46.02	28.215	16.87	11.511	7.6611	5.6615
0.6	27.271	18.146	11.212	7.7223	5.1727	3.8285
0.8	17.331	12.429	7.9477	5.5355	3.7355	2.771
1	11.54	8.8633	5.8689	4.1419	2.818	2.0964
1.2	7.954	6.5036	4.4602	3.1942	2.1934	1.638
1.4	5.6448	4.8813	3.4663	2.5208	1.7488	1.3114
1.6	4.0992	3.7304	2.7409	2.0258	1.4206	1.0708
1.8	3.0423	2.8947	2.1976	1.6515	1.1712	0.8881
2	2.297	2.2787	1.7828	1.3621	0.9781	0.7457
2.2	1.7655	1.8131	1.4607	1.1347	0.8256	0.6331
2.4	1.3745	1.4604	1.207	0.9531	0.7027	0.5428

Moments

L/D Comparison, varying Diameter

H'	4	6	8	9.78	12	14
0.2	-75.35	-39.23	-23.87	-16.65	-11.45	-8.593
0.4	-34.39	-18.18	-11.05	-7.671	-5.222	-3.872
0.6	-19.45	-10.67	-6.568	-4.587	-3.137	-2.33
0.8	-12.1	-6.94	-4.353	-3.068	-2.116	-1.581
1	-7.978	-4.792	-3.072	-2.188	-1.522	-1.145
1.2	-5.475	-3.442	-2.259	-1.627	-1.143	-0.865
1.4	-3.877	-2.545	-1.711	-1.248	-0.885	-0.674
1.6	-2.816	-1.925	-1.325	-0.979	-0.701	-0.537
1.8	-2.09	-1.482	-1.045	-0.782	-0.566	-0.436
2	-1.581	-1.159	-0.836	-0.634	-0.463	-0.36
2.2	-1.216	-0.919	-0.677	-0.52	-0.385	-0.3
2.4	-0.949	-0.736	-0.554	-0.432	-0.322	-0.253

L/D Comparison, varying PMB

H'	4.13	6	8	9.78	12	14
0.2	-124.7	-52.85	-26.38	-16.65	-10.05	-7.171
0.4	-57.23	-25.85	-12.6	-7.671	-4.467	-3.095
0.6	-31.59	-15.41	-7.609	-4.587	-2.641	-1.804
0.8	-19.06	-10.03	-5.085	-3.068	-1.765	-1.196
1	-12.18	-6.888	-3.601	-2.188	-1.263	-0.852
1.2	-8.133	-4.905	-2.65	-1.627	-0.945	-0.637
1.4	-5.621	-3.592	-2.007	-1.248	-0.73	-0.492
1.6	-4	-2.69	-1.552	-0.979	-0.579	-0.391
1.8	-2.919	-2.051	-1.221	-0.782	-0.467	-0.317
2	-2.173	-1.59	-0.975	-0.634	-0.383	-0.261
2.2	-1.649	-1.25	-0.787	-0.52	-0.318	-0.217
2.4	-1.274	-0.995	-0.643	-0.432	-0.267	-0.183

Segmented Results

Forebody Length Comparison

H'	1.0D	1.4D	2.0D	2.5D	3.0D
0.2	20.846	19.481	17.773	16.63	15.76
0.4	12.07	11.511	10.725	10.153	9.683
0.6	8.0074	7.7223	7.286	6.945	6.65
0.8	5.6998	5.5355	5.2679	5.046	4.847
1	4.2463	4.1419	3.9645	3.812	3.671
1.2	3.265	3.1942	3.0702	2.961	2.856
1.4	2.5719	2.5208	2.4294	2.348	2.267
1.6	2.0649	2.0258	1.9561	1.892	1.829
1.8	1.682	1.6515	1.596	1.546	1.495
2	1.3871	1.3621	1.3175	1.276	1.235
2.2	1.1554	1.1347	1.0977	1.064	1.029
2.4	0.9715	0.9531	0.9226	0.894	0.865

Afterbody Length Comparison

H'	1.0D	2.0D	2.72D	3.0D	4.0D	5.0D
0.2	22.327	20.641	19.481	19.077	17.79	16.76
0.4	12.72	12.042	11.511	11.314	10.646	10.058
0.6	8.3533	8.0117	7.7223	7.6092	7.2066	6.8226
0.8	5.9109	5.7129	5.5355	5.4637	5.1961	4.9241
1	4.3888	4.2604	4.1419	4.0918	3.9014	3.6969
1.2	3.3727	3.2802	3.1942	3.1583	3.0136	2.8537
1.4	2.6579	2.5872	2.5208	2.4925	2.3794	2.2488
1.6	2.1367	2.0791	2.0258	2.0029	1.9094	1.8017
1.8	1.7451	1.6961	1.6515	1.6319	1.5536	1.4622
2	1.4426	1.4002	1.3621	1.3458	1.2783	1.2
2.2	1.2065	1.1685	1.1347	1.1206	1.0618	0.9944
2.4	1.0172	0.9835	0.9531	0.9411	0.8899	0.8301

Forebody Length Comparison

H'	1.0D	1.4D	2.0D	2.5D	3.0D
0.2	-23.16	-16.65	-9.072	-4.364	-0.7
0.4	-10.49	-7.671	-4.077	-1.686	0.247
0.6	-6.102	-4.587	-2.538	-1.109	0.074
0.8	-3.982	-3.068	-1.782	-0.853	-0.07
1	-2.785	-2.188	-1.326	-0.687	-0.142
1.2	-2.041	-1.627	-1.021	-0.562	-0.167
1.4	-1.548	-1.248	-0.804	-0.464	-0.17
1.6	-1.204	-0.979	-0.644	-0.386	-0.16
1.8	-0.956	-0.782	-0.524	-0.323	-0.147
2	-0.771	-0.634	-0.43	-0.271	-0.131
2.2	-0.63	-0.52	-0.357	-0.229	-0.117
2.4	-0.521	-0.432	-0.299	-0.195	-0.103

Afterbody Length Comparison

H'	1.0D	2.0D	2.72D	3.0D	4.0D	5.0D
0.2	2.8914	-9.132	-16.65	-19.16	-26.83	-32.62
0.4	1.9856	-3.764	-7.671	-9.034	-13.39	-16.85
0.6	1.0549	-2.248	-4.587	-5.426	-8.178	-10.44
0.8	0.571	-1.541	-3.068	-3.625	-5.484	-7.042
1	0.3224	-1.13	-2.188	-2.577	-3.892	-5.007
1.2	0.19	-0.861	-1.627	-1.91	-2.873	-3.693
1.4	0.1164	-0.673	-1.248	-1.46	-2.184	-2.801
1.6	0.0739	-0.537	-0.979	-1.142	-1.698	-2.17
1.8	0.0485	-0.435	-0.782	-0.91	-1.345	-1.712
2	0.0327	-0.357	-0.634	-0.736	-1.081	-1.37
2.2	0.023	-0.295	-0.52	-0.602	-0.88	-1.11
2.4	0.0167	-0.247	-0.432	-0.499	-0.724	-0.909

Segmented Results

Forebody Fullness Factor Comparison

H'	2.0	2.2	2.4	2.6
0.2	19.115	19.481	19.912	19.971
0.4	11.33	11.511	11.731	11.722
0.6	7.6146	7.7223	7.8572	7.8344
0.8	5.4637	5.5355	5.6269	5.6041
1	4.0907	4.1419	4.2082	4.1886
1.2	3.1562	3.1942	3.2443	3.2291
1.4	2.4903	2.5208	2.56	2.548
1.6	2.0008	2.0258	2.0573	2.0475
1.8	1.6308	1.6515	1.6776	1.6689
2	1.3447	1.3621	1.3839	1.3774
2.2	1.1206	1.1347	1.1532	1.1478
2.4	0.9411	0.9531	0.9694	0.965

Afterbody Fullness Factor Comparison

H'	2.0	2.2	2.4	2.6	2.8	3.0
0.2	19.481	19.596	19.717	19.839	19.961	20.08
0.4	11.511	11.567	11.626	11.684	11.74	11.795
0.6	7.7223	7.755	7.7887	7.8213	7.8518	7.8822
0.8	5.5355	5.5573	5.579	5.5986	5.6182	5.6367
1	4.1419	4.1571	4.1723	4.1865	4.1995	4.2126
1.2	3.1942	3.2062	3.2182	3.2291	3.2388	3.2486
1.4	2.5208	2.5306	2.5404	2.5491	2.5567	2.5643
1.6	2.0258	2.0345	2.0421	2.0486	2.0562	2.0617
1.8	1.6515	1.658	1.6657	1.6722	1.6776	1.6831
2	1.3621	1.3687	1.3752	1.3806	1.385	1.3904
2.2	1.1347	1.1413	1.1467	1.1511	1.1554	1.1598
2.4	0.9531	0.9596	0.9639	0.9683	0.9726	0.977

Forebody Fullness Factor Comparison

H'	2	2.2	2.4	2.60
0.2	-14.68	-16.65	-18.84	-19.87
0.4	-6.708	-7.671	-8.737	-9.132
0.6	-4.024	-4.587	-5.202	-5.39
0.8	-2.706	-3.068	-3.458	-3.565
1	-1.94	-2.188	-2.451	-2.52
1.2	-1.451	-1.627	-1.813	-1.863
1.4	-1.117	-1.248	-1.383	-1.421
1.6	-0.88	-0.979	-1.08	-1.111
1.8	-0.706	-0.782	-0.859	-0.885
2	-0.574	-0.634	-0.694	-0.716
2.2	-0.472	-0.52	-0.567	-0.586
2.4	-0.392	-0.432	-0.469	-0.485

Afterbody Fullness Factor Comparison

H'	2	2.2	2.4	2.60	2.8	3
0.2	-16.65	-15.52	-14.44	-13.41	-12.43	-11.5
0.4	-7.671	-7.041	-6.447	-5.89	-5.366	-4.874
0.6	-4.587	-4.192	-3.822	-3.478	-3.158	-2.86
0.8	-3.068	-2.801	-2.552	-2.323	-2.11	-1.912
1	-2.188	-1.997	-1.821	-1.658	-1.508	-1.37
1.2	-1.627	-1.486	-1.343	-1.236	-1.126	-1.025
1.4	-1.248	-1.14	-1.041	-0.95	-0.866	-0.789
1.6	-0.979	-0.895	-0.817	-0.747	-0.682	-0.622
1.8	-0.782	-0.715	-0.654	-0.598	-0.546	-0.499
2	-0.634	-0.58	-0.53	-0.485	-0.444	-0.405
2.2	-0.52	-0.476	-0.435	-0.399	-0.365	-0.334
2.4	-0.432	-0.395	-0.362	-0.331	-0.303	-0.277

Segmented Results

Pitch Angle Comparison

H'	10	5	2.5	0	-2.5	-5	-10
0.2			19.332	19.481	33.433		
0.4		13.712	11.589	11.511	13.859	24.607	
0.6	15.175	8.6155	7.7365	7.7223	8.6482	11.265	
0.8	8.8059	5.9424	5.5236	5.5355	6.0077	7.1446	17.349
1	5.7575	4.3409	4.1223	4.1419	4.416	5.0177	8.6688
1.2	4.0755	3.2954	3.1736	3.1942	3.3672	3.7208	5.554
1.4	3.0332	2.5719	2.5012	2.5208	2.6372	2.8592	3.9145
1.6	2.3369	2.0508	2.0084	2.0258	2.1063	2.2532	2.9103
1.8	1.8463	1.6613	1.6363	1.6515	1.7092	1.8104	2.2423
2	1.4861	1.3643	1.3491	1.3621	1.4046	1.4764	1.7723
2.2	1.2152	1.1326	1.1239	1.1347	1.1674	1.2196	1.4285
2.4	1.0064	0.9498	0.9443	0.9531	0.9792	1.0172	1.1696

Pitch Angle Comparison

H'	10	5	2.5	0	-2.5	-5
0.2	0	10.257	1.0683	-16.65	-71.04	0
0.4	0	5.091	1.4125	-7.671	-21.27	-60.04
0.6	18.917	2.4384	0.2052	-4.587	-10.84	-21.81
0.8	10.959	1.141	-0.317	-3.068	-6.462	-11.54
1	5.7183	0.4797	-0.511	-2.188	-4.195	-6.951
1.2	3.1326	0.1343	-0.56	-1.627	-2.881	-4.513
1.4	1.765	-0.047	-0.545	-1.248	-2.062	-3.084
1.6	1.0013	-0.138	-0.503	-0.979	-1.525	-2.19
1.8	0.5585	-0.18	-0.452	-0.782	-1.157	-1.605
2	0.2955	-0.195	-0.401	-0.634	-0.897	-1.206
2.2	0.1376	-0.195	-0.353	-0.52	-0.709	-0.926
2.4	0.0424	-0.186	-0.309	-0.432	-0.568	-0.724

Segmented Results

Moment Arms

L/D Comparison, varying Diameter

H'	4	6	8	9.78	12	14
0.2	0.05	0.07	0.08	0.09	0.10	0.11
0.4	0.05	0.05	0.06	0.07	0.07	0.08
0.6	0.05	0.05	0.06	0.06	0.06	0.07
0.8	0.04	0.05	0.05	0.06	0.06	0.06
1	0.04	0.05	0.05	0.05	0.06	0.06
1.2	0.04	0.05	0.05	0.05	0.05	0.06
1.4	0.04	0.04	0.05	0.05	0.05	0.05
1.6	0.04	0.04	0.05	0.05	0.05	0.05
1.8	0.04	0.04	0.05	0.05	0.05	0.05
2	0.04	0.04	0.04	0.05	0.05	0.05
2.2	0.04	0.04	0.04	0.05	0.05	0.05
2.4	0.04	0.04	0.04	0.05	0.05	0.05

L/D Comparison, varying PMB

H'	4.13	6	8	9.78	12	14
0.2	0.14	0.11	0.09	0.09	0.08	0.08
0.4	0.12	0.09	0.07	0.07	0.06	0.05
0.6	0.12	0.08	0.07	0.06	0.05	0.05
0.8	0.11	0.08	0.06	0.06	0.05	0.04
1	0.11	0.08	0.06	0.05	0.04	0.04
1.2	0.10	0.08	0.06	0.05	0.04	0.04
1.4	0.10	0.07	0.06	0.05	0.04	0.04
1.6	0.10	0.07	0.06	0.05	0.04	0.04
1.8	0.10	0.07	0.06	0.05	0.04	0.04
2	0.09	0.07	0.05	0.05	0.04	0.03
2.2	0.09	0.07	0.05	0.05	0.04	0.03
2.4	0.09	0.07	0.05	0.05	0.04	0.03

Segmented Results

Forebody Length Comparison

H'	1.0D	1.4D	2.0D	2.5D	3.0D
0.2	0.11	0.09	0.05	0.03	0.00
0.4	0.09	0.07	0.04	0.02	-0.00
0.6	0.08	0.06	0.03	0.02	-0.00
0.8	0.07	0.06	0.03	0.02	0.00
1	0.07	0.05	0.03	0.02	0.00
1.2	0.06	0.05	0.03	0.02	0.01
1.4	0.06	0.05	0.03	0.02	0.01
1.6	0.06	0.05	0.03	0.02	0.01
1.8	0.06	0.05	0.03	0.02	0.01
2	0.06	0.05	0.03	0.02	0.01
2.2	0.05	0.05	0.03	0.02	0.01
2.4	0.05	0.05	0.03	0.02	0.01

Afterbody Length Comparison

H'	1.0D	2.0D	2.72D	3.0D	4.0D	5.0D
0.2	-0.01	0.04	0.09	0.10	0.15	0.19
0.4	-0.02	0.03	0.07	0.08	0.13	0.17
0.6	-0.01	0.03	0.06	0.07	0.11	0.15
0.8	-0.01	0.03	0.06	0.07	0.11	0.14
1	-0.01	0.03	0.05	0.06	0.10	0.14
1.2	-0.01	0.03	0.05	0.06	0.10	0.13
1.4	-0.00	0.03	0.05	0.06	0.09	0.12
1.6	-0.00	0.03	0.05	0.06	0.09	0.12
1.8	-0.00	0.03	0.05	0.06	0.09	0.12
2	-0.00	0.03	0.05	0.05	0.08	0.11
2.2	-0.00	0.03	0.05	0.05	0.08	0.11
2.4	-0.00	0.03	0.05	0.05	0.08	0.11

Segmented Results

Forebody Fullness Factor Comparison

H'	2.0	2.2	2.4	2.6
0.2	0.08	0.09	0.09	0.10
0.4	0.06	0.07	0.07	0.08
0.6	0.05	0.06	0.07	0.07
0.8	0.05	0.06	0.06	0.06
1	0.05	0.05	0.06	0.06
1.2	0.05	0.05	0.06	0.06
1.4	0.04	0.05	0.05	0.06
1.6	0.04	0.05	0.05	0.05
1.8	0.04	0.05	0.05	0.05
2	0.04	0.05	0.05	0.05
2.2	0.04	0.05	0.05	0.05
2.4	0.04	0.05	0.05	0.05

Afterbody Fullness Factor Comparison

H'	2.0	2.2	2.4	2.6	2.8	3.0
0.2	0.09	0.08	0.07	0.07	0.06	0.06
0.4	0.07	0.06	0.06	0.05	0.05	0.04
0.6	0.06	0.05	0.05	0.04	0.04	0.04
0.8	0.06	0.05	0.05	0.04	0.04	0.03
1	0.05	0.05	0.04	0.04	0.04	0.03
1.2	0.05	0.05	0.04	0.04	0.03	0.03
1.4	0.05	0.05	0.04	0.04	0.03	0.03
1.6	0.05	0.04	0.04	0.04	0.03	0.03
1.8	0.05	0.04	0.04	0.04	0.03	0.03
2	0.05	0.04	0.04	0.04	0.03	0.03
2.2	0.05	0.04	0.04	0.03	0.03	0.03
2.4	0.05	0.04	0.04	0.03	0.03	0.03

Segmented Results

	Pitch Angle Comparison							
-10	H'	10	5	2.5	0	-2.5	-5	-10
0	0.2			-0.01	0.09	0.21		
0	0.4		-0.04	-0.01	0.07	0.15	0.24	
0	0.6	-0.12	-0.03	-0.00	0.06	0.13	0.19	
-47.63	0.8	-0.12	-0.02	0.01	0.06	0.11	0.16	0.27
-20.08	1	-0.10	-0.01	0.01	0.05	0.09	0.14	0.23
-11.03	1.2	-0.08	-0.00	0.02	0.05	0.09	0.12	0.20
-6.753	1.4	-0.06	0.00	0.02	0.05	0.08	0.11	0.17
-4.413	1.6	-0.04	0.01	0.03	0.05	0.07	0.10	0.15
-3.021	1.8	-0.03	0.01	0.03	0.05	0.07	0.09	0.13
-2.142	2	-0.02	0.01	0.03	0.05	0.06	0.08	0.12
-1.563	2.2	-0.01	0.02	0.03	0.05	0.06	0.08	0.11
-1.169	2.4	-0.00	0.02	0.03	0.05	0.06	0.07	0.10

Segmented Results

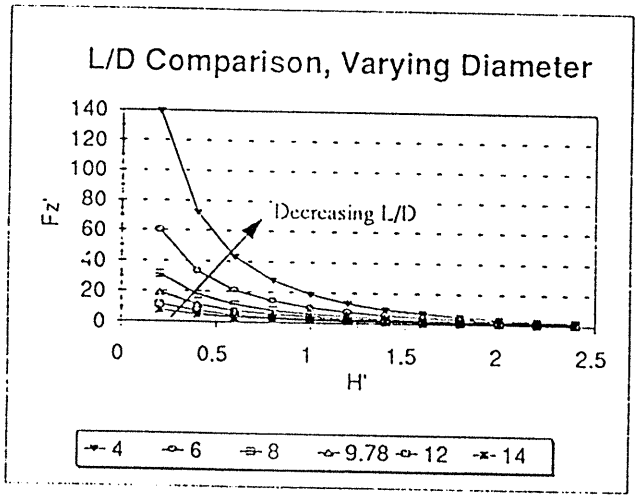

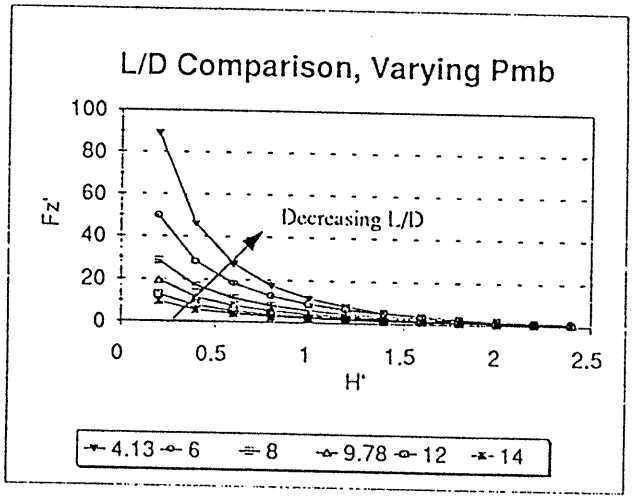

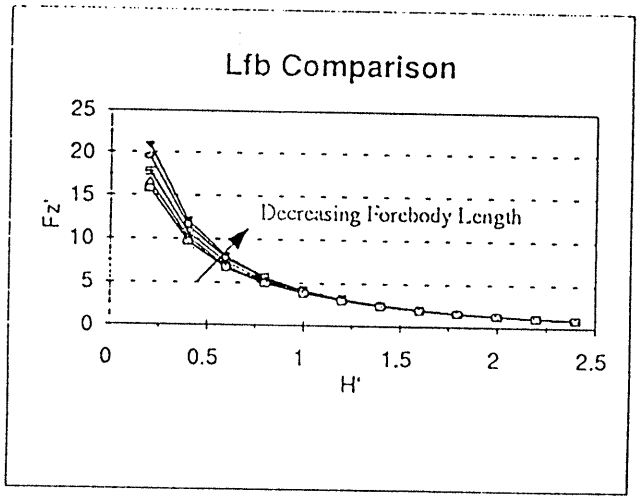

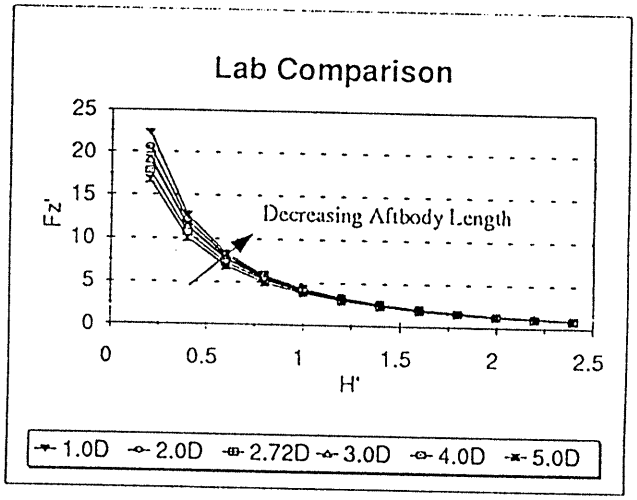

Segmented Results

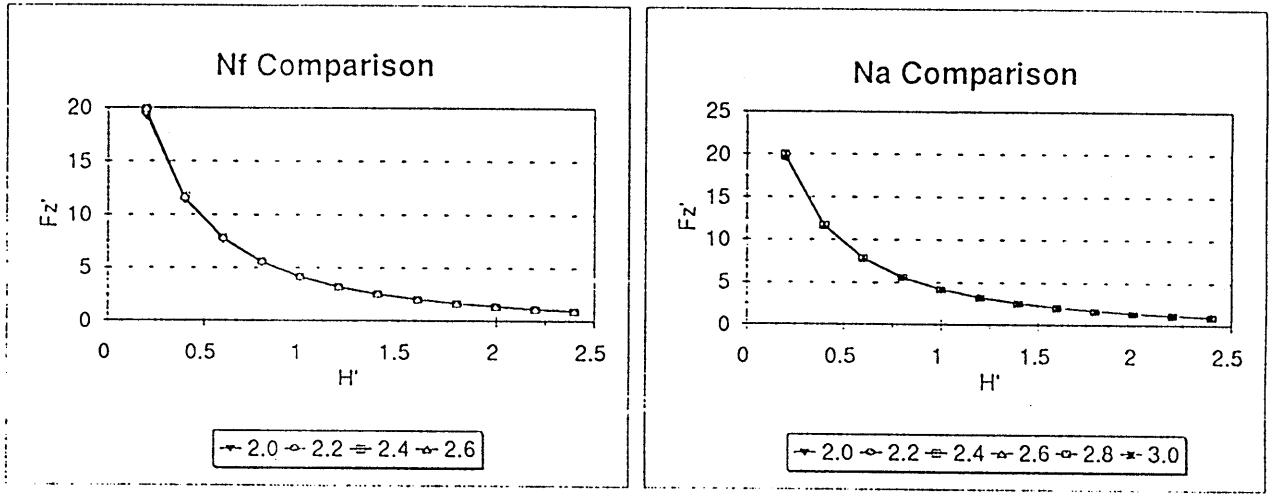

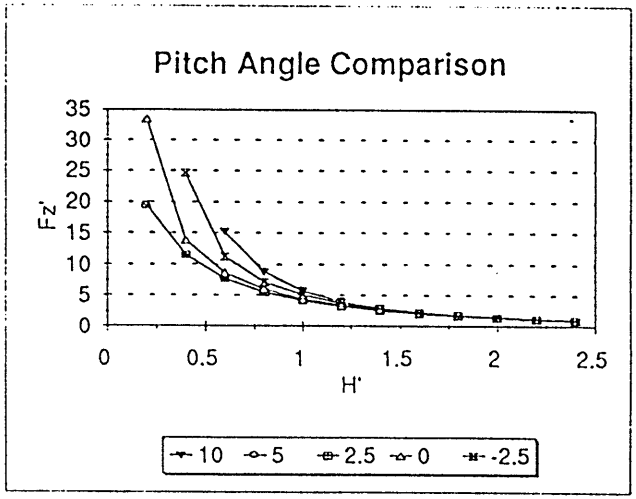

Segmented Results

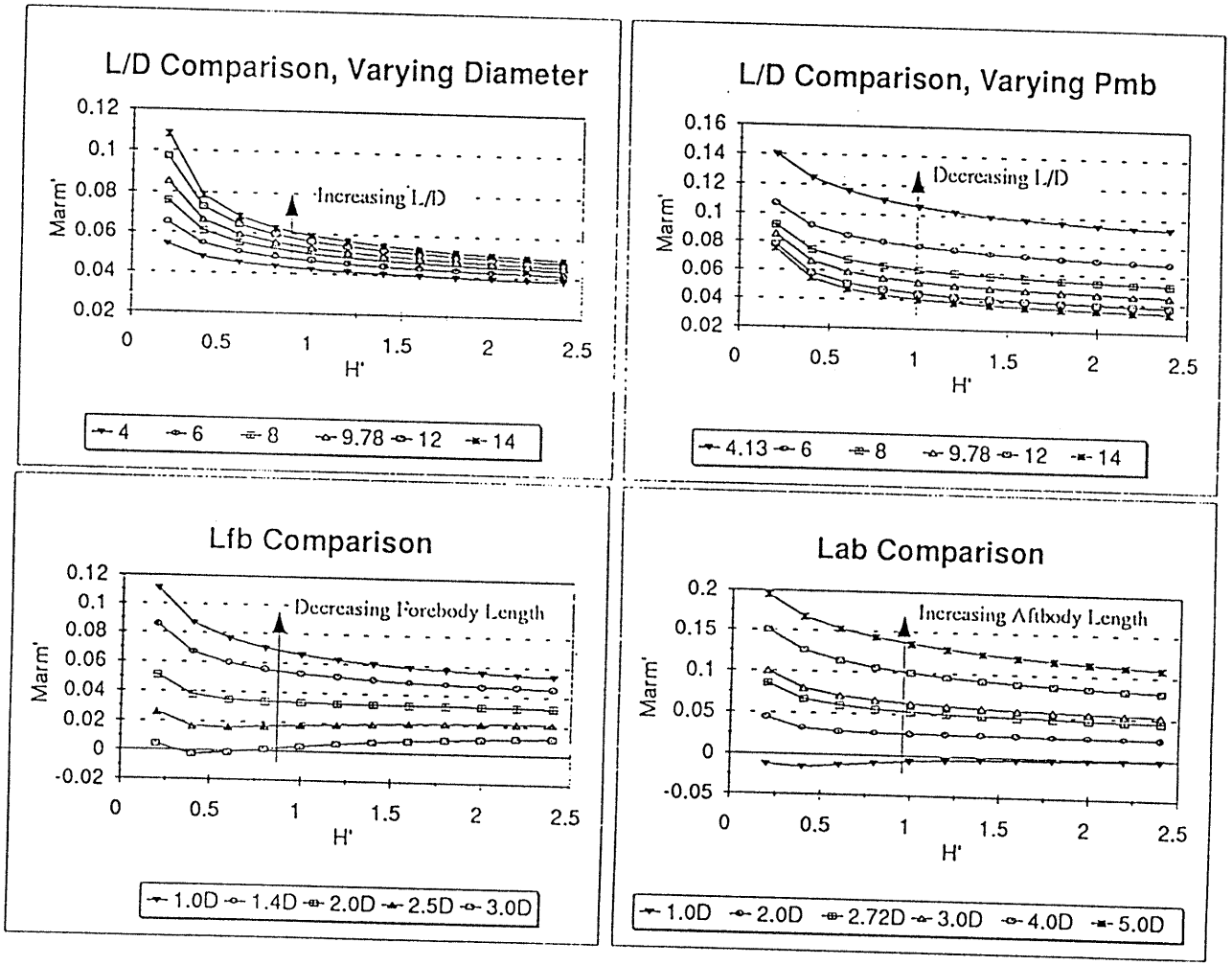

Segmented Results

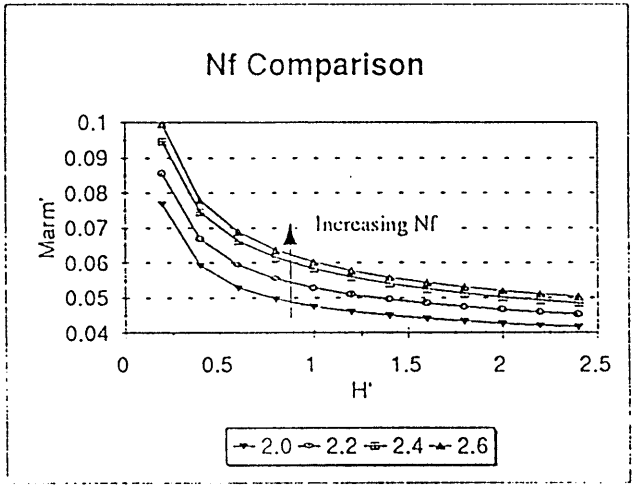

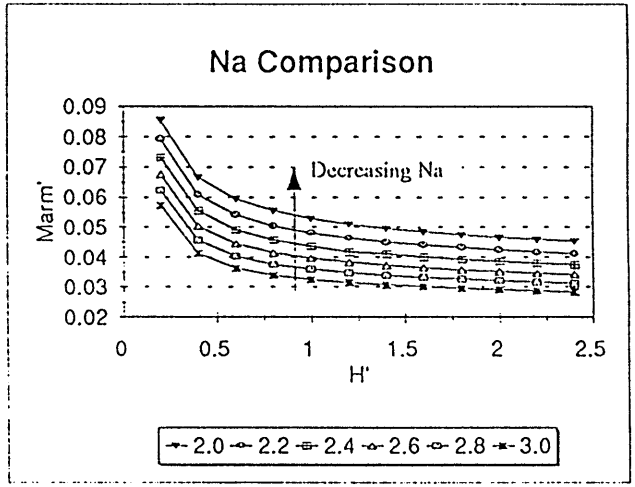

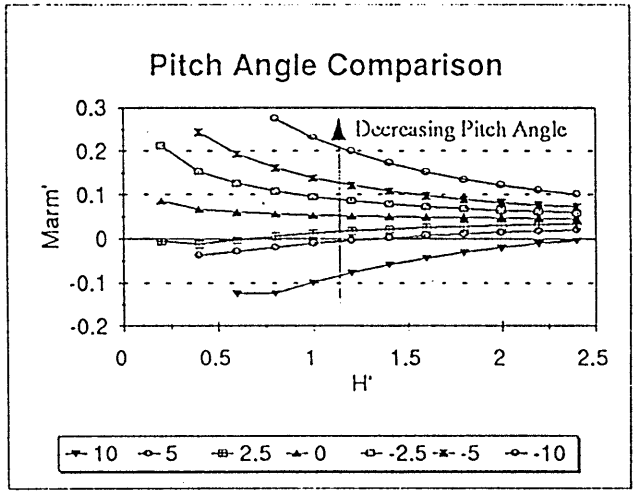

Appendix 3 : NB_OPS

The computer models discussed throughout this thesis are available in one program under the name of NB_OPS.FOR. By combining the theories into one code, the overall input and output structures were standardized.

NB_OPS.FOR requires the user to define the submarine's dimensions, it's orientation, and the analysis method desired. These values are entered through an input file which the user specified at the begining of the program. The parameters are as follows:

LENGTH	=	Overall submarine length, ft.
DIA	=	Submarine diameter, ft. (if using an elliptical body, this is the length of the semi-minor axis)
E	=	Eccentricity of submarine cross-section
LFB	=	Length of the forebody, ft.
NF	=	Forebody fullness factor
LAB	=	Length of the afterbody, ft.
NA	=	Afterbody fullness factor
FVEL	=	Forward velocity, kts.
ACCEL	=	Acceleration, kts/min.
VVEL	=	Vertical velocity, kts.
WVEL	=	Angular velocity, rad/sec.
PITCH	=	Pitch angle, deg.
METHOD	=	Evaluation method, B=baseline, S=Segmented, N=Newman's slender body theory
# HEIGHTS	=	Number of heights for evaluation
INIT HEIGHT	=	The initial non-dimensionalized height, (H/Diameter)
HT STEP	=	The increment by which to step from the initial height through the number of heights
SHAPE	=	Body Shape, R=Slender Spheroid, elliptical fore & aft; J=Jackson submarine shape

RHO	=	Water density, typically 2.0 lbf-s^2/ft^4
MAX_DATA	=	The number of evaluation points
MAX_ITER	=	The number of iterations for the correct source/dipole configuration, typically 5 is used
TSTEP =		The time step for unsteady motions

The data for each run are stored in an output file named by the user at the beginning of the program. The output format differs slightly with each method but always contains the actual and non-dimensionalized forces and moments computed for each height specified.

A listing of the computer program, NB_OPS.FOR is presented below:

```
*************************************************************************
*
*  NEAR BOTTOM OPERATIONS
*
*************************************************************************

    PROGRAM NEAR_BOT
*
*  This program simulates a submarine of user defined dimensions as it
*  operates near obstacles, i.e. the ocean bottom, a larger submarine,
*  the ocean surface. The program calculates the forces and moments which
*  arise from near bottom operations according to any of three methods;
*  baseline theory, segmented theory or slender body theory. The program
*  is also capable of handling a hull body of elliptical cross-section.
*  The submarine dimensions and control variables are entered through an
*  input file that the user is prompted for and written to a user-defined
*  output file
*
          IMPLICIT NONE
          PARAMETER PI=3.14159
          PARAMETER MAX_ARRAY=6400
          INTEGER*4 I,J,K,MAX_DATA,MAX_ITER,TSTEP,BEGINPMB,ENDPMB,
     &     FBSTATION,NUMHTS,NUMOFF
          INTEGER*4 M(0:MAX_ARRAY),MM(0:MAX_ARRAY),MFB(0:MAX_ARRAY)

          REAL*8 DIST, XMID, ZMID, X,TEMP,ICR
          REAL*8 FXPRIME,FZPRIME,MYPRIME,HPRIME,ZO_ROM, FZMAX,
FZ_FZMAX,FZSTAR,INITHT,HTSTEP

      REAL*8 LENGTH, DIA, E, LFB, NF, LAB, NA, FVEL, H, PITCH, ACCEL,
     &     VVEL, WVEL,ROW,S,FXTOTAL,FZTOTAL,MYTOTAL,FACTOR

      REAL*8 RAD1(0:MAX_ARRAY), RADP1(0:MAX_ARRAY),RAD2(0:MAX_ARRAY),
     &           RADP2(0:MAX_ARRAY), RADC(0:MAX_ARRAY),ZI(0:MAX_ARRAY),
     &     HPR(100),XVAL(500),RVAL(500),RADPP(0:MAX_ARRAY),
     &     AR(4*MAX_ARRAY),XOUT(MAX_ARRAY)

      COMMON /PARAM1/LENGTH, DIA, E, LFB, NF, LAB, NA, FVEL, H, PITCH,
     &           ACCEL,VVEL,WVEL,ROW,S,FXTOTAL,FZTOTAL,MYTOTAL
      COMMON /PARAM2/M,MM,MFB
      COMMON /PARAM3/ MAX_DATA, MAX_ITER, TSTEP, BEGINPMB,ENDPMB,
     &      FBSTATION
      COMMON /PARAM4/RAD1, RADP1, RAD2, RADP2, RADC, ZI

      CHARACTER*1 METHOD,SHAPE,DTYPE,ANS
      CHARACTER*11 INNAME, OUTNAME

C*********************************************************************

10        FORMAT(/,13(F10.3,2(/)),A1,2(/),I4,2(/),2(F10.3,2(/)),
     &     A1,2(/),F10.3,2(/),2(I4,2(/)),I4)

99    FORMAT(/,10(F10.3,2(/)),A1,2(/),I4,2(/),3(F10.3,2(/)),
     &     3(I4,2(/)),I4)

11        FORMAT(A11)
20        FORMAT(A15,2F15.5)
25        FORMAT(F15.5)
30        FORMAT(/,3A15)
35        FORMAT(3G15.8)
40        FORMAT(/,4A15)
45        FORMAT(4F15.8)
60    FORMAT(/,2A20)
65    FORMAT(2F20.5)

          WRITE(6,*) 'OFFSETS(O) OR JACKSON(J) DATA?'
          READ(6,'(A1)') DTYPE

          WRITE(6,*) 'PLEASE INPUT THE NAME OF THE INPUT FILE.'
          READ(6,11) INNAME
```

```
          WRITE(6,*) 'PLEASE INPUT THE NAME OF THE OUTPUT FILE.'
          READ(6,11) OUTNAME

          OPEN (UNIT=13, FILE=OUTNAME,STATUS='UNKNOWN')
          OPEN (UNIT=12, FILE=INNAME,STATUS='OLD')

*
* If reading in a Jackson Type submarine input file ...
*
          IF (DTYPE.EQ.'J'.OR.DTYPE.EQ.'j') THEN

       WRITE (6,*)'Reading Submarine Data ...'
       READ (12,10)LENGTH,DIA,E,LFB,NF,LAB,NA,FVEL,ACCEL,VVEL,
     &         WVEL,H,PITCH,METHOD,NUMHTS,INITHT,HTSTEP,SHAPE,
     &         ROW,MAX_DATA,MAX_ITER,TSTEP

            WRITE(13,*) 'Input data'
       WRITE(13,10)LENGTH,DIA,E,LFB,NF,LAB,NA,FVEL,ACCEL,VVEL,
     &         WVEL,H,PITCH,METHOD,NUMHTS,INITHT,HTSTEP,SHAPE,
     &         ROW,MAX_DATA,MAX_ITER,TSTEP
          ELSE

*
* If reading in an Offsets input file...
*
       WRITE(6,*)'Reading Submarine Data ...'
       READ(12,99) LENGTH,DIA,E,LFB,LAB,FVEL,ACCEL,VVEL,WVEL,PITCH,
     &          METHOD,NUMHTS,INITHT,HTSTEP,ROW,MAX_DATA,
     &          MAX_ITER,TSTEP,NUMOFF

       WRITE(13,*) 'Input Data'
       WRITE(13,99) LENGTH,DIA,E,LFB,LAB,FVEL,ACCEL,VVEL,WVEL,PITCH,
     &          METHOD,NUMHTS,INITHT,HTSTEP,ROW,MAX_DATA,
     &          MAX_ITER,TSTEP,NUMOFF

            DO J = 1,NUMOFF
                  READ(12,*) XVAL(J),RVAL(J)
      END DO
     ENDIF

*
* Set the number of points for convergence
*
          FACTOR = (NF**6.0/((LFB/LENGTH*100)**0.5))
          WRITE(6,*) 'FOREBODY FACTOR = ',FACTOR
          MAX_DATA = (INT((-395+10.5*FACTOR+4275/FACTOR)/10.))*10.
          IF (METHOD.EQ.'B') THEN
            IF (MAX_DATA.LE.50) THEN
                  MAX_DATA = 50
            ENDIF
          ENDIF
          IF (METHOD.EQ.'S') THEN
            IF (MAX_DATA.LE.100) THEN
                  MAX_DATA = 100
            ENDIF
          ENDIF
          IF (METHOD.EQ.'N') THEN
             MAX_DATA = MAX_DATA*4.0
          ENDIF
          WRITE(6,*) 'THE NUMBER OF POINTS IS : ', MAX_DATA

* Set the H' array to the heights off the bottom
          HPR(1) = INITHT
          DO J = 2, NUMHTS
            HPR(J) = HPR(J-1)+HTSTEP
          END DO

*
* Check to be sure max_data is an even number less than max_array
* Divide sub body into s segments of equal length
*
```

```
          IF (MAX_DATA .GT. MAX_ARRAY) THEN
           MAX_DATA = MAX_ARRAY
           WRITE(6,*) 'NOTE *** MAX_DATA TOO LARGE, REDUCED TO MAX_ARRAY'
           WRITE(13,*) 'NOTE *** MAX_DATA TOO LARGE, REDUCED TO
          MAX_ARRAY'
          ELSE IF (MAX_DATA/2*2 .NE. MAX_DATA) THEN
           MAX_DATA = MAX_DATA + 1
           WRITE(6,*) 'NOTE ********* MAX_DATA MUST BE AN EVEN NUMBER'
           WRITE(13,*) 'NOTE ********* MAX_DATA MUST BE AN EVEN NUMBER'
          END IF

    S = LENGTH / MAX_DATA
*
* Find the number of stations in the forebody, make it an even number
*
          FBSTATION = INT(LFB/S)
          IF (FBSTATION/2*2 .NE. FBSTATION) THEN
           FBSTATION = FBSTATION + 1
          END IF

*
* If the input is for a Jackson type hull then...
*
    IF (DTYPE.EQ.'J'.OR.DTYPE.EQ.'j') THEN
*
* Calculate offsets and slopes of submarine at axial increments of J
*
           IF (SHAPE .EQ. 'R') THEN
            WRITE(13,*) 'FORE-AFT SLENDER SPHEROIDS BEING USED'
           END IF
           DO J = 0, MAX_DATA
             DIST = S*J
             IF (DIST .GT. LFB) THEN
        IF (DIST .GT. (LENGTH-LAB)) THEN
*
* Afterbody offsets and slopes
                    IF (SHAPE .EQ. 'R') THEN  !AFTERBODY A SLNDR SPHEROID
                        X = DIST-(LENGTH-LAB)
                            IF (X .GE. LAB) THEN
                                X = LAB - S/100.
                            END IF
                        RAD1(J) = (DIA/2.0)*(1-(X/LAB)**NA)**(1/NA)
                        RADP1(J) = (DIA/2.0)*(1/LAB)**NA*(X**(NA-1)) *
  &          (1-(X/LAB)**NA)**((1/NA)-1)
                        RAD2(J)=(1-E)*RAD1(J)/(1-E**2)**0.5
                        RADP2(J)=(1-0)*RADP1(J)/(1-E**2)**0.5
                        RADC(J)=E*RAD1(J)/(1-E**2)**0.5
                    ELSE ! JACKSON AFTERBODY
                        X = DIST-(LENGTH-LAB)
                        RAD1(J) = (DIA/2.0)*(1-(X/LAB)**NA)
                        RADP1(J) = NA*DIA/2.0/(LAB)**NA*X**(NA-1)
                        RAD2(J)=(1-E)*RAD1(J)/(1-E**2)**0.5
                        RADP2(J)=(1-0)*RADP1(J)/(1-E**2)**0.5
                        RADC(J)=E*RAD1(J)/(1-E**2)**0.5
                    END IF
            ELSE
*
* Parallel middle body offsets and slopes
              RAD1(J) = DIA/2
              RADP1(J) = 0
              RAD2(J)=(1-E)*RAD1(J)/(1-E**2)**0.5
              RADP2(J)=0
              RADC(J) = E*RAD1(J)/(1-E**2)**0.5
                  ENDPMB = J+1
            END IF

           ELSE
*
* Forebody offsets and slopes
             IF (DIST .EQ. 0) THEN
                 DIST = S/100.0
```

```
                END IF
                X = LFB - DIST
                RAD1(J) = (DIA/2.0)*(1-(X/LFB)**NF)**(1/NF)
                RADP1(J) = -(DIA/2.0)*(1/LFB)**NF*(X)**(NF-1) *
     &          (1-(X/LFB)**NF)**((1/NF)-1)
                RAD2(J) = (1-E)*RAD1(J)/(1-E**2)**0.5
                RADP2(J)=-(1-0)*RADP1(J)/(1-E**2)**0.5
                RADC(J) = E*RAD1(J)/(1-E**2)**.5
                BEGINPMB = J+1
              END IF

      END DO

      ELSE
*
* If the input is given in the form of offsets...
*
            XOUT(1) = S/10.
        DO J = 2,MAX_DATA+1
            XOUT(J) = J*S-S
        ENDDO
*
* Fit a spline through the input (UGLYDK), evaluate the spline along the
* length for max_data points (EVALDK), and get the slopes by taking the
* derivative (DRIVDK)
*
            CALL UGLYDK(NUMOFF,1,4,XVAL,RVAL,1,1,AR,ICR)
        CALL EVALDK(NUMOFF,MAX_DATA,XVAL,XOUT,RAD1,AR,ICR)
        CALL DRIVDK(NUMOFF,MAX_DATA,XVAL,XOUT,RADP1,RADPP,AR,ICR)
        DO J = 0,MAX_DATA
            RAD2(J) = (1-E)*RAD1(J)/(1-E**2)**0.5
            RADP2(J)=-(1-0)*RADP1(J)/(1-E**2)**0.5
            RADC(J) = E*RAD1(J)/(1-E**2)**.5
        ENDDO
      ENDIF
*
* End of section for different input types
*


*
* If there is no pmb, correct endpmb value
*
          IF (ENDPMB .EQ. 0) THEN
            ENDPMB = BEGINPMB
          END IF

*
* Set simpson's multipliers in array M
*
          DO J = 0 , MAX_DATA
            IF (J/2 .EQ. REAL(J)/2.) THEN
              M(J) = 2
            ELSE
              M(J) = 4
            END IF
        MM(J) = M(J)
        MFB(J) = M(J)
          END DO
          M(0) = 1
          M(MAX_DATA) = 1
          DO J = FBSTATION, MAX_DATA
            IF (J/2 .EQ. REAL(J)/2.) THEN
              MM(J) = 2
            ELSE
              MM(J) = 4
            END IF
          ENDDO
      MM(FBSTATION) = 1
      MM(MAX_DATA) = 1
      MFB(0) = 1
      MFB(FBSTATION) = 1
```

```
      IF (TSTEP .EQ. 0) THEN
       WRITE(6,*) 'NOTE**TIME STEP CANT BE 0, CHANGING IT TO 60 SEC'
       TSTEP = 60
      END IF

      PITCH = PITCH * PI / 180.0      ! Convert to radians
      FVEL = 1.689 * FVEL                     ! Convert to f/s
      ACCEL = 1.689 * ACCEL/60    ! Convert to f/s^2
      FVEL = FVEL-ACCEL*TSTEP  ! Decrement speed for first time step

*
* For every height wanted, continue with the calculations
*
    DO K = 1, NUMHTS
     H = HPR(K)*DIA

*
* Adjust distance to bottom for pitched vehicle
*
      ZMID = 2*(RAD1(INT(MAX_DATA/2))*COS(PITCH) + H)
      XMID = S*INT(MAX_DATA/2)
      DO I = 0, MAX_DATA
       DIST = S*I
       ZI(I) = ZMID + 2 * ( (XMID-DIST)*SIN(PITCH) )
*
* Check for possible contact with bottom caused by pitch
*
       IF (ZI(I) .LE. 0) THEN
        WRITE(13,*) '******** ERROR: BOTTOM CONTACT *********'
        WRITE(13,*) '********  PROGRAM ABORTING  *********'
        WRITE(6,*) '******** ERROR: BOTTOM CONTACT *********'
        WRITE(6,*) '********  PROGRAM ABORTING  *********'
        STOP
       END IF
      END DO
*
* Call the appropriate subroutine and perform force calculations
*
      IF (METHOD.EQ.'N' .AND. E.EQ.0) THEN
       CALL SLENDER
      ELSE IF (METHOD.EQ.'B' .AND. E.EQ.0) THEN
       CALL BASELINE
      ELSE
       IF (METHOD.EQ.'S') THEN
        CALL SEGMENTED
       ELSE IF (E.NE.0) THEN
        CALL ECCENTRIC
       ELSE
        WRITE(6,*)'******* INVALID ANALYSIS PARAMETERS ********'
        WRITE(6,*)'*******      CHECK INPUT FILE     ********'
       END IF
      END IF

*
* Process Output
*
      HPRIME  = H/DIA
      FXPRIME = FXTOTAL*2/(ROW*LENGTH**2*FVEL**2*1E-4)
      FZPRIME = FZTOTAL*2/(ROW*LENGTH**2*FVEL**2*1E-4)
      MYPRIME = MYTOTAL*2/(ROW*LENGTH**3*FVEL**2*1E-5)
      FZMAX = 2*PI*ROW*FVEL**2*(DIA/2)**3/LENGTH
      FZ_FZMAX = FZTOTAL/FZMAX
      ZO_ROM = (H+DIA/2)/(DIA/2)
      FZSTAR = FZTOTAL*2/(ROW*(LFB+LAB)**2*FVEL**2*1E-4)

      WRITE(13,40)'H','FXTOTAL','FZTOTAL','MYTOTAL'
      WRITE(13,45)H,FXTOTAL,FZTOTAL,MYTOTAL
      WRITE(6,40)'H','FXTOTAL','FZTOTAL','MYTOTAL'
      WRITE(6,45)H,FXTOTAL,FZTOTAL,MYTOTAL
```

```
            WRITE(13,40)'HPRIME','FXPRIME','FZPRIME','MYPRIME'
            WRITE(13,45)HPRIME,FXPRIME,FZPRIME,MYPRIME
            WRITE(6,40)'HPRIME','FXPRIME','FZPRIME','MYPRIME'
            WRITE(6,45)HPRIME,FXPRIME,FZPRIME,MYPRIME

            WRITE(13,40)'Z0_ROM','FZMAX','FZSTAR','FZ_FZMAX'
            WRITE(13,45) ZO_ROM,FZMAX,FZSTAR,FZ_FZMAX
            WRITE(6,40)'Z0_ROM','FZMAX','FZSTAR','FZ_FZMAX'
            WRITE(6,45) ZO_ROM,FZMAX,FZSTAR,FZ_FZMAX

     END DO

     END

*************************************************************************
*
*  SUBROUTINE SLENDER
*
*************************************************************************

          SUBROUTINE SLENDER

          IMPLICIT NONE
          PARAMETER PI=3.14159
          PARAMETER MAX_ARRAY=6400

          INTEGER*4 J,MAX_DATA,MAX_ITER,TSTEP,BEGINPMB,ENDPMB,FBSTATION
          INTEGER*4 M(0:MAX_ARRAY), MM(0:MAX_ARRAY), MFB(0:MAX_ARRAY)

          REAL*8 Z, X, LENGTH, DIA, E,LFB,NF, LAB, NA, FVEL, H, PITCH,
     &       ACCEL,VVEL,WVEL,ROW,S,FXTOTAL,FZTOTAL,MYTOTAL,
     &       FSUM,MSUM

     REAL*8 RAD1(0:MAX_ARRAY),RADP1(0:MAX_ARRAY),RAD2(0:MAX_ARRAY),
     &                 RADP2(0:MAX_ARRAY),RADC(0:MAX_ARRAY),ZI(0:MAX_ARRAY),
     &      FZ(0:MAX_ARRAY),MY(0:MAX_ARRAY)

          CHARACTER*1 ANS

          COMMON /PARAM1/LENGTH, DIA, E, LFB, NF, LAB, NA, FVEL, H, PITCH,
     &                 ACCEL,VVEL,WVEL,ROW,S,FXTOTAL,FZTOTAL,MYTOTAL
          COMMON /PARAM2/M,MM,MFB
     COMMON /PARAM3/ MAX_DATA, MAX_ITER, TSTEP, BEGINPMB,ENDPMB,
     &          FBSTATION
     COMMON /PARAM4/RAD1, RADP1, RAD2, RADP2, RADC, ZI

*************************************************************************

C 30      FORMAT(/,3A15)
C 35      FORMAT(3G15.6)

          WRITE(13,*)
          WRITE(13,*) '******* NEWMAN"S METHOD *******'
          WRITE(13,*)

          FXTOTAL = 0
          FZTOTAL = 0
          MYTOTAL = 0
          Z = (DIA/2+H)


          DO J=0,MAX_DATA
            X=LENGTH/2-J*S
            FZ(J)=PI*ROW*FVEL**2.*((RAD1(J)*RADP1(J))**2/
     &      (Z**2-RAD1(J)**2)**0.5)*M(J)
            MY(J)=-PI*ROW*FVEL**2.*((RAD1(J)*RADP1(J))**2/
     &      (Z**2-RAD1(J)**2)**0.5)*X*M(J)
            FSUM = FZ(J)/M(J)/2.594 + FSUM
            MSUM = MY(J)/M(J)/2.594 + MSUM
       FZTOTAL = FZ(J) + FZTOTAL
            MYTOTAL = MY(J) + MYTOTAL
```

```
        END DO
        CLOSE(15)

        FSUM = FSUM/MAX_DATA
        MSUM = MSUM/MAX_DATA

        FZTOTAL=FZTOTAL*S/3  !TO CORRECT FOR SIGN CONVENTION
        MYTOTAL=MYTOTAL*S/3

  RETURN
  END

*************************************************************************
*
*  SUBROUTINE BASELINE
*
*************************************************************************

        SUBROUTINE BASELINE

        IMPLICIT NONE
        PARAMETER PI=3.14159
        PARAMETER MAX_ARRAY=6400

        INTEGER*4 I, J,L,P,MAX_DATA,MAX_ITER,TSTEP, TIME_LOOP,BEGINPMB,
     &     ENDPMB,FBSTATION
        INTEGER*4 M(0:MAX_ARRAY), MM(0:MAX_ARRAY), MFB(0:MAX_ARRAY)

        REAL*8 LENGTH, DIA, E, LFB, NF, LAB, NA, FVEL, H, PITCH, ACCEL,
     &              PPHIXZA, PPHIZZA, PPHIXZ1, PPHIZZ1,UU1,WW1,R,X,Z,
     &              FXTOTAL,FZTOTAL,MYTOTAL,SOURCESUM,DIPOLESUM,TEMP,
     &     FSUM,MSUM

  REAL*8  S,ROW,STREAMA,STREAMB,POTENTIALA,POTENTIALB,
     &     DSOURCE,DDIPOLE,DDIPOLEW,DW,VVEL,WVEL,UQA1,UQN1,
     &     DUQNDT

        REAL*8 PHIXZ(0:MAX_ARRAY), PHIZZ(0:MAX_ARRAY),
     &              SOURCE(0:MAX_ARRAY), SOURCE0(0:MAX_ARRAY),
     &              DIPOLE(0:MAX_ARRAY), DIPOLE0(0:MAX_ARRAY),
     &              U(0:MAX_ARRAY), U2(0:MAX_ARRAY),
     &              W(0:MAX_ARRAY), W2(0:MAX_ARRAY)

  REAL*8  XI(0:MAX_ARRAY), XJ(0:MAX_ARRAY),
     &              FX(0:MAX_ARRAY), FZ(0:MAX_ARRAY),MY(0:MAX_ARRAY),
     &              RAD1(0:MAX_ARRAY),RADP1(0:MAX_ARRAY),RAD2(0:MAX_ARRAY),
     &              RADP2(0:MAX_ARRAY),RADC(0:MAX_ARRAY), ZI(0:MAX_ARRAY),
     &     DIPOLEV(0:MAX_ARRAY),DIPOLEW(0:MAX_ARRAY),
     &     W0(0:MAX_ARRAY), DIPOLEW0(0:MAX_ARRAY)

  REAL*8 FXSS(0:MAX_ARRAY),FXTR(0:MAX_ARRAY),FZSS(0:MAX_ARRAY),
     &     FZTR(0:MAX_ARRAY),MYSS(0:MAX_ARRAY),MYTR(0:MAX_ARRAY),
     &     MYO(0:MAX_ARRAY), WM(0:MAX_ARRAY), WD(0:MAX_ARRAY),
     &     UQA(0:MAX_ARRAY), UQN(0:MAX_ARRAY),UQN0(0:MAX_ARRAY)

        CHARACTER*1 ANS

        COMMON /PARAM1/LENGTH, DIA, E, LFB, NF, LAB, NA, FVEL, H, PITCH,
     &              ACCEL,VVEL,WVEL,ROW,S,FXTOTAL,FZTOTAL,MYTOTAL
        COMMON /PARAM2/M,MM,MFB
  COMMON /PARAM3/ MAX_DATA, MAX_ITER, TSTEP, BEGINPMB,ENDPMB,
     &        FBSTATION
  COMMON /PARAM4/RAD1, RADP1, RAD2, RADP2, RADC, ZI

*************************************************************************
30      FORMAT(/,3A15)
35      FORMAT(3E15.5)
40      FORMAT(/,4A15)
45      FORMAT(4F15.5)
60   FORMAT(/,2A20)
```

```
65    FORMAT(2F20.5)

          WRITE(13,*)
          WRITE(13,*) '******* BASELINE METHOD *******'
          WRITE(13,*)

          IF (ACCEL .NE. 0) THEN
           TIME_LOOP = 1
          ELSE
           TIME_LOOP = 0
          END IF
          DO L =0,TIME_LOOP
*
* Loop for initial and accelerated source strengths
*
            IF (L.NE.0) THEN                    ! Not initial time step
              FVEL=FVEL+ACCEL*TSTEP             ! Then increment speed
              VVEL=VVEL+ACCEL*TSTEP
            END IF

            DO J= 0, MAX_DATA
              SOURCE(J) = -FVEL*RAD1(J)*RADP1(J)/2
       END DO

            DO J = 0, MAX_DATA
              U2(J) = 0
              W2(J) = 0
              DIPOLE(J) = 0
              DIPOLEV(J) = 0
         DIPOLEW(J) = 0
            END DO
*
* Iteration loop
*
            DO P=1, MAX_ITER

              DO I=0, MAX_DATA
                XI(I) = LENGTH/2 - I*S
                WW1 = 0
                      DO J=0, MAX_DATA
                        XJ(J) = LENGTH/2 - J*S
                        X = (XI(I) - XJ(J)) * COS(PITCH)
                        Z = ZI(I) - (XI(I) - XJ(J)) * SIN(PITCH)
                        R = (X**2 + (Z-RAD1(I))**2)**.5
                        IF (R**5 .NE. 0) THEN
                          WW1 = ((-(DIPOLE(J)+DIPOLEW(J)+DIPOLEV(J)) +
  &           SOURCE(J)*(Z-RAD1(I)))/R**3 +
  &                     (3*(DIPOLE(J)+DIPOLEW(J)+DIPOLEV(J))*
  &           (Z-RAD1(I))**2)/R**5)*M(J)+WW1
                UQA1 = (WM(I)*(Z-RAD1(I))/R**3. +
  &           (3*WD(I)*X*(Z-RAD1(I))/R**5.)) *M(J)+UQA1
                        UQN1 = (WM(I)*(Z-RAD1(I))/R**3. +
  &           (3*WD(I)*(Z-RAD1(I))**2./R**5.))*M(J)+UQN1
                        END IF
                END DO
                      W(I) = S*WW1/3
           UQA(I) = S*UQA1/3.
                      UQN(I) = S*UQN1/3.
              END DO

              DO I=0, MAX_DATA
                DIPOLE(I) = W(I)*RAD1(I)**2./2.
                DIPOLEV(I) = VVEL*RAD1(I)**2./2.
                      DIPOLEW(I) = 2*WVEL*(LENGTH/2.-I*S)*RAD1(I)**2.
           WM(I)= UQA(I)*RAD1(I)*RADP1(I)/2.
                      WD(I) = UQN(I)*RAD1(I)**2./2.
              END DO

              DO I=0, MAX_DATA
                UU1 = 0
                WW1 = 0
```

```
                DO J=0, MAX_DATA
              X = (XI(I)-XJ(J)) * COS(PITCH)
                Z = ZI(I) - (XI(I) - XJ(J)) * SIN(PITCH)
                R = (X**2 + Z**2) **.5
                IF (R**5 .NE. 0) THEN
          UU1 = (SOURCE(J)*X/R**3 +
&           (3*(DIPOLE(J)+DIPOLEV(J)+DIPOLEW(J))*Z*X)/
&           (R**5))*M(J)+UU1
          WW1 = ((-(DIPOLE(J)+DIPOLEV(J)+DIPOLEW(J))+
&           SOURCE(J)*Z)/R**3 +
&           (3*(DIPOLE(J)+DIPOLEV(J)+DIPOLEW(J))*
&           (Z**2))/(R**5))*M(J)+WW1
          UQA1 = (WM(I)*Z/R**3. +
&           (3*WD(I)*X*Z/R**5.)) *M(J)+UQA1
                  UQN1 = (WM(I)*Z/R**3. +
&           (3*WD(I)*Z**2./R**5.))*M(J)+UQN1

                END IF
            END DO
            U(I) = S*UU1/3.
            W(I) = S*WW1/3.
        UQA(I) = S*UQA1/3.
                UQN(I) = S*UQN1/3.
          END DO

          DO J = 0, BEGINPMB
            SOURCE(J) = -(FVEL-U(J))*RAD1(J)*RADP1(J)/2
          END DO
          DO J = ENDPMB, MAX_DATA
            SOURCE(J) = -(FVEL-U(J))*RAD1(J)*RADP1(J)/2
          END DO

        END DO                                          ! P loop

        IF (L.EQ.0) THEN   ! First time, save source,dipole
          WRITE(6,*) 'INITIAL TIME STEP'

          DO J = 0, MAX_DATA
            SOURCE0(J) = SOURCE(J)
            DIPOLE0(J) = DIPOLE(J)
                UQN0(J) = UQN0(J)
                DIPOLEW0(J) = DIPOLEW(J)
          END DO

        ELSE
          WRITE(6,*) 'FINAL TIME STEP'
        END IF

      END DO                                                ! L LOOP
        SOURCESUM = 0
        DIPOLESUM = 0
    DO J = 0,MAX_DATA
          SOURCESUM = SOURCESUM + SOURCE(J)
          DIPOLESUM = DIPOLESUM + DIPOLE(J)
    END DO
        WRITE(6,60)'SOURCESUM','DIPOLESUM'
        WRITE(6,65) SOURCESUM, DIPOLESUM
        WRITE(13,60)'SOURCESUM','DIPOLESUM'
        WRITE(13,65) SOURCESUM, DIPOLESUM
*
* Cross flow velocity calculations
*
        DO I=0, MAX_DATA
          UU1 = 0
          WW1 = 0
          DO J=0, MAX_DATA
            X = (XI(I) - XJ(J)) * COS(PITCH)
            Z = ZI(I) - (XI(I) - XJ(J)) * SIN(PITCH)
            R = (X**2 + Z**2) **.5
      UU1 = (SOURCE(J)*X/R**3 +
&       (3*(DIPOLE(J)+DIPOLEV(J)+DIPOLEW(J))*Z*X)/
```

```
     &      (R**5))*M(J)+UU1
            WW1 = ((-(DIPOLE(J)+DIPOLEV(J)+DIPOLEW(J))+
     &      SOURCE(J)*Z)/R**3 +
     &      (3*(DIPOLE(J)+DIPOLEV(J)+DIPOLEW(J))*
     &      (Z**2))/(R**5))*M(J)+WW1
            UQA1 = (WM(I)*Z/R**3. +
     &      (3*WD(I)*X*Z/R**5.)) *M(J)+UQA1
            UQN1 = (WM(I)*Z/R**3. +
     &      (3*WD(I)*Z**2./R**5.))*M(J)+UQN1

              END DO
              U(I) = S*UU1/3.
              W(I) = S*WW1/3.
          UQA(I) = S*UQA1/3.
              UQN(I) = S*UQN1/3.
            END DO

            DO I=0, MAX_DATA
              PHIXZ(I) = 0
              PHIZZ(I) = 0
              PPHIXZA = 0
              PPHIZZA = 0
              DO J=0, MAX_DATA
                X = (XI(I) - XJ(J)) * COS(PITCH)
                Z = ZI(I) - (XI(I) - XJ(J)) * SIN(PITCH)
                R = (X**2 + Z**2)**.5
                PPHIXZ1 = -3*X*(SOURCE(J)*Z-(DIPOLE(J)+DIPOLEV(J)+
     &        DIPOLEW(J)))/R**5
           PPHIXZA = (PPHIXZ1 - 15*(DIPOLE(J)+DIPOLEV(J)+
     &        DIPOLEW(J))*X*Z**2/R**7)*M(J) + PPHIXZA
                PPHIZZ1 = -3*Z*(SOURCE(J)*Z - 3*(DIPOLE(J)+DIPOLEV(J)+
     &        DIPOLEW(J)))/ R**5
           PPHIZZA = (PPHIZZ1 + SOURCE(J)/R**3-15*(DIPOLE(J)+
     &        DIPOLEV(J)+DIPOLEW(J))*Z**3/R**7)*M(J)+PPHIZZA
              END DO

              PHIXZ(I) = S/3.*PPHIXZA
              PHIZZ(I) = S/3.*PPHIZZA
            END DO

            FXTOTAL = 0
            FZTOTAL = 0
            MYTOTAL = 0

            DO I=0,MAX_DATA
              DSOURCE = (SOURCE(I)-SOURCE0(I))/TSTEP
              DDIPOLE = (DIPOLE(I)-DIPOLE0(I))/TSTEP
              DDIPOLEW = (DIPOLEW(I)-DIPOLEW0(I))/TSTEP
              DUQNDT = (UQN(I)-UQN0(I))/TSTEP

              FXSS(I) = (-4*PI*ROW*(SOURCE(I)*U(I)+
     &         (-DIPOLE(I)-DIPOLEV(I)-DIPOLEW(I))*PHIXZ(I)))*M(I)
              FXTR(I) = -4*PI*ROW*XI(I)*DSOURCE*M(I)
              FX(I) = FXSS(I) + FXTR(I)
C       FX(I) = -4*PI*ROW*(SOURCE(I)*U(I)+(-DIPOLE(I))*PHIXZ(I) +
C     &        XI(I)*(SOURCE(I)-SOURCE0(I))/TSTEP)*M(I)
              FZSS(I) = (-4*PI*ROW*(SOURCE(I)*W(I)+
     &         (-DIPOLE(I)-DIPOLEV(I)-DIPOLEW(I))*PHIZZ(I)))*M(I)
              FZTR(I) = -4*PI*ROW*DDIPOLE*M(I)
              FZ(I) = FZSS(I) + FZTR(I)

C             FZ(I) = -4*PI*ROW*(SOURCE(I)*W(I) + (-DIPOLE(I))*PHIZZ(I)+
C     &        (DIPOLE(I)-DIPOLE0(I))/TSTEP)*M(I)
              MYSS(I) =XI(I)*FZSS(I) +
     &        4*PI*ROW*((U(I)*(-DIPOLEW(I)-DIPOLEV(I))) -
     &        DIPOLE(I)*(U(I)-FVEL))*M(I)
          MYTR(I) = 4*PI*ROW*(-DIPOLEW(I)*DUQNDT+UQN(I)*DDIPOLEW)*M(I)
          MY(I) = MYSS(I) + MYTR(I)
              MYO(I) = (XI(I)*FZ(I)) + 4*PI*ROW*(-DIPOLE(I))*U(I)*M(I)

              FSUM = -FZ(I)/M(I) + FSUM
```

```
            MSUM = MY(I)/M(I) + MSUM

            FXTOTAL = FX(I) + FXTOTAL
            FZTOTAL = FZ(I) + FZTOTAL
            MYTOTAL = MY(I) + MYTOTAL
          END DO

          FSUM = FSUM/MAX_DATA
          MSUM = MSUM/MAX_DATA

          FXTOTAL =  FXTOTAL*S/3
          FZTOTAL = -FZTOTAL*S/3                    ! TO CORRECT SIGN CONVENTION
          MYTOTAL =  MYTOTAL*S/3

    RETURN
    END

*************************************************************************
*
* SUBROUTINE SEGMENTED
*
*************************************************************************

    SUBROUTINE SEGMENTED

          IMPLICIT NONE

          PARAMETER PI = 3.14159
          PARAMETER  MAX_ARRAY = 6400

          INTEGER*4 I, J, L, P, MAX_DATA, MAX_ITER, TSTEP,BEGINPMB,
     &       ENDPMB,FBSTATION
          INTEGER*4 M(0:MAX_ARRAY), MM(0:MAX_ARRAY), MFB(0:MAX_ARRAY)

          REAL*8 LENGTH,DIA,E,LFB,NF,LAB,NA,FVEL,H,PITCH,ACCEL,ROW,S,
     &       FZTOTAL, MY1TOTAL, MY2TOTAL, MYTOTAL,
     &              FBVIRTMASS,FBLOVRD, EFB, M33PRIME, BETA,FBAVGACC,FBVOL,
     &       FBCENTR, FBMASS,SOURCESUM, DIPOLESUM,R,X,Z,
     &       DDQZ1DZ,DDQZ2DZ, DDQZ2DY, DDQZ1DX,UU1,UU2,VV2,WW1,WW2,
     &       FXTOTAL,FZMAX, FZ1TOTAL, FZ2TOTAL,VVEL,WVEL

          REAL*8  DQZ1DZ(0:MAX_ARRAY), DQZ2DZ(0:MAX_ARRAY),
     &       DQZ2DY(0:MAX_ARRAY),DQZ1DX(0:MAX_ARRAY),
     &       SOURCE1(0:MAX_ARRAY),SOURCE2(0:MAX_ARRAY),
     &       DIPOLEZ1(0:MAX_ARRAY),DIPOLEZ2(0:MAX_ARRAY),
     &       DIPOLEY2(0:MAX_ARRAY),U1(0:MAX_ARRAY), U2(0:MAX_ARRAY),
     &              V2(0:MAX_ARRAY), W1(0:MAX_ARRAY), W2(0:MAX_ARRAY),
     &              XI(0:MAX_ARRAY),XJ(0:MAX_ARRAY),FZ1(0:MAX_ARRAY),
     &       FZ2(0:MAX_ARRAY), MY1(0:MAX_ARRAY),MY2(0:MAX_ARRAY),
     &              RAD1(0:MAX_ARRAY), RADP1(0:MAX_ARRAY), RAD2(0:MAX_ARRAY),
     &              RADP2(0:MAX_ARRAY),RADC(0:MAX_ARRAY),ZI(0:MAX_ARRAY)

          CHARACTER*1 ANS

          COMMON /PARAM1/LENGTH, DIA, E, LFB, NF, LAB, NA, FVEL, H, PITCH,
     &              ACCEL,VVEL,WVEL,ROW,S,FXTOTAL,FZTOTAL,MYTOTAL
          COMMON /PARAM2/M,MM,MFB
      COMMON /PARAM3/ MAX_DATA, MAX_ITER, TSTEP, BEGINPMB,ENDPMB,
     &        FBSTATION
      COMMON /PARAM4/RAD1, RADP1, RAD2, RADP2, RADC, ZI

C*************************************************************************

 20       FORMAT(2F15.5,A15)
 30       FORMAT(/,3A15)
 35       FORMAT(3F15.5)
 40       FORMAT(/,4A15)
 45       FORMAT(4F15.5)
 50       FORMAT(/,5A15)
 55    FORMAT(5F15.5)
 60       FORMAT(/,2A20)
```

```
65      FORMAT(2F20.5)

        WRITE(13,*)
        WRITE(13,*) '******* SEGMENTED METHOD *******'
        WRITE(13,*)


*
* Find nondim. added mass of forebody hemiellipsoid.  use lamb's article 115
* but take the average of result and 1, which is the nondim. added mass of a
* cylinder.
*
        FBLOVRD =(2*LFB*(1-E**2)**.5)/DIA
        EFB = (1 -(1/FBLOVRD)**2)**.5
        BETA = 1/EFB**2 - (1-EFB**2)/(2*EFB**3) * LOG((1+EFB)/(1-EFB))
        M33PRIME = BETA / (2-BETA)
        M33PRIME = (M33PRIME+1)/2

c       WRITE(13,40)'FOREBODY L/D','ECCENTRICITY','BETA','M33PRIME'
c       WRITE(13,45)FBLOVRD,EFB,BETA,M33PRIME

*
* Size initial source strengths
*
        DO J = 0, MAX_DATA
     SOURCE1(J) = -FVEL*RAD1(J)*RADP1(J)*(1 - E**2/(2*(1-E**2)))
  &    /(2-E**2)

         U1(J) = 0
         U2(J) = 0
         V2(J) = 0
         W1(J) = 0
         W2(J) = 0
         DIPOLEZ1(J) = 0
         DIPOLEZ2(J) = 0
         DIPOLEY2(J) = 0
        END DO
*
* Start iteration on source and dipole strengths
*
        DO P=1, MAX_ITER
*
* Calculate cross flow velocities on body axis
*
        DO I=0, MAX_DATA
          XI(I) = LENGTH/2 - I*S
          VV2 = 0
          DO J=0, MAX_DATA
            XJ(J) = LENGTH/2 - J*S
            X = (XI(I) - XJ(J)) * COS(PITCH)
            R = (X**2 + (RADC(I)-RAD2(I))**2)**.5
            IF ((R**3) .NE. 0.0) THEN
                  VV2 = (SOURCE1(J)*(RADC(I)-RAD2(I)))/R**3*M(J)+VV2
            END IF
          END DO
          V2(I) = S*VV2/3
        END DO

        DO I=0, MAX_DATA
          WW1 = 0
          WW2 = 0
          DO J=0, MAX_DATA
            X = (XI(I) - XJ(J)) * COS(PITCH)
            Z = ZI(I) - (XI(I) - XJ(J)) * SIN(PITCH)
            R = (X**2 + (RAD1(I)-Z)**2)**.5
            IF ((R**5) .NE. 0) THEN
                  WW1 = ((-DIPOLEZ1(J) + SOURCE1(J)*(RAD1(I)-Z))/R**3 +
  &                        (3*DIPOLEZ1(J)*((RAD1(I)-Z)**2)) / (R**5) +
  &                        2*(-DIPOLEZ2(J)+SOURCE2(J)*(RAD1(I)-Z)) /
  &                        (R**2 + RADC(I)**2)**(3/2) +
  &                        (6*DIPOLEZ2(J)*((RAD1(I)-Z)**2)) /
```

```
     &                          (R**2 + RADC(I)**2)**(5/2))*M(J) + WW1
               END IF
             END DO
             W1(I) = S*WW1/3
           END DO
*
* Size dipoles
*
           DO I=0, MAX_DATA
             DIPOLEZ1(I) = W1(I)*RAD1(I)**2/2
           END DO
*
* Calculate induced axial velocities U1 & U2
*
           DO I=0, MAX_DATA
             UU1 = 0
             DO J=0, MAX_DATA
               X = (XI(I) - XJ(J)) * COS(PITCH)
               Z = ZI(I) - (XI(I) - XJ(J)) * SIN(PITCH)
               R = (X**2 + RADC(I)**2) **.5
               IF ((R**5) .NE. 0) THEN
          UU1 = (SOURCE2(J)*X/R**3 + (3*DIPOLEY2(J)*(-RADC(I)*X))
     &            /(R**5) +SOURCE1(J)*X/(X**2 +Z**2)**(3.0/2.0)+
     &            3*DIPOLEZ1(J)*(-Z)*X/(X**2 + Z**2)**(5.0/2.0)+
     &                          2*SOURCE2(J)*X/(R**2 + Z**2)**(3.0/2.0) +
     &                          6*DIPOLEZ2(J)*(-Z)*X/(R**2 + Z**2)**(5.0/2.0))
     &                          *M(J) + UU1
               END IF
             END DO
             U1(I) = S*UU1/3
           END DO
*
* ADJUST SOURCE STRENGTHS
*
           DO J = 0, MAX_DATA
        SOURCE1(J) = -(FVEL-U1(J))*RAD1(J)*RADP1(J)*(1 - E**2/
     &       (2*(1-E**2)))/(2-E**2)
           END DO

           END DO                                    ! End of iteration (p loop)
*
* Calculate cross flow velocities at surface of body W1,W2,U1,U2
*

           DO I = 0,MAX_DATA
             WW1 = 0
             DO J=0, MAX_DATA
               X = (XI(I) - XJ(J)) * COS(PITCH)
               Z = ZI(I) - (XI(I) - XJ(J)) * SIN(PITCH)
               R = (X**2 + (-Z)**2)**.5
               IF ((R**5) .NE. 0) THEN
                     WW1 = ((-DIPOLEZ1(J) + SOURCE1(J)*(-Z))/R**3 +
     &                          (3*DIPOLEZ1(J)*((-Z)**2)) / (R**5) +
     &                          2*(-DIPOLEZ2(J)+SOURCE2(J)*(-Z)) /
     &                          (R**2 + RADC(I)**2)**(3/2) +
     &                          (6*DIPOLEZ2(J)*((-Z)**2)) /
     &                          (R**2 + RADC(I)**2)**(5/2))*M(J) + WW1
               END IF
             END DO
             W1(I) = S*WW1/3
           END DO

           DO I=0, MAX_DATA
             UU1 = 0
             DO J=0, MAX_DATA
               X = (XI(I) - XJ(J)) * COS(PITCH)
               Z = ZI(I) - (XI(I) - XJ(J)) * SIN(PITCH)
               R = (X**2 + RADC(I)**2) **.5
               IF ((R**2) .NE. 0) THEN
                     UU1 = (SOURCE1(J)*X/(X**2 + Z**2)**(3.0/2.0) +
     &                          3*DIPOLEZ1(J)*(-Z)*X/(X**2 + Z**2)**(5.0/2.0) +
```

```
     &                          2*SOURCE2(J)*X/(R**2 + Z**2)**(3.0/2.0) +
     &                          6*DIPOLEZ2(J)*(-Z)*X/(R**2 + Z**2)**(5.0/2.0))
     &                          *M(J) + UU1
               END IF
             END DO
             U1(I) = S*UU1/3
           END DO

           WRITE(6,*) 'STARTING FORCE CALCULATIONS'
*
* Calculate velocity gradients
*
           DO I=0,MAX_DATA
             DQZ1DX(I) = 0
             DQZ1DZ(I) = 0
             DDQZ1DX = 0
             DDQZ1DZ = 0
             DO J=0, MAX_DATA
               X = (XI(I) - XJ(J)) * COS(PITCH)
               Z = ZI(I) - (XI(I) - XJ(J)) * SIN(PITCH)
               R = (X**2 + Z**2)**.5
               DDQZ1DX = (-3*(-DIPOLEZ1(J) + SOURCE1(J)*(-Z)*X)/R**5 -
     &                          (15*DIPOLEZ1(J)*((-Z)**2)*X) / (R**7) -
     &                          6*(-DIPOLEZ2(J)+SOURCE2(J)*(-Z)*X) /
     &                          (R**2 + RADC(I)**2)**(5.0/2.0) -
     &                          (30*DIPOLEZ2(J)*((-Z)**2)*X)/
     &                          (R**2 + RADC(I)**2)**(7.0/2.0)) *M(J) + DDQZ1DX
               DDQZ1DZ = (SOURCE1(J)/R**3 + 3*Z*(3*DIPOLEZ1(J) -
     &                          Z*SOURCE1(J))/R**5 - 15*Z**3*DIPOLEZ1(J)/R**7 +
     &                          2*SOURCE2(J)/(R**2 + RADC(I)**2)**(3.0/2.0) +
     &                          3*Z*(6*DIPOLEZ2(J) - 2*Z*SOURCE2(J))/
     &                          (R**2 + RADC(I)**2)**(5.0/2.0) -
     &            30*Z**3*DIPOLEZ2(J)/(R**2 + RADC(I)**2)**
     &            (7.0/2.0)) *M(J) + DDQZ1DZ
             END DO
             DQZ1DX(I) = S/3*DDQZ1DX
             DQZ1DZ(I) = S/3*DDQZ1DZ
           END DO

*
* Calculate force and moment for all but forebody
*
           FZ1TOTAL = 0
           FZ2TOTAL = 0
           MY1TOTAL = 0
           MY2TOTAL = 0

           DO I=FBSTATION,MAX_DATA
         FZ1(I) = 2*PI*ROW*RAD1(I)**2/(1-E**2)**.5*
     &      (W1(I)*DQZ1DZ(I) +
     &                  (U1(I)-FVEL)*DQZ1DX(I))*MM(I)
             MY1(I) = -XI(I)*FZ1(I)

             FZ1TOTAL = FZ1(I) + FZ1TOTAL
             MY1TOTAL = MY1(I) + MY1TOTAL
           END DO

           FZ1TOTAL = FZ1TOTAL*S/3
           MY1TOTAL = MY1TOTAL*S/3
*
* Calculate forebody force and moment terms
*
           FBAVGACC = 0.0
           FBVOL = 0.0
           FBCENTR = 0.0
           FBMASS = 0.0
           FBVIRTMASS = 0.0

           DO I=0,FBSTATION
         FBAVGACC = W1(I)*DQZ1DZ(I) + (U1(I)-FVEL)*DQZ1DX(I) +
     &     FBAVGACC
```

```
            FBVOL =  PI*RAD1(I)**2/(1-E**2)**.5*MFB(I) + FBVOL
            FBCENTR = PI*RAD1(I)**2/(1-E**2)**.5*MFB(I)*S*I + FBCENTR
          END DO

          FBAVGACC = FBAVGACC/(FBSTATION+1)
          FBMASS = ROW*FBVOL*S/3
          FBCENTR = FBCENTR/FBVOL
          FBVIRTMASS = (1 + M33PRIME) * FBMASS

c         WRITE(13,30)'FBSTATION','FBVOL','FBAVGACC'
c         WRITE(13,35)REAL(FBSTATION),FBVOL,FBAVGACC
c         WRITE(13,30)'FBCENTR','FBMASS','FBVIRTMASS'
c         WRITE(13,35)FBCENTR,FBMASS,FBVIRTMASS

*
* Add forebody force and moment to the rest of the body
*

          WRITE(13,40) 'PARTIAL VALUES',' PMB & AB','FZTOTAL','MYTOTAL'
          WRITE(13,45) 0.0,0.0,FZ1TOTAL,MY1TOTAL

          FZ1TOTAL = FZ1TOTAL + FBAVGACC*FBVIRTMASS
          MY1TOTAL = MY1TOTAL - FBAVGACC*FBVIRTMASS*(LENGTH/2-FBCENTR)

          FZTOTAL = FZ1TOTAL + 2*FZ2TOTAL
          MYTOTAL = MY1TOTAL + 2*MY2TOTAL

    RETURN
    END

*************************************************************************
*
* SUBROUTINE ECCENTRIC
*
*************************************************************************

    SUBROUTINE ECCENTRIC

          IMPLICIT NONE
          PARAMETER PI=3.14159
          PARAMETER MAX_ARRAY=6400

          INTEGER*4 I, J, L,P,MAX_DATA,MAX_ITER,TSTEP,BEGINPMB,
     &       ENDPMB,FBSTATION
          INTEGER*4 M(0:MAX_ARRAY), MM(0:MAX_ARRAY), MFB(0:MAX_ARRAY)

     REAL*8  LENGTH,DIA,E,LFB,NF,LAB,NA,FVEL,H,PITCH,ACCEL,S,ROW,
     &       DDQZ1DZ, DDQZ2DZ, DDQZ2DY,UU1,UU2,VV1,WW1,WW2,
     &       FZMAX, FZ1TOTAL, FZ2TOTAL, FZTOTAL,
     &       MY1TOTAL, MY2TOTAL, MYTOTAL,FZPRIME, MYPRIME, HPRIME,
     &       FXTOTAL,R, X, Z,POTENTIALA,POTENTIALB,STREAMA,STREAMB
      REAL*8 VVEL,WVEL

          REAL*8 DQZ1DZ(0:MAX_ARRAY),DQZ2DZ(0:MAX_ARRAY),
     &       DQZ2DY(0:MAX_ARRAY),SOURCE1(0:MAX_ARRAY),
     &       SOURCE2(0:MAX_ARRAY), DIPOLEZ1(0:MAX_ARRAY),
     &       DIPOLEZ2(0:MAX_ARRAY),DIPOLEY2(0:MAX_ARRAY),
     &       U1(0:MAX_ARRAY), U2(0:MAX_ARRAY), V2(0:MAX_ARRAY),
     &       W1(0:MAX_ARRAY), W2(0:MAX_ARRAY),XI(0:MAX_ARRAY),
     &       XJ(0:MAX_ARRAY),FZ1(0:MAX_ARRAY),FZ2(0:MAX_ARRAY),
     &       MY1(0:MAX_ARRAY),MY2(0:MAX_ARRAY),
     &       RAD1(0:MAX_ARRAY), RADP1(0:MAX_ARRAY), RAD2(0:MAX_ARRAY),
     &       RADP2(0:MAX_ARRAY),RADC(0:MAX_ARRAY), ZI(0:MAX_ARRAY)

          CHARACTER*1 ANS

          COMMON /PARAM1/LENGTH, DIA, E, LFB, NF, LAB, NA, FVEL, H, PITCH,
     &                ACCEL,VVEL,WVEL,ROW,S,FXTOTAL,FZTOTAL,MYTOTAL
          COMMON /PARAM2/M,MM,MFB
      COMMON /PARAM3/ MAX_DATA, MAX_ITER, TSTEP, BEGINPMB,ENDPMB,
     &          FBSTATION
```

```
      COMMON /PARAM4/RAD1, RADP1, RAD2, RADP2, RADC, ZI

C*********************************************************************
 20         FORMAT(A15,2F15.5)
 30         FORMAT(/,3A15)
 35         FORMAT(3F15.5)
 40         FORMAT(/,4A15)
 45         FORMAT(4F15.5)
 50         FORMAT(/,5A15)
 55    FORMAT(5F15.5)
 60         FORMAT(/,2A20)
 65         FORMAT(2F20.5)

            WRITE(13,*) 'ORIGINAL SOURCES :'
            DO J = 0, MAX_DATA
       SOURCE1(J) = -FVEL*RAD1(J)*RADP1(J)*(1 - E**2/(2*(1-E**2)))/
     &    (2-E**2)
             SOURCE2(J) = -FVEL*RAD1(J)*RADP1(J)/2 - SOURCE1(J)
             WRITE(13,*) J, SOURCE1(J), SOURCE2(J)
             U1(J) = 0
             U2(J) = 0
             V2(J) = 0
             W1(J) = 0
             W2(J) = 0
             DIPOLEZ1(J) = 0
             DIPOLEZ2(J) = 0
             DIPOLEY2(J) = 0
            END DO

            DO P=1, MAX_ITER

             WRITE(6,*) 'STARTING ITERATION # = ',P
             DO I=0, MAX_DATA
                      XI(I) = LENGTH/2 - I*S
                      VV1 = 0
                      DO J=0, MAX_DATA
                               XJ(J) = LENGTH/2 - J*S
                               X = XI(I) - XJ(J)
                               R = (X**2 + (RADC(I)-RAD2(I))**2)**.5
                               IF ((R**3) .NE. 0.0) THEN
               VV1 = (SOURCE1(J)*(RADC(I)-RAD2(I)))/
     &                 R**3*M(J) + VV1
                               END IF
                      END DO
                      V2(I) = S*VV1/3
             END DO

             DO I=0, MAX_DATA
              WW1 = 0
              WW2 = 0
              DO J=0, MAX_DATA
                      X = (XI(I) - XJ(J))*COS(PITCH)
                      Z = ZI(I) - (XI(I) - XJ(J))*SIN(PITCH)
                      R = (X**2 + (RAD1(I)-Z)**2)**.5
                      IF ((R**5) .NE. 0) THEN
                       WW1 = ((-DIPOLEZ1(J) + SOURCE1(J)*(Z-RAD1(I)))/R**3 +
     &                               (3*DIPOLEZ1(J)*((Z-RAD1(I))**2)) / (R**5) +
     &                               2*(-DIPOLEZ2(J)+SOURCE2(J)*(RAD1(I)-Z)) /
     &           (R**2 + RADC(I)**2)**(3/2) +
     &                               (6*DIPOLEZ2(J)*((RAD1(I)-Z)**2))/
     &           (R**2 + RADC(I)**2)**(5/2))*M(J) + WW1
                      END IF
                      R = (X**2 + (RAD2(I)-Z)**2)**.5
                      IF ((R**5) .NE. 0) THEN
                       WW2 = ((-DIPOLEZ2(J) + SOURCE2(J)*(RAD2(I)-Z))/R**3 +
     &                               (3*DIPOLEZ2(J)*((RAD2(I)-Z)**2)) / (R**5) +
     &                               (-DIPOLEZ1(J)+SOURCE1(J)*(RAD2(I)-Z)) /
     &                               (R**2 + RADC(I)**2)**(3.0/2.0) +
     &                               (3*DIPOLEZ1(J)*((RAD2(I)-Z)**2))/
     &                               (R**2 + RADC(I)**2)**(5.0/2.0) +
     &                               (-DIPOLEZ2(J) + SOURCE2(J)*(RAD2(I)-Z))/
```

```
&                          (R**2 + 4*RADC(I)**2)**(3.0/2.0) +
&                          (3*DIPOLEZ2(J)*((RAD2(I)-Z)**2)) /
&                          (R**2 + 4*RADC(I)**2)**(5.0/2.0) +
&                          (DIPOLEY2(J)*(2*RADC(I))*(RAD2(I)-Z)) /
&                          (R**2 + 4*RADC(I)**2)**(5.0/2.0))*M(J) + WW2
                END IF
            END DO
            W1(I) = S*WW1/3
            W2(I) = S*WW2/3
          END DO

          DO I=0, MAX_DATA
            IF (E .NE. 0) THEN
                DIPOLEY2(I) = V2(I)*RAD2(I)**2/2
                DIPOLEZ2(I) = W2(I)*RAD2(I)**2/2
            END IF
            DIPOLEZ1(I) = W1(I)*RAD1(I)**2/2
          END DO

          DO I=0, MAX_DATA
            UU1 = 0
            UU2 = 0
            DO J=0, MAX_DATA
                X = (XI(I) - XJ(J))*COS(PITCH)
                Z = ZI(I) - (XI(I) - XJ(J))*SIN(PITCH)
                R = (X**2 + RADC(I)**2) **.5
                IF ((R**5) .NE. 0) THEN
        UU1 = (SOURCE2(J)*X/R**3 + (3*DIPOLEY2(J)*
&           (-RADC(I))*X)/(R**5) +
&                          SOURCE1(J)*X/(X**2 + Z**2)**(3.0/2.0) +
&                          3*DIPOLEZ1(J)*(-Z)*X/(X**2 + Z**2)**(5.0/2.0) +
&                          2*SOURCE2(J)*X/(R**2 + Z**2)**(3.0/2.0) +
&                          6*DIPOLEZ2(J)*(-Z)*X/(R**2 + Z**2)**(5.0/2.0))
&                          *M(J) + UU1
                 UU2 = (SOURCE1(J)*X/R**3 +
&                          SOURCE2(J)*X/(X**2 + Z**2)**(3.0/2.0) +
&                          3*DIPOLEZ2(J)*(-Z)*X/(X**2 + Z**2)**(5.0/2.0) +
&                          SOURCE1(J)*X/(R**2 + Z**2)**(3.0/2.0) +
&                          3*DIPOLEZ1(J)*(-Z)*X/(R**2 + Z**2)**(5.0/2.0) +
&           SOURCE2(J)*X/(X**2 + 4*RADC(I) + Z**2)**
&           (3.0/2.0) +3*DIPOLEZ2(J)*(-Z)*X/(X**2+4*RADC(I)
&           +Z**2)**(5.0/2.0) +
&           3*DIPOLEY2(J)*2*RADC(I)*X/(X**2+4*RADC(I)+Z**2)
&           **(5.0/2.0))*M(J) + UU2
                END IF
    END DO
        U1(I) = S*UU1/3
        U2(I) = S*UU2/3
        END DO

         DO J = 0, MAX_DATA
    SOURCE1(J) = -(FVEL-U1(J))*RAD1(J)*RADP1(J)*(1 - E**2/
&     (2*(1-E**2)))/(2-E**2)
          SOURCE2(J) = -(FVEL-U1(J))*RAD1(J)*RADP1(J)/2 - SOURCE1(J)
         END DO
        END DO                                  ! P LOOP

        DO I=0, MAX_DATA
          WW1 = 0
          WW2 = 0
          DO J=0, MAX_DATA
                X = (XI(I) - XJ(J))*COS(PITCH)
                Z = ZI(I) - (XI(I) - XJ(J))*SIN(PITCH)
                R = (X**2 + (-Z)**2)**.5
                IF ((R**5) .NE. 0) THEN
                 WW1 = ((-DIPOLEZ1(J) + SOURCE1(J)*(-Z))/R**3 +
&                          (3*DIPOLEZ1(J)*((-Z)**2)) / (R**5) +
&                          2*(-DIPOLEZ2(J)+SOURCE2(J)*(-Z)) /
&           (R**2 + RADC(I)**2)**(3/2) +
&                          (6*DIPOLEZ2(J)*((-Z)**2))/
&           (R**2 + RADC(I)**2)**(5/2))*M(J) + WW1
```

```
                END IF
                R = (X**2 + (-Z)**2)**.5
                IF ((R**5) .NE. 0) THEN
                 WW2 = ((-DIPOLEZ2(J) + SOURCE2(J)*(-Z))/R**3 +
&                       (3*DIPOLEZ2(J)*((-Z)**2)) / (R**5) +
&                       (-DIPOLEZ1(J)+SOURCE1(J)*(-Z)) /
&                       (R**2 + RADC(I)**2)**(3.0/2.0) +
&                       (3*DIPOLEZ1(J)*((-Z)**2))/
&                       (R**2 + RADC(I)**2)**(5.0/2.0) +
&                       (-DIPOLEZ2(J) + SOURCE2(J)*(-Z))/
&                       (R**2 + 4*RADC(I)**2)**(3.0/2.0) +
&                       (3*DIPOLEZ2(J)*((-Z)**2)) /
&                       (R**2 + 4*RADC(I)**2)**(5.0/2.0) +
&                       (DIPOLEY2(J)*(2*RADC(I))*(-Z)) /
&                       (R**2 + 4*RADC(I)**2)**(5.0/2.0))*M(J) + WW2
                END IF
          END DO
          W1(I) = S*WW1/3
          W2(I) = S*WW2/3
        END DO

        DO I=0, MAX_DATA
          UU1 = 0
          UU2 = 0
          DO J=0, MAX_DATA
                X = (XI(I) - XJ(J))*COS(PITCH)
                Z = ZI(I) - (XI(I) - XJ(J))*SIN(PITCH)
                R = (X**2 + RADC(I)**2) **.5
                IF ((R**2) .NE. 0) THEN
                 UU1 = (SOURCE1(J)*X/(X**2 + Z**2)**(3.0/2.0) +
&                       3*DIPOLEZ1(J)*(-Z)*X/(X**2 + Z**2)**(5.0/2.0) +
&                       2*SOURCE2(J)*X/(R**2 + Z**2)**(3.0/2.0) +
&                       6*DIPOLEZ2(J)*(-Z)*X/(R**2 + Z**2)**(5.0/2.0))
&                       *M(J) + UU1
                 UU2 = (SOURCE2(J)*X/(X**2 + Z**2)**(3.0/2.0) +
&                       3*DIPOLEZ2(J)*(-Z)*X/(X**2 + Z**2)**(5.0/2.0) +
&                       SOURCE1(J)*X/(R**2 + Z**2)**(3.0/2.0) +
&                       3*DIPOLEZ1(J)*(-Z)*X/(R**2 + Z**2)**(5.0/2.0) +
&          SOURCE2(J)*X/(X**2 + 4*RADC(I) + Z**2)**
&          (3.0/2.0) +3*DIPOLEZ2(J)*(-Z)*X/(X**2+4*
&          RADC(I)+Z**2)**(5.0/2.0) +
&          3*DIPOLEY2(J)*2*RADC(I)*X/(X**2+4*RADC(I)+
&          Z**2)**(5.0/2.0))*M(J) + UU2
                END IF
          END DO
          U1(I) = S*UU1/3
          U2(I) = S*UU2/3
        END DO

        WRITE(13,*) 'STARTING FORCE CALCULATIONS'

        DO I=0, MAX_DATA
         DQZ1DZ(I) = 0
         DQZ2DZ(I) = 0
         DQZ2DY(I) = 0
         DDQZ1DZ = 0
         DDQZ2DZ = 0
         DDQZ2DY = 0
         DO J=0, MAX_DATA
                X = (XI(I) - XJ(J))*COS(PITCH)
                Z = ZI(I) - (XI(I) - XJ(J))*SIN(PITCH)
                R = (X**2 + Z**2)**.5

                DDQZ1DZ = (SOURCE1(J)/R**3 + 3*Z*(3*DIPOLEZ1(J) -
&                       Z*SOURCE1(J))/R**5 - 15*Z**3*DIPOLEZ1(J)/R**7 +
&                       2*SOURCE2(J)/(R**2 + RADC(I)**2)**(3.0/2.0) +
&                       3*Z*(6*DIPOLEZ2(J) - 2*Z*SOURCE2(J))/
&                       (R**2 + RADC(I)**2)**(5.0/2.0) -
&          30*Z**3*DIPOLEZ2(J)/(R**2 + RADC(I)**2)**
&          (7.0/2.0)) *M(J) + DDQZ1DZ
                DDQZ2DZ = (SOURCE2(J)/R**3 + 3*Z*(3*DIPOLEZ2(J)-
```

```
&                         Z*SOURCE2(J))/R**5 - 15*Z**3*DIPOLEZ2(J)/R**7 +
&                         SOURCE1(J)/(R**2 + RADC(I)**2)**(3.0/2.0) +
&                         3*Z*(3*DIPOLEZ1(J) - Z*SOURCE1(J))/
&                         (R**2 + RADC(I)**2)**(5.0/2.0) -
&          15*Z**3*DIPOLEZ1(J)/(R**2 + RADC(I)**2)**
&          (7.0/2.0) +
&                         SOURCE2(J)/(R**2 + 4*RADC(I)**2)**(3.0/2.0) +
&                         3*Z*(3*DIPOLEZ2(J) - Z*SOURCE2(J))/
&                         (R**2 + 4*RADC(I)**2)**(5.0/2.0) -
&          15*Z**3*DIPOLEZ2(J)/(R**2+4*RADC(I)**2)**
&          (7.0/2.0) +DIPOLEY2(J)*2*RADC(I)/(R**2+
&          4*RADC(I)**2)**(5.0/2.0) -5*DIPOLEY2(J)*2*
&          RADC(I)*Z**2/(R**2+4*RADC(I)**2)**(7.0/2.0))*
&                         M(J) + DDQZ2DZ
                DDQZ2DY = ((-3*SOURCE1(J)*Z - DIPOLEZ1(J))*RADC(I)/
&                         (R**2 + RADC(I)**2)**(5.0/2.0) -
&                         15*Z**2*RADC(I)*DIPOLEZ1(J) /
&                         (R**2 + RADC(I)**2)**(7.0/2.0) -
&                         6*(SOURCE2(J)*Z - DIPOLEZ2(J))*RADC(I) /
&                         (R**2 + 4*RADC(I)**2)**(5.0/2.0) -
&                         30*Z**2*RADC(I)*DIPOLEZ2(J) /
&                         (R**2 + 4*RADC(I)**2)**(7.0/2.0) +
&          DIPOLEY2(J) * Z / (R**2 + 4*RADC(I)**2)**
&          (5.0/2.0) -20*DIPOLEY2(J)*RADC(I)**2*Z /
&                         (R**2 + 4*RADC(I)**2)**(7.0/2.0)) *
&                         M(J) + DDQZ2DY
          END DO
          DQZ1DZ(I) = S/3*DDQZ1DZ
          DQZ2DZ(I) = S/3*DDQZ2DZ
          DQZ2DY(I) = S/3*DDQZ2DY
        END DO

        FZ1TOTAL = 0
        FZ2TOTAL = 0
        MY1TOTAL = 0
        MY2TOTAL = 0

        WRITE(13,*) 'FINAL SOURCES'
        WRITE(13,*) 'I, SOURCE, DIPOLE, M'
        DO I=0,MAX_DATA
          WRITE(13,*)I,SOURCE1(I),DIPOLEZ1(I),M(I)

    FZ1(I) = -4*PI*ROW*(SOURCE1(I)*W1(I) + (-DIPOLEZ1(I))*
&       DQZ1DZ(I))*M(I)
    FZ2(I) = -4*PI*ROW*(SOURCE2(I)*W2(I) + (-DIPOLEZ2(I))*
&       DQZ2DZ(I) +(-DIPOLEY2(I))*DQZ2DY(I))*M(I)
          MY1(I) = -(XI(I)*FZ1(I)) + 4*PI*ROW*(-DIPOLEZ1(I))*U1(I)*M(I)
          MY2(I) = -(XI(I)*FZ2(I)) + 4*PI*ROW*(-DIPOLEZ2(I))*U2(I)*M(I)

          FZ1TOTAL = FZ1(I) + FZ1TOTAL
          FZ2TOTAL = FZ2(I) + FZ2TOTAL
          MY1TOTAL = MY1(I) + MY1TOTAL
          MY2TOTAL = MY2(I) + MY2TOTAL
        END DO

        FZ1TOTAL = FZ1TOTAL*S/3
        FZ2TOTAL = FZ2TOTAL*S/3
        MY1TOTAL = MY1TOTAL*S/3
        MY2TOTAL = MY2TOTAL*S/3
        FZTOTAL = FZ1TOTAL + 2* FZ2TOTAL
        MYTOTAL = MY1TOTAL + 2*MY2TOTAL

        WRITE(13,20)'1: ',FZ1TOTAL, MY1TOTAL
    WRITE(13,20)'2: ',FZ2TOTAL, MY2TOTAL

RETURN
END
```

5595-38